proton scattering studies: 70 to 140 mev.

A THESIS SUBMITTED FOR THE DEGREE OF DOCTOR OF PHILOSOPHY

IN THE UNIVERSITY OF OXFORD

BY

m. ramsay wigan.

SEPTEMBER 1967

HERTFORD COLLEGE. OXFORD.

CONTENTS

LIST OF TABLES

D.Phil.

Notification of Acceptance as an Advanced Student

University Registry,
Clarendon Building,
Oxford.

2 November 1964

The Secretary of Faculties is authorized to state that the applicant named below has been accepted for admission.

Name E. R. Wigan

College or other Society Hertford College

Board of Faculty Physical Sciences

Subject of Research Nucleon Scattering studies at 140 mev.

Supervisor D. . . . Jarvis

Initialed for the Secretary of Faculties.

[P.T.O. IMPORTANT

1,000: 9.62.

1. *The Term of admission* will be that in which the admission fee and first terminal fee are paid.

2. *Fees payable:* Admission £5; each term for the first six terms £3, and each term in which supervision is received £8; 10 on application for leave to supplicate for the degree £ 25

3. *Method of payment:*
   Admission and terminal fees can be paid only through the student's College, Hall, or other Society.

4. Forms are supplied at the University Registry for use when a student applies for leave to supplicate. One of these is enclosed with this notice.

5. The work must be carried out in Oxford for six terms, except that for a student who holds the degree of B.Phil. this shall be three terms. Leave of absence may be granted by the board for not more than three of the six terms, unless the student is a Bachelor of Letters or of Science, in which case leave of absence may be granted for the whole period.

6. Statutory residence must have been kept for six terms before the degree can be taken.

7. The name of an Advanced Student must be kept on the books of his society continuously from the date of admission.

8. The earliest term in which a student can apply for leave to supplicate is his sixth, and the latest his twelfth, as an Advanced Student, e.g.:

Admitted	Michaelmas Term 1962.
Earliest term for applying for leave to supplicate .	Trinity Term 1964.
Latest term for applying for leave to supplicate .	Trinity Term 1966.

9. For further details see the latest edition of the *Examination Statutes.*

FOR A CANDIDATE FOR THE DEGREES OF
B.D., B.LITT., B.SC., or D.PHIL., or for the
DIPLOMA IN LAW

THE Secretary of Faculties writes to inform you that the following have been appointed your examiners:—

1. Dr. M. A. Grace

2 Dr. J. J. Thresher

Your thesis is in their hands, and they will inform you in due course of the date of your examination. You are responsible for ensuring that any letter sent to you at your College (or Hall or Society) or at any other address which you may have is forwarded without delay, and you should at once acknowledge the receipt of any letter from your examiners. You are *not* expected to take the initiative in communicating with them.

Initialed for the
Secretary of Faculties MCS.

To M. R. Vigan, Esq.
7 Stratfield Road,
Oxford.

2,000:—7.65.

UNIVERSITY REGISTRY
CLARENDON BUILDING
BROAD STREET
OXFORD

31 October 1967

Dear Sir,

I have much pleasure in informing you that the Board of the Faculty of Physical Sciences has granted you leave to supplicate for the Degree of

Doctor of Philosophy

A notice to this effect will be published in the *University Gazette*.

Will you please make your arrangements for supplicating for the Degree through the proper officer of your College.

Yours faithfully

L. Hamond

Secretary of Faculties

To M.R. Wigan, Esq.,

1000:—8.65.

LIST OF FIGURES

Abstract

The work reported in this thesis covers the latter part of a programme undertaken at A.E.R.E. Harwell to collect data on the nucleon-nucleon scattering problem at energies accessible to the Harwell 280 cm synchrocyclotron. The experiments described belong to the second phase of data collection at these energies in that they do not of themselves determine a unique set of phase shifts in a modified phase-shift analysis, but resolve ambiguities in the earlier data available, or improve the precision to a significant degree.

The first chapter contains a review of the nucleon-nucleon scattering problem, and provides a common context for the different types of experiment described. The second chapter is devoted to a description of the development and final form of a polarised proton target for use in the 70-150 Mev region for proton-proton scattering. Radiation damage resulted in a decay of the polarisation produced in this target, and a brief study of this phenomenon (described in Chapter II) was required to supplement the polarisation decay data collected in the spin correlation experiment reported in the third chapter.

The third and fourth chapters contain the experimental method and analysis of experiments using the polarised target to determine the spin correlation parameter Cnn in proton-proton scattering at 90^{o} centre of mass for three energies: 74, 98, and 143 Mev; and at 61.8^{o} centre of mass at 143 Mev only. A typical precision of $\pm$ 0.05 was obtained for this parameter.

The fifth chapter contains a description of the apparatus and methods used for measurements of polarisation

in the 98 Mev region: the experiment at 98 Mev to determine $P(\theta)$ in p-p scattering is described and analysed in chapter six. Due to a recent remeasurement of the polarisation of the Harwell 142 Mev polarised proton beam, absolute polarisation values were obtained, to a typical precision of $\pm$ 2% of the peak value of the asymmetry. The 98 Mev data provide a notably more stringent restriction on phase-shift fits at this energy than previous polarisation information.

The preliminary results of a measurement of the absolute differential cross-section for p-p scattering at 98.8 Mev are included in a phase-shift analysis at 95 Mev. Analyses at 73, 95, 140 Mev are briefly discussed, and the chapter concluded with a compilation of the N-N scattering data now available in the energy range 60-160 Mev.

Acknowledgements

During the last three years I have been working with the Harwell Synchrocyclotron Group in a number of collaborations. Throughout this time, the help and encouragement of Drs. O.N.Jarvis, B.Rose, and J.Butterworth have been invaluable; I would particularly like to thank Dr.B.Rose for making the arrangements for me to work on the Harwell synchrocyclotron.

I would also like to thank: J.Orchard-Webb, T.W.P.Brogden, and J.C.Waldron for their work on and for the polarised target during my stay: P.Martin and R.A.Bell for their contribution to the 98 Mev liquid hydrogen work: Drs.J.K.Perring and J.P.Scanlon for many stimulating discussions: the engineer and the operating staff of the synchrocyclotron for their willing assistance at all times; and L.R.Caldecourt and K.C.Done for their unfailing engineering support.

The work was supported by a U.K.A.E.A. research grant which I gratefully acknowledge.

Particular thanks are due to my wife for her moral and financial support, and her efforts in the production of this thesis.

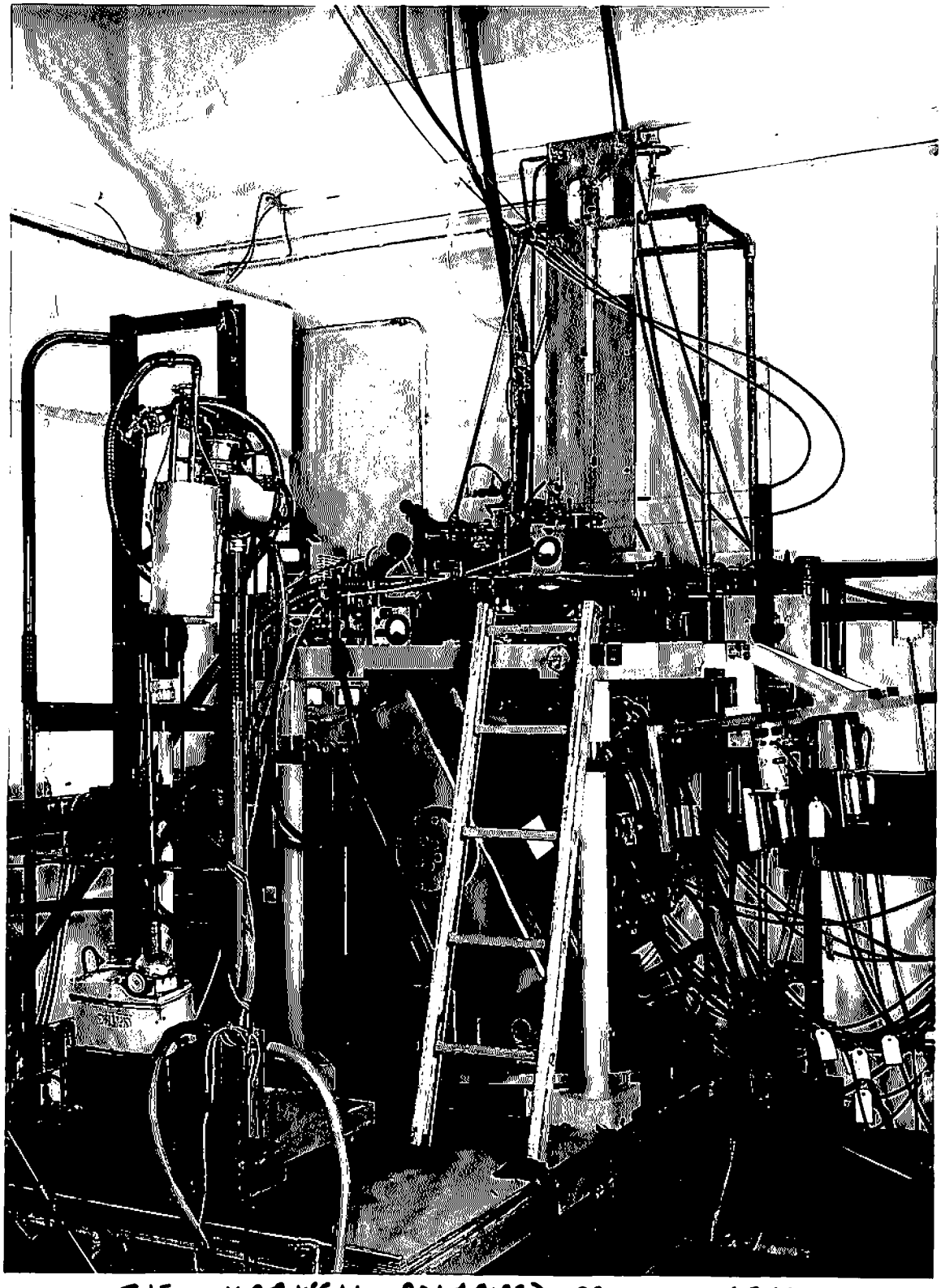

THE HARWELL POLARISED PROTON TARGET

I. Nucleon-Nucleon scattering up to 400 Mev.

1.1 N-N interaction in a general context

The study of the nucleon-nucleon (N-N) interaction is one of the basic themes of nuclear physics,[1)2)] and should provide the connecting link between elementary particle studies and more specifically nuclear investigations. Attempts to utilise knowledge of the basic nucleon-nucleon interactions to understand nuclear properties have not been very successful in the past,[4)] although nucleon-nucleus scattering may be described in terms of nucleon-nucleon phase shifts.[3)(31)] However there are indications that the data and the theory of the two-body problem are now reaching a stage where more success may be expected. Recent approaches include the use of the phenomenological potentials for nuclear matter calculations,[5)6)] and the calculation of nuclear spin-orbit-splittings using the two-nucleon phase shifts directly.[7)]

The theoretical calculation of the two-nucleon potential has been a long standing problem in elementary particle theory, and the approach through meson exchange models has a long history. The readily calculable one-pion exchange contribution was at first sufficient to describe the long range part of the interaction,[8)] to the precision then available. With the rapid collection of a wide range of p-p information, and an increase in the amount of n-p data available, more detailed and testing models could be studied.[9)10)11)] The precision of the p-p data is now comparatively good; recent measurements of polarisation and cross-section in p-p scattering at 140 Mev at Harwell have achieved an absolute precision of the order of 1%,[13)] and

work reported in this thesis extends the data to a similar precision at 100 Mev.

Even at these comparatively low energies the effects of other mesons such as the ρ, ω, η, f [126] and ϕ are observable and models using several mesons have been developed which give a good qualitative fit to both n-p and p-p data up to 400 Mev, some using as few as 4 [12] adjustable parameters (Amati et al 1963, [9] Signell 1964, [10] Scotti et al 1965, [11] Köpp 1965, [14] Arndt et al 1965, [15] and literature cited by them). The precision of the phase-shift sets now obtained from the data by phase-shift analysis lends some support to the assumption of charge independence (Arndt and MacGregor 1966), [16] as the values of the pion-nucleon coupling constant obtained from n-p and p-p data are in agreement.

The data are now sufficiently numerous and precise to allow the determination of unique phase-shift solutions for both n-p and p-p scattering from 10-350 [16] [91] Mev. Present experimental work is concentrated on improving on the precision and reducing the ambiguities of the data, and future effort is likely to be concentrated on the n-p system.

Calculation of p-p bremsstrahlung cross-sections has now reached a stage where satisfactory agreement with the data [17] [138] can be obtained, and further measurements on the off-the-energy-shell elements of the scattering matrix are being planned.

1.2 General formalism

In this field, theory has lagged behind experiment, so phenomenological models have been developed to reduce the different data to a convenient and coherent form for later comparison with more basic theoretical descriptions, and to help with the planning of experiments. A general

formalism derived by Wolfenstein (1952,1958)[19] is used to describe experimentally measurable parameters of the two-nucleon system in a convenient manner. This formalism has the Pauli exclusion principle, time reversal invariance (T) and parity conservation (P) built into it, and charge conjugation invariance by implication of the P.C.T. theorem: the effects of any small deviation from these symmetries have been considered by Woodruff (1959)[19] and Phillips (1958,[20] 1966)[21]. Thorndike[34] has studied TP invariance to see if any infomation could be extracted from the p-p data, and shown that there is no evidence for the violation of either invariance, although the limits on the invariance-breaking amplitudes are poorly determined. The treatment is non-relativistic, and the corrections required for this have been studied by Stapp,[29] Sprung,[32] and Garren. The corrections do not affect $P(\theta)$ and Cnn, and the non-relativistic formalism developed below is correct, when $P(\theta)$ is interpreted as a 4-vector.

Wolfenstein and Ashkin (1952)[18] use a scattering matrix in the spin space of the two nucleons. Each nucleon is described by a Pauli spinor, giving a total of four dimensions in the combined spin space. The wave function describing the scattering in the centre of mass system has four components:

$$(1)\quad \psi_i = a_i e^{i\underline{k}.\underline{r}} + \frac{e^{ikr}}{r} \sum_{j=1}^{4} M_{ij}(\theta,\phi)\, a_j$$

Where the four a_i refer to the incident spin states, M is the scattering matrix, $\underline{r}$ is the distance between the two nucleons and $\hbar\,\underline{k}$ is the incident momentum in the centre of

FIG. 1.

VECTOR SYSTEMS USED IN THE WOLFENSTEIN FORMALISM

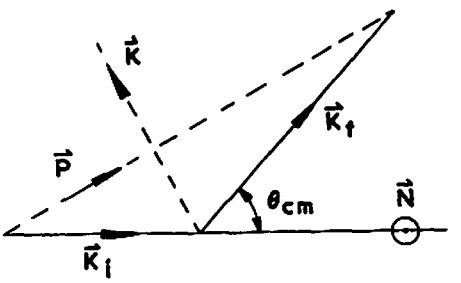

(a) CENTRE OF MASS FRAME

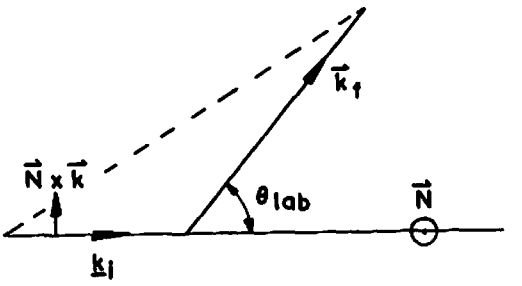

(b) LABORATORY FRAME

$$\vec{N} = \frac{\vec{K}_i \times \vec{K}_f}{|\vec{K}_i \times \vec{K}_f|} \qquad \vec{K} = \frac{\vec{K}_f - \vec{K}_i}{|\vec{K}_f - \vec{K}_i|} \qquad \vec{P} = \frac{\vec{K}_f + \vec{K}_i}{|\vec{K}_f + \vec{K}_i|}$$

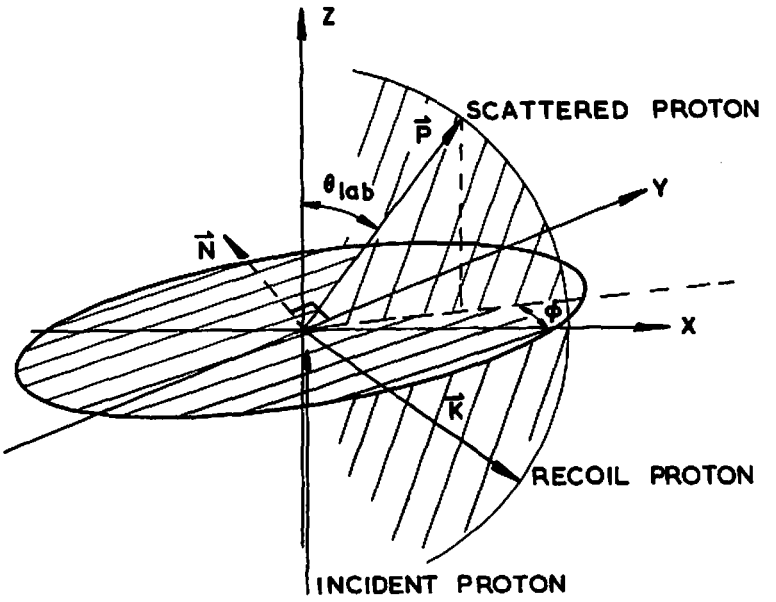

$\vec{N} = (-\sin\phi,\ \cos\phi,\ 0)$
$\vec{P} = (\sin\theta\cos\phi,\ \sin\theta\sin\phi,\ \cos\phi)$
$\vec{K} = (\cos\theta\cos\phi,\ \cos\theta\sin\phi,\ -\sin\theta)$

(c) PROTON - PROTON SCATTERING IN LAB. FRAME.

mass system. We thus obtain $4 \times 4 = 16$ complex elements of M in the general case. However there are several symmetry properties which appear to hold for strong interactions, i.e.,

1) The Pauli exclusion principle.
2) Time reversal invariance.
3) Parity - corresponding to invariance under reflection.
4) Angular momentum - corresponding to invariance under rotations.
5) Charge conjugation invariance: equivalent to (2)+(3) by the P.C.T. theorem.

By applying these restrictions, Wolfenstein[18] shows that the scattering matrix may be written:

$$M = a+c(\underline{\sigma_1}.\underline{n}+\underline{\sigma_2}.\underline{n}) +m(\underline{\sigma_1}.\underline{n})(\underline{\sigma_2}.\underline{n}) +g[(\underline{\sigma_1}.\underline{p})(\underline{\sigma_2}.\underline{p}) + (\underline{\sigma_1}.\underline{k})(\underline{\sigma_2}.\underline{k})] \quad (2)$$
$$+h\,[(\underline{\sigma_1}.\underline{p})(\underline{\sigma_2}.\underline{p}) - (\underline{\sigma_1}.\underline{k})(\underline{\sigma_2}.\underline{k})]$$

where $\underline{\sigma_1}$, $\underline{\sigma_2}$ are the Pauli spin matrices for the two nucleons, and a,c,m,g,h, are complex functions of energy and scattering angle (θ). The vectors $\underline{n}$, $\underline{p}$, $\underline{k}$ form a right handed set as shown in FIG. 1.

This shows that at any given energy and angle 10 independent experiments are required to determine the matrix M at that energy and angle. Puzikov (1957)[22] has shown that five relations between the coefficients a,c,m,g,h, may be found by applying the requirements of particle conservation (unitarity): this is evidently valid in the elastic scattering region, and reduces the minimum number of experiments required to five at a given energy over the angular range $o-\pi$ in the centre of mass. ~~For p-p scattering, the identity of the particles further reduces this range to $o-\pi/2$.~~

These minimum requirements must always be exceeded

give:

$$(4) \qquad \langle \bar{A} \rangle = \frac{Tr(\varrho A)}{Tr(\varrho)}$$

As we are concerned with spin 1/2 particles, the information contained in the density matrix of the incident beam is essentially the polarisation vector ($\underline{P}$) of the beam. A separate density matrix is needed to describe the beam and the target, giving a density matrix in the combined spin space.

The form of M described previously together with relation (3) may be used to derive several important conclusions for N-N scattering.

I) Using space-reflection invariance, it may be shown[18] that in the scattering of an unpolarised beam from an unpolarised target the scattering particles will (if polarised at all) be polarised in direction perpendicular to the scattering plane.

II) Using time reversal invariance[18], the cross-section for the scattering of a polarised beam from an unpolarised target is:

$$(5) \qquad I(\theta, \phi) = Io(\theta)[1 + \underline{P}_I \cdot \underline{N} P(\theta)]$$

where $Io(\theta)$ is the cross-section for the scattering of an unpolarised beam from an unpolarised target through an angle θ, ϕ is the azimuth angle, $\underline{P}_I$ is the polarisation of the incident beam, $P(\theta)$ is the polarisation produced in scattering an unpolarised beam on the target, and $\underline{N}$ (see FIG 1) is a unit vector perpendicular to the scattering plane [from (1)].

We thus obtain a measurable quantity ε, a left-right asymmetry;

in practice, as experimental data is not acquired either with infinite precision or continuously as a function of scattering angle.

1.3 Definition of experimentally measurable quantities

So far only pure initial spin states have been considered. Under experimental conditions neither the incident beam nor the target is in a pure spin state. The beams termed 'unpolarised' in fact contain every possible pure spin state with an equal weight, and the target nucleon spins are randomly oriented. The beams termed 'polarised' contain a mixture of spin states of unequal weights, giving a net non-zero spin angular momentum in some direction. Such beams may be produced by scattering an unpolarised beam off a suitable target, or by accelerating a beam of polarised particles produced by a special ion source in the accelerator.[26] Unpolarised targets generally are used, however polarised proton targets have recently been developed, and polarised deuteron[24] targets are now becoming practicable.

To describe the spin states of such beams and targets, the statistical density matrix ϱ is used.[18)28] If we write ϱ_I for the initial density matrix, the form of ϱ_F the density matrix describing the system after scattering is given by:

$$\varrho_F = M \varrho_I M^+ \tag{3}$$

where M is the scattering matrix defined in the previous section. To obtain the average value over all particles, of any spin operator A, the density matrix may be used to

$$(6) \qquad \mathcal{E} = \frac{I(\theta, o) - I(\theta, \pi)}{I(\theta, o) + I(\theta, \pi)}$$

where $\mathcal{E} = P_I . P(\theta)$ from (5).

This polarisation-asymmetry equality provides a test for time reversal, and several measurements have been made to test it, notably by Hillman[25] and Thorndike.[34] No evidence has yet been obtained to challenge the validity of the equality

III) Extending the formalism to the polarisation ($\underline{P}_F$) produced in the scattering of a polarised beam ($\underline{P}_I$) on an unpolarised target,

$$(7) \qquad \underline{P}_F = \frac{1}{(1+\underline{P}_I \cdot \underline{n}P)} [(P+D\underline{P}_I \cdot \underline{n})(\underline{n}) + (A\underline{P}_I \cdot k + R\ \underline{P}_I \cdot \underline{n} \wedge \underline{k})\underline{n} \wedge \underline{k} + (A' \cdot \underline{P}_I \cdot \underline{k} + R' \cdot \underline{P}_I \underline{n} \wedge \underline{k})\underline{k}]$$

where P, D, R, A, R', A', are all functions of scattering angle and energy, and the last five are the Wolfenstein parameters for triple-scattering.

IV) When the target also is polarised, the form of the density matrix is:[23]

$$(8) \qquad \varrho = 1 + \underline{P}_I \cdot \underline{\sigma}_I + \underline{P}_T \cdot \underline{\sigma}_T + C_{jk}\, \underline{\sigma}_{Ij}\, \underline{\sigma}_{Tk}$$

where $\underline{P}_I$ is the incident beam polarisation, $\underline{P}_T$ target polarisation, and C_{jk} are the spin correlation parameters and j,k can be any pair of $\underline{k}$, $\underline{p}$, $\underline{n}$ spatial directions of FIG 1. Applying (III) and restricting $\underline{P}_I$ and $\underline{P}_T$ to be both in the same plane, at $\phi = 0$; the cross-section is given by:

$$(9) \qquad I = I_o[\, 1 + (P_I + P_T)P + P_I\, P_T\, C_{nn}]$$

where I, Io , P, Cnn, are all functions of scattering angle and of energy, P is the polarisation produced in scattering

an unpolarised beam and unpolarised target, Cnn is the spin correlation parameter, a measurement of which is described in this thesis.

These four results provide an experimental framework to obtain the elements of the scattering matrix. By using (III), (IV) all the measurable parameters may be expressed in terms of the elements of the scattering matrix.[32] In principle 256 different experiments may be carried out on the p-p system, depending on different polarisation states of incident beam and target, and the different measurements that can be made on the recoil and scattered beams. Below the pion threshold only five experiments are completely independent for the p-p system, and measurements may be taken at finite intervals over the angular range by making the assumption of analyticity,[120] which is essentially the assumption that data points will be on smooth curves. Result (I) gives us a method of polarising an incident beam; (II) and (IV) allow us to affect this incident polarisation, and (II) enables us to measure the polarisation of the final scattered or recoil beams.

Thus (a) the measurement of differential cross-section Io (θ)- or $\sigma_o(\theta)$ - requires only the measurement of a singly scattered unpolarised beam.

(b) The measurement of polarisation P(θ) requires at least two scatterings, and the measurement of a left to right asymmetry in a scattered beam.

(c) The measurement of spin correlation parameter Cnn requires at least two scatterings and the measurement of an asymmetry in a scattered beam. The two

approaches are:

(1) to analyse the recoil and scattered particle polarisations produced when an unpolarised beam is scattered off an unpolarised target: this needs three scatterings,

(2) to scatter a polarised beam off a polarised target with both polarisations in the same plane, and to examine the left to right asymmetry in the plane perpendicular to the plane of the incident polarisation, as before.

1.4 Phase-shift analysis

The basic theory of nucleon-nucleon interactions is not adequate to provide a direct comparison with measured quantities as defined above. Thus a phenomenological approach is required, which uses reasonable physical assumptions to reduce the differing forms of measured data to as few parameters as possible. The theory may then be aimed at reproducing these parameters, and the experimental effort directed at obtaining sufficient information to fix the phenomenological parameters accurately and uniquely. The approach used for this phenomenological parametrisation is to define phase shifts through the asymptotic behaviour of the scattering wave function.[33] The angular momentum states allowed for the proton-proton system are

$$^1S_0 \ , \ ^3P_{0,1,2} \ , \ ^1D_2 \ , \ ^3F_{2,3,4} \ , \ ^1G_4 \ \text{ etc.}$$

where $^{2S+1}L_J$ is the general form and S is the total spin of the two protons: J being the total angular momentum, and L the relative orbital angular momentum, in spectroscopic notation. The description of neutron-proton scattering has about twice as many states available as in the proton-proton case. The restriction of the exclusion principle requiring the wave function to be anti-symmetric

reduces the number of allowed states.

For each state a phase shift δ_L is defined; however for such states as $^3P_1$ and $^3F_2$ which have the same parity and angular momentum, it is necessary to define a mixing parameter ε_1 to complete the representation. The orbital angular momentum itself is not necessarily conserved due to the presence of the tensor force in the two-nucleon interaction. It is also necessary to allow for the effect of the Coulomb forces.

Rewriting equation (1) in terms of the scattering amplitudes $f_c(\theta)$, we have

$$(10) \qquad \psi = a_c e^{ik\cdot r} + \frac{e^{ikr}}{r} f_c(\theta)$$

It may be shown that[113]

$$(11) \qquad f_c(\theta) = \frac{-1}{2ik} \sum_{\ell=0}^{\infty} (2\ell+1)[e^{2i(\sigma_\ell+\delta_\ell)}-1]P_\ell(\cos(\theta))$$

where σ_ℓ are the phase shifts contributed by the Coulomb force, and $P_\ell(\cos\theta)$ are the Legendre polynomials.

The restrictions of unitarity, parity, and time reversal invariance are readily built into the phase-shift parametrisation.[120] Unitarity is obtained by restricting the phase shifts to be real: this applies only up to the meson threshold, as beyond this point the phase shifts become complex to allow for inelasticity. Parity conservation is applied by forbidding the mixing of states such as $^1S_0$ and $^3P_0$. Time reversal invariance is applied by defining a single parameter ε_2 (ε_4, ε_6 ...etc.) to describe the mixing of the pairs of states $^3P_2$ and $^3F_2$ ($^3F_4$ and $^3H_4$ etc.).[34] Woodruff[19] and Phillips[20,21]

have also explored the effects of relaxing the restrictions, and show that considerable experimental precision is required to detect any such deviation.

If we write $\underline{S}$ = total spin angular momentum vector of the two particles, $\underline{L}$ = total relative angular momentum, and $\underline{J}$ (= $\underline{L}$ + $\underline{S}$) as the total angular momentum of the system; then only J and Jz (the z-component of $\underline{J}$) are constants of the motion. This means that only the quantum numbers J and Jz can be used to specify the states of the two-nucleon system. Also, states with even L have even parity, and states with odd L have odd parity; thus to retain parity conservation they may not mix. The investigations of Woodruff and Phillips[19)20)21)] introduce mixing parameters between such states to investigate the effects of parity non-conservation and time reversal non-invariance.

To define a unique phase shift for triplet states with L = J $\pm$ 1 under these conditions, it is necessary to define a nondiagonal matrix to relate amplitudes of the states L = J + 1 after collision to those before. This requires the phases $\bar{\delta}_{J,J+1}$; $\bar{\delta}_{J,J-1}$ and a coupling parameter $\bar{\varepsilon}_J$. The matrix is usually written:

$$(12)\quad \begin{bmatrix} \bar{\delta}_{J,J+1} & 0 \\ 0 & \bar{\delta}_{J,J-1} \end{bmatrix} \begin{bmatrix} \cos 2\bar{\varepsilon}_J & \sin 2\bar{\varepsilon}_J \\ -\sin 2\bar{\varepsilon}_J & \cos 2\bar{\varepsilon}_J \end{bmatrix} \begin{bmatrix} \bar{\delta}_{J,J+1} & 0 \\ 0 & \bar{\delta}_{J,J-1} \end{bmatrix}$$

and the phases are called nuclear bar phases, to distinguish them from the less convenient parametrisation of Blatt and Biedenharn.[37)] The effects of the Coulomb force are readily included in the nuclear bar parametrisation as the nuclear and Coulomb phases then add directly.[2)]

All measurable quantities may be expressed in terms

of phase shifts,[32] as the M matrix elements may be written as functions of the phase shifts, and the relations between the observable and the M matrix elements may then be used. The phase-shift parametrisation has several useful features. The higher partial waves, corresponding to high relative angular momentum states, may be neglected in an approximate treatment as they can be assumed not to come within the short range of the interaction. As a refinement the higher phases may be calculated theoretically by the use of a meson exchange model, and where fairly small phase shifts are still well determined by experimental data, comparisons of the meson models with 'experiment' may be made.

Although the experimentally measured quantities may be related to the phase shifts, the functional form of these relations makes it impossible to obtain an analytical form for the phases from the experimental data.[23] The form of the phase-shift analysis is thus fixed by the need to search for a 'best set' of phases to fit all data simultaneously. The criterion[35] used is the χ^2 sum for all the data points:

$$\chi^2 = \sum_i \left[\frac{Xi - Ei(\delta)}{\sigma_i} \right]^2 \qquad (13)$$

Where $Xi \pm \sigma_i$ is the measured value of a quantity with a standard deviation σ_i : $Ei(\delta)$ is the computed value of the quantity using the values of the phase shifts δ. The phase-shift set may now be varied to minimise the χ^2 sum over all the data. As some sets of data have overall normalisations quoted for them - e.g. a series of relative measurements of differential cross-sections may have a

quoted (measured) normalisation as an additional datum to give the absolute scale of the relative measurements - these normalisations are included in the χ^2 search by writing the χ^2 sum as:

$$(14)\quad \chi^2 = \sum_i \left\{ \frac{y^{(n)} Xi - E_i(\delta)}{\sigma_i} \right\}^2 + \sum_n \left\{ \frac{y^{(n)} - 1}{\sigma_y^{(n)}} \right\}^2$$

where $y^{(n)} \pm \sigma_y^{(n)}$ are the normalisations and standard errors of the nth set of data.

When the first phase shift analyses were carried out they were done using data close to a single energy, and neglected phase shifts for higher than a semi-arbitrarily decided value of L. Semi-classical arguments were used to give a reasonable estimate of this maximum value of L. The advent of the modified phase-shift analysis, using estimates for the higher phases derived from the one-pion exchange (OPE) model, was a notable advance.[36] The lower phases were allowed to vary to obtain the best fit, and the changeover point to OPE could be varied to check its validity. This approach achieved considerable success, and was extended to attempt to fit all the data over an energy range from 0-400 Mev simultaneously.[37] The form of the energy dependence of these phase shifts is controlled by new parameters, which are also varied in the search for minimum χ^2.

The ambiguities and local minima found in such a search and the more arbitrary elements of the procedure - such as the choice of an OPE changeover point - caused considerable difficulties until the advent of more powerful computers than those available for the early work. The data available for the earlier analyses were not restrictive

enough to ensure unique solutions, and experimental effort was directed toward distinguishing between solutions. Unique solutions of p-p scattering are now available at several energies, notably 25, 50, 98, 140, 210, 320 Mev,[16] and the multi energy analyses have achieved unique solutions from 0-400 Mev. The n-p data alone are inadequate to produce unique solutions; however by combining them with the p-p data solutions can be found over the same energy range.

The neutron and the proton can be considered to be the two states of a single entity of spin projection $\pm$ 1/2; this spin is called isobaric spin (T). When the Pauli principle is applied only T=1 states are allowed for p-p scattering, although either T=1 or T=0 states are available to the n-p system. The T=1 states for the n-p system are considered to be the same as the T=1 states of the p-p system, with the Coulomb interaction removed. The π -N coupling constants obtained from phase-shift analysis provide some of the evidence that this procedure is justified. The T=0 phase shifts are not known to as high a precision as those for T=1.

The scattering matrix is now considered (MacGregor and Arndt[16]) to be determined quantitatively for the T=1 phases and at least qualitatively for the T=0 phases. The direction of experimental effort at the present time is to refine the data to remove inconsistencies and add measurements of new parameters.

The work reported in this thesis is part of an experimental programme at Harwell to carry out these aims in the 70-150 Mev region. The Cnn measurements reported here at 73, 98, 143 Mev[38] are measurements of a new parameter at these energies, and the polarisation values reported here

at 98 Mev[39] are a considerable advance on the previous data. Already published are precise measurements of polarisation and cross-section in p-p scattering at 140 Mev,[13] which have adequately resolved the uncertainties at that energy.

1.5 Present state of the theory

The description of the nucleon-nucleon interaction by a potential has a long history. Over 25 years ago[40] the basic components of a potential assuming the restrictions of charge independence, time reversal and parity were delineated, and as the data have improved all these components have been found necessary to explain the experimental results. This form[2] is:

$$V = Vci + Vsc\ \underline{\sigma_1}\cdot\underline{\sigma_2} + Vt\left(\frac{3\,\underline{\sigma_1}\cdot\underline{r}\ \underline{\sigma_2}\cdot\underline{r}}{r^2} - \underline{\sigma_1}\cdot\underline{\sigma_2}\right) \quad (15)$$

$$+ Vls\,(\underline{\sigma_1} + \underline{\sigma_2})\cdot\underline{r}\times\underline{p} + Vq\,[(\underline{\sigma_1} + \underline{\sigma_2})\cdot\underline{r}\times\underline{p}]$$

where Vci is a spin independent central potential, Vsc the spin dependent central potential, Vt the tensor potential, Vls the spin-orbit potential; and Vq the quadratic spin-orbit potential, which may be energy dependent or energy independent depending on the form of invariants used . A recent phenomenological energy independent potential has been given by Hamada and Johnston,[41] which reduces to a one-pion potential at large distances and has a repulsive core. The best evidence for this repulsive core is given by the behaviour of $^1S_0$ and $^1D_2$ phases as a function of energy.[42] The $^1S_0$ rises initially to a maximum, and then falls, becoming negative at $\sim$250 Mev, indicating a repulsion at close distances. The $^1S_0$ is more sensitive to short range interactions than the $^1D_2$, which remains positive to about 400 Mev.

The Hamada potential gives a fairly good representation

of the data, both n-p and p-p, over the energy range 0-320 Mev. This potential is very nearly as general as the most general form allowed, and further attempts to fit the data may require the full generality.

A potential is essentially a non-relativistic representation of the data; however, a good fit to the data (such as that achieved by the Hamada potential[41]) can be obtained over as wide an energy range as 0-400 Mev. A potential representation is required for nuclear physics calculations which may need 'off the energy shell' matrix elements, and good calculations of nuclear bindings and saturation[4] have been made using the Bressel[43] and Hamada-Johnston[41] potentials. The meson theory has not been very successful in deriving a potential to fit the data, and the more direct approach to data fitting using dispersion relations is now favoured.

Most attempts to describe the nucleon-nucleon interaction in terms of a basic theory spring from the Yukawa meson exchange potential, for which the heavier the meson exchanged, the shorter is the range of the force produced. The N-N interaction can then be considered in the three regions[2]:

(1) the long range part of the interaction, which is dominated by the lightest meson, the π;

(2) an intermediate region, where 2-π interactions, and the effects of heavier mesons - such as the ρ, ω, η - are appreciable;

(3) the innermost region, dominated by heavy meson exchange.

The calculation of the one-pion exchange contribution can be made accurately, however for two- and more-pion

exchange effects the difficulties and approximation involved increase rapidly. The long range parts of the interaction have been satisfactorily accounted for, and several approaches have achieved fair success in the intermediate distance region.

The earlier attempts to describe the N-N interaction in terms of mesons used field theory to obtain a potential, and proceeded from this potential to obtain phase shifts. The earlier calculations were not able to utilise information such as π-N scattering or scattering lengths, and it was difficult to allow for relativistic effects. A recent calculation by Green and Sawada,[45] using an intermediary relativistic potential, has obtained good qualitative agreement with the experimental data.

Recently it has become common to calculate the phase shifts directly by dispersion theory, as further information such as π-N scattering may then be used. Dispersion theory is based[2] on causality, unitarity, and crossing symmetry (which relates any reaction with those obtained from it by the interchange of incoming and outgoing states), and can more readily take relativistic effects into account. New information is required, as the unitarity restriction demands a sum over all intermediate states. In this context this means that results on π - π and π-N scattering are necessary.

The scattering amplitude is expressed as an analytic function of the (complex) energy variable, and a singularity in this amplitude corresponds to each intermediate state. In close analogy to the earlier meson approaches the theory can be applied in steps:[2] the long range part of the interaction being due to singularities close to the physical region, and the shorter range parts to those further removed.

The one-pion contribution arises from the singularity closest to the physical region, and can be accurately calculated. This part of the phase shift is built into the modified phase-shift analyses, where this one-pion term is used to replace the higher phases, while the remainder are determined directly by the experimental data. The main difficulty in the dispersion relation calculation arises from the two-pion exchange terms. These provide most of the attraction in the interaction, and it is therefore important that they be calculated correctly.

The N-N interaction is at this stage described in terms of the π-N and $\pi-\pi$ interactions, and the calculations are both lengthy and complex. There are three types of contribution to the two-pion term. These arise from the exchange of two pions with relative angular momenta of L=1, 2, and $\geq$2. The first term turns out to give almost identical results to calculations based on the exchange of a single, scalar meson[115] known as the σ.

This entity, with the constants ($J^P = 0^+$; $g_\sigma \sim 2.9$, $M_\sigma \sim 45$ Mev),[14] has been postulated by several workers to help interpret the N-N interaction. The L=1 exchange is closely connected to ϱ-meson exchange, as the ϱ is a resonant L=1 state of two pions. Thus the ϱ may be used to attempt to describe this effect. Amati et al,[9] Arndt et al,[15] Scotti et al[11] and others have used these approximations together with the exchange of single mesons (π, η, ρ, ω, ϕ) and the empirical S-wave scattering lengths to give good qualitative fits to the observed phase shifts up to $\sim$ 300 Mev by varying the coupling constants involved. The values of the coupling constants obtained in this way are in reasonable agreement with available measured values.[14] Bryan and Scott[12] did not use the empirical S-wave data, and obtained a similar fit using only four

variable parameters (i.e. the coupling constants), to be compared with ~12 for the other references quoted.[9)11)15]

Unfortunately the two-pion exchange terms for pions in relative angular momentum states L>2 were not included in these calculations, and would be expected to have a significant effect if they were.[115)]

The overall fits to the data are quantitatively poor, and Signell succeeded[91)] in obtaining a fit of the same quality by using a ten-parameter representation for the phase shifts, with no particular physical basis. Thus as phenomenological models, the meson models are not yet adequate, although the theory is qualitatively most successful.

Arndt[99)] et al have recently investigated the group theory schemes, popular in high energy physics, and their predictions for N-N scattering. The predictions of various 12-dimensional groups such as SU_{12}, M_{12}, $\tilde{U}_{12}$, for the vanishing of one of the invariant amplitudes of nucleon-nucleon scattering have been compared directly with the values of that amplitude computed from the energy dependent analysis[16)] of the data over the energy range 20-350 Mev. There is complete disagreement between the group theory prediction and the 'experimental' values.

1.6 Experimental data in the 60-160 Mev region

A survey of all the data at present available in this energy region is included in chapter VIII. Here the discussion will be limited to the p-p information near 74, 98, 143 Mev, being the energies of interest in the present work.

At about 140 Mev a considerable body of experimental data exists, and at the time the work for this thesis was begun,

many inconsistencies and ambiguities were to be found between data from different laboratories. 140 Mev is a unique energy in that a 'complete' set of experiments (σ, P, D, R, R', A) for the p-p system has been carried out at two separate laboratories (Harwell, Harvard), and part of a set (σ, P, D) at another (Orsay). Cnn has been measured only at Harwell.[38] This wealth of information is not available at other energies, and the inconsistencies shown up in the experimental data serve to show the advisability of independent measurements of the same quantity at the same energy.

Recent energy dependent phase-shift analyses[13,16] have found a unique solution for both T=1 and T=0 phases from 25-310 Mev, and has shown up such disagreements. The cross-section data of both Harvard[47] and Harwell[49] were discarded by MacGregor,[16] and the Orsay[53] data used. The Harwell data shows a rise between 45° and 90°c of m, while the Harvard data shows a fall in this region, which is even larger in the Orsay data. In addition the absolute scale of the different measurements was in poor agreement. The polarisation data showed remarkable agreement until the work of Jarvis and Rose[50] showed that the absolute scales of the polarisation measurements were in error. The Orsay polarisation data shows a certain reluctance to pass through zero at 90° c of m, which suggests undetected systematic asymmetries.

The recent measurements of σ, P at Harwell[12] carried out over the last few years have resolved these difficulties.

At 98 Mev, the MacGregor analyses showed that the data was reasonably consistent, but comment[16] that this is mainly due to the poor experimental precision.

The polarisation data of both Harwell [47] and Harvard [49] were subject to the same objection as the 155 Mev Orsay measurements, and the shape and absolute values of the cross-section data were not accurately known. The Harwell measurements of R, R' at 98 Mev [51], together with the Harvard D, [62] enabled a unique solution to be found in the 98 Mev region. The present measurements of Cnn, P, σ improve the situation.

Near 70 Mev very precise cross-section measurements exist at 68.3 Mev, [54] and some polarisation [47] [55] data. There is also a total cross-section [56] measurement at 70 Mev. The present value of Cnn improves the data set, as Cnn is varying rapidly with energy in this region and present precise data sets exist at 50 [92] and 140 Mev.

1.7 Conclusion

We have seen that the data are now sufficient to enable a qualitative understanding of the low energy (<400 Mev) N-N system to be made, and further work will concentrate on improving the precision and consistency of the data especially in the n-p system. Themeson exchange models are now able to account for the present data as well as such fitted potentials as that of Hamada-Johnston, as recently demonstrated by Noyes et al. [91] Other approaches [120] developed in high energy physics are increasingly being applied to the N-N problem: group theory [99] [126] classification schemes and Regge poles [114] [119] are two examples of such techniques.

II A polarised target for medium energy scattering experiments.

2.1 Design requirements

The use of a polarised proton target in nucleon-nucleon scattering studies has recently become possible, and provides a good method of measuring spin correlation parameters. The conventional "triple scattering" experiment starts with an unpolarised beam which is then scattered from an unpolarised hydrogen target. The polarisations of both scattered and recoil particles are analysed simultaneously by second scatterings. In the energy region 50-200 Mev, the analysing powers of suitable materials for the third scattering are all rather small, and the time reverse of the experiment may be more practicable.

Here an incident polarised beam is scattered from a polarised target, and the cross-section for this scattering is measured. This avoids the difficulties caused by the low analysing powers available in this energy region. The form of this cross-section is discussed in 1.3 equation (9), and when P_I , P_T are normal to the plane of scattering:

(9) $$\sigma = \sigma_o(1 + [P_I + P_T] P_I + P_T P \quad P \quad Cnn)$$

where σ, σ_o, P, Cnn are all functions of the scattering angle (θ) and of energy. P_I, P_T , P are the polarisations of the incident beam, the target, and that produced in p-p scattering, respectively. σ_o is the unpolarised cross-section.

As P=0 at 90° c of m, it is necessary to measure P_T.P at some other angle, say 61.8°, to provide a nuclear physics method for checking the polarisation of the target. This also has the advantage, providing the measurements are made at both

angles simultaneously, of giving a ratio Cnn (61.8° c of m): Cnn(90° c of m) independent of the behaviour of the target polarisation. As these targets are subject to large background effects, the scattered and recoil protons should be recorded in coincidence to reduce these backgrounds: for this experiment 61.8° c of m was the nearest obtainable angle to the maximum polarisation in p-p scattering (at ~ 40° c of m) for a reasonable thickness of target material, consistent with this coincident detection condition.

The experimental requirements were:

(1) a target with at least a 60° exit window, measured in the lab. from the horizontal plane, with a minimum of material in the path of the scattered protons. This meant that helium could not be allowed in the microwave cavity.

(2) a polarisation of at least 25 %. The polarised proton beam available was ~ 10^7 protons/sec at a polarisation of 47.2 ± 0.4 [57]. As Cnn (90°) at ~ 140 Mev was expected to be near unity, this target polarisation was expected to be sufficient to determine Cnn to ± 5 % in less than a day.

(3) some method of continuous measuring and monitoring the target polarisation, other than the nuclear physics method of using an unpolarised incident beam. Here (9) becomes $\sigma = \sigma_0(1 + P\ P_T)$, and the polarisation of the target may be deduced from a knowledge of the experimental asymmetry produced, and the value of P from the value of the asymmetry with incident beam polarised and the target unpolarised, or other work[13]; during Cnn measurements, however, this method cannot be used, and some continuous monitor is required to ensure that the target

FIG. 2

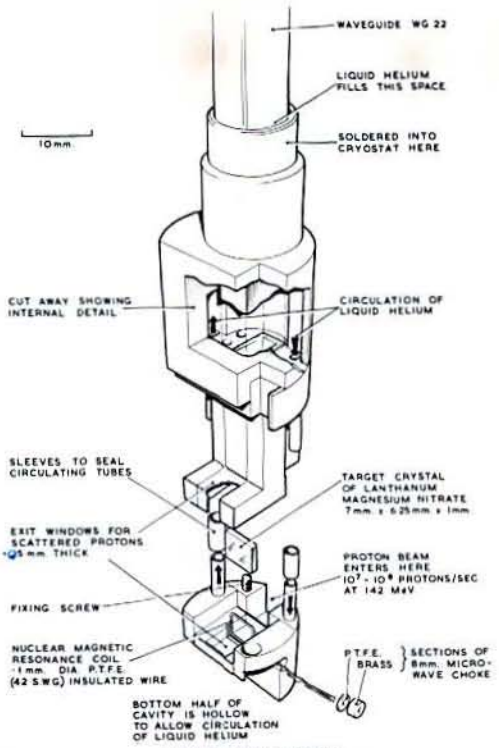

POLARISED TARGET CAVITY
TE012 MODE RESONANT AT 35·2 Gc/s.

	COL. 1. ENERGIES	COL. 2. ZERO ORDER WAVE FUNCTIONS	COL. 3. FIRST ORDER WAVE FUNCTIONS	COL. 4. THERMAL EQUIL. POPULATIONS
		M m		
①	$\delta = \frac{h\nu_n}{kT}$	$\left\|\frac{1}{2}, -\frac{1}{2}\right\rangle$	$\left\|\frac{1}{2}, -\frac{1}{2}\right\rangle + \alpha\left\|\frac{1}{2}, \frac{1}{2}\right\rangle$	$N_1 = e^{-\Delta-\delta}$
②		$\left\|\frac{1}{2}, \frac{1}{2}\right\rangle$	$\left\|\frac{1}{2}, \frac{1}{2}\right\rangle - \alpha\left\|\frac{1}{2}, -\frac{1}{2}\right\rangle$	$N_2 = e^{-\Delta}$
	$\Delta = \frac{h\nu_e}{kT}$			
③		$\left\|-\frac{1}{2}, -\frac{1}{2}\right\rangle$	$\left\|-\frac{1}{2}, -\frac{1}{2}\right\rangle - \alpha\left\|-\frac{1}{2}, \frac{1}{2}\right\rangle$	$N_3 = e^{-\delta}$
④	δ	$\left\|-\frac{1}{2}, \frac{1}{2}\right\rangle$	$\left\|-\frac{1}{2}, \frac{1}{2}\right\rangle + \alpha\left\|-\frac{1}{2}, -\frac{1}{2}\right\rangle$	$N_4 = 1$

FIG. 3

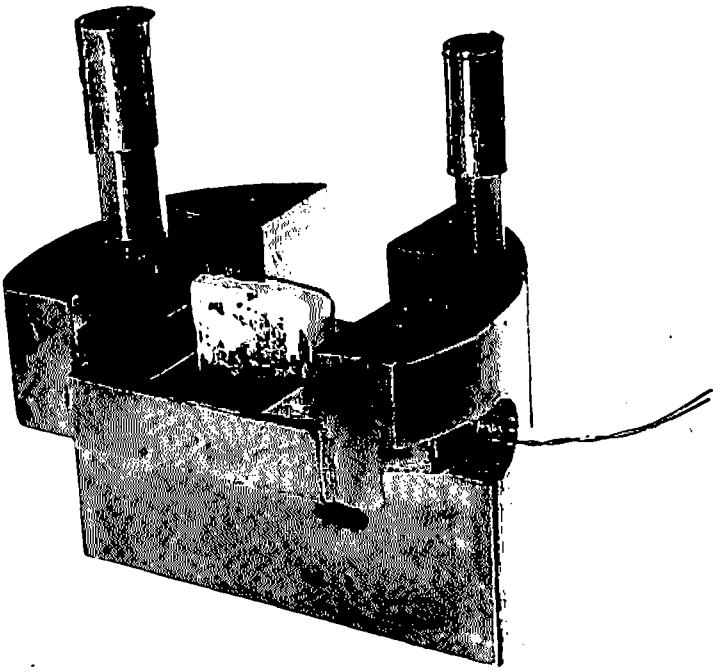

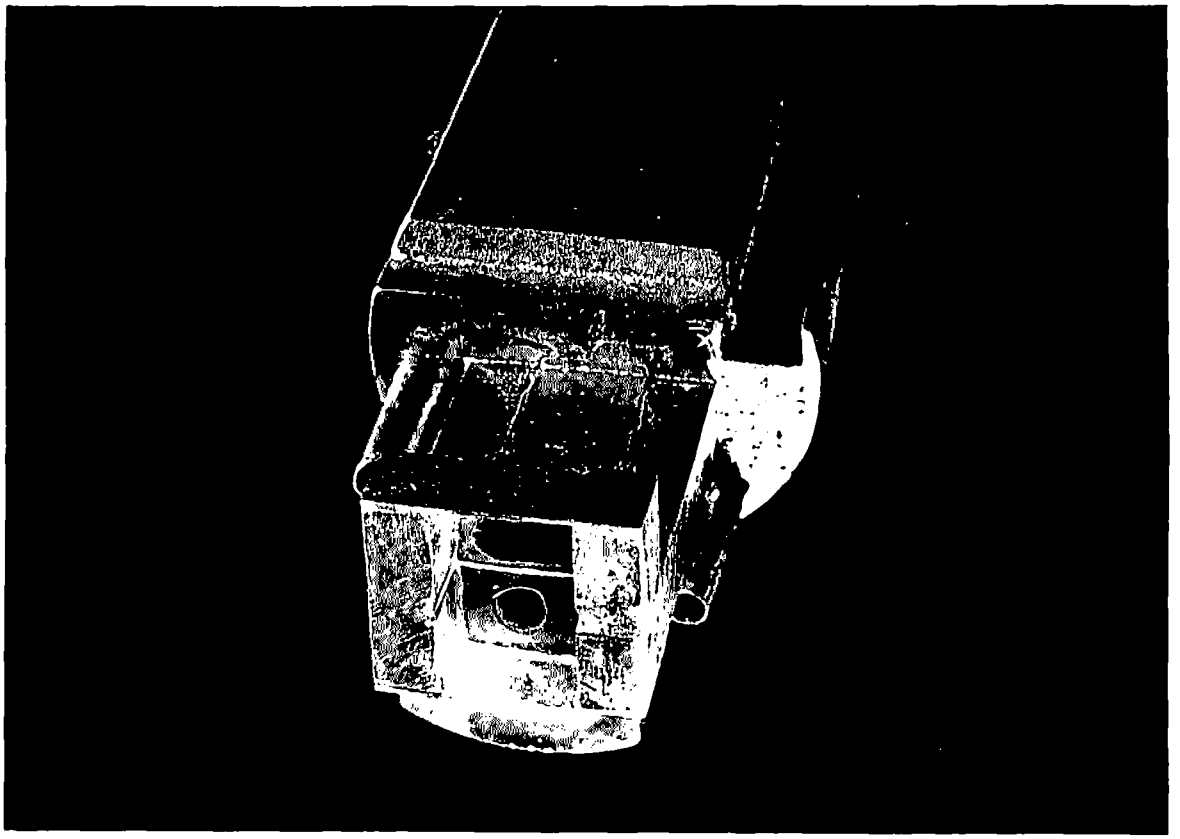

polarisation is maintained at its maximum value.

2.2 Dynamic polarisation of protons by the solid effect

The target material chosen was the crystal Lanthanum Magnesium Nitrate, $[La_2Mg_3(NO_3)_{12};(H_2O)_{24}]$ grown in a solution with ~1% of the lanthanum replaced by Nd^{144} or Nd^{146}. The method of dynamic polarisation was used, which will be described here, although it is now well known.[58][59]

Two spin systems are involved, the spins of the protons in the water of crystallisation and the spins of the Nd^{+++} ions distributed through the lattice. At helium temperatures the Nd^{+++} ions have an effective spin S= 1/2. The energy level diagram of the proton-'electron' system is shown in FIG. 3. where M, m are the magnetic quantum numbers of electron and proton respectively, and the levels are split by a static magnetic field H. The second column shows the zero order wave functions. If we now consider the weak dipolar interaction between the 'electron' and the proton separated by a distance r, the mixing parameter $|\alpha|$ is proportional to $1/r^3 H$ (with a further angular dependence). The 'electron' system is assumed to be tightly coupled to the temperature of the helium bath (T°) through the electron spin-lattice relaxation rate. The thermal equilibrium populations of the states are shown in column 4, and the proton polarisation P_l is given by:

$$(16) \qquad P_l = \frac{(N_2 + N_4) - (N_1 + N_3)}{(N_2 + N_4) + (N_1 + N_3)} = \tanh(\delta / 2kT)$$

where N_i is the population of state i, and k is the Boltzman constant.

For H = 10 Kg, $T = 1.3^\circ K$, $P \sim 7 \times 10^{-4}$

The Nd^{+++} ion in this lattice is anisotropic, with

$g_\perp = 2.70$. By using only even mass isotopes, neodymium hyperfine effects are eliminated. The electron spin-lattice mechanisms for this system have been studied[60] and allow rapid transitions between states 1-3 and 2-4 at 1.3°K.

The proton spin-lattice relaxation takes place via the dipolar interaction between the protons and the electron spins, which weakly allow transitions 1-4, 2-3. These transitions are weaker by a factor $\sim \alpha^2$ than 1-3, 2-4, and are of the same order as transitions induced by the dipolar interaction between 1-2, 3-4. Leakage transitions due to extraneous paramagnetic impurities give an extra transition rate between 1-2, 3-4. Thus it is important to use crystals as free as possible from paramagnetic impurities.

When K = 9.3 Kgauss, the transitions 1-3, 2-4 occur at 35.2 GHz with the crystal-axis oriented perpendicular to the magnetic field ($g_\perp$-orientation). The proton levels are split by $\pm$ 11 gauss, at a frequency of $\pm \nu_N = 39.4$ MHz. If the transition 2-3, (or 1-4) is saturated by microwave power, N_2 becomes equal to N_3 . The relatively fast electron spin-lattice relaxation maintains $\frac{N_1}{N_3} = \frac{N_2}{N_4} = e^{-\frac{\Delta}{KT}}$

(17) Hence: $P_2 = \tanh(\Delta / 2kT)$

This process may be more clearly understood if the effect of the microwave power is considered promoting the (electron + proton) system through a mutual spin reversal, from which state the electron relaxes relatively rapidly to its former orientation, leaving the proton in its new spin state. Each 'electron' (paramagnetic centre) has a sphere of influence of $\sim 10^3$ protons, and below $\sim 2^\circ$ K the electron spin-lattice relaxation rate is sufficiently

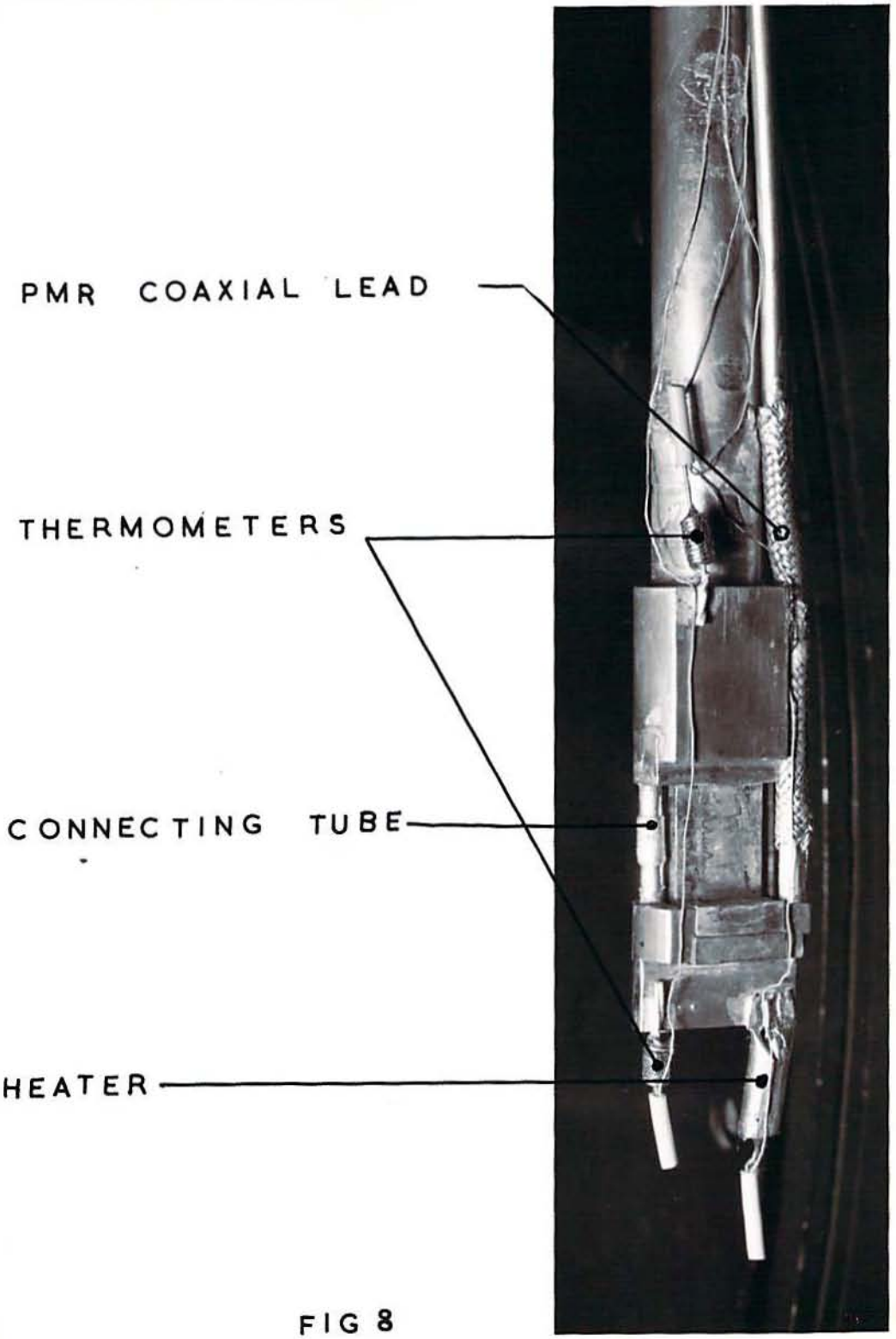

FIG 8

FIG. 4

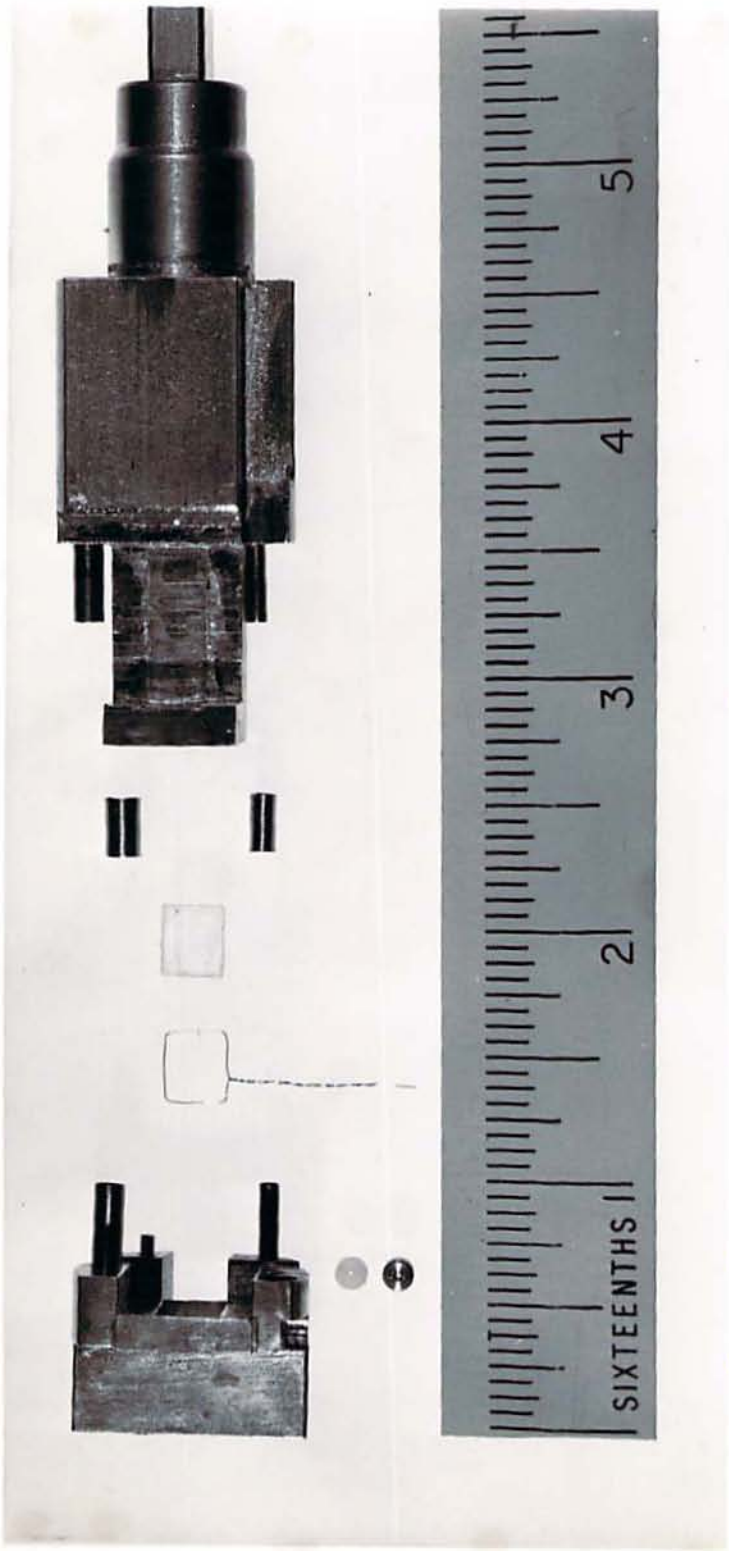

8mm WAVEGUIDE

IRIS COUPLING TO MICROWAVE CAVITY

SLEEVES FOR He^4 TUBES

L.M.N. CRYSTAL

P.M.R. PICKUP COIL

N4 R.F. CHOKE

HOLLOW LOWER PART OF CAVITY ASSEMBLY

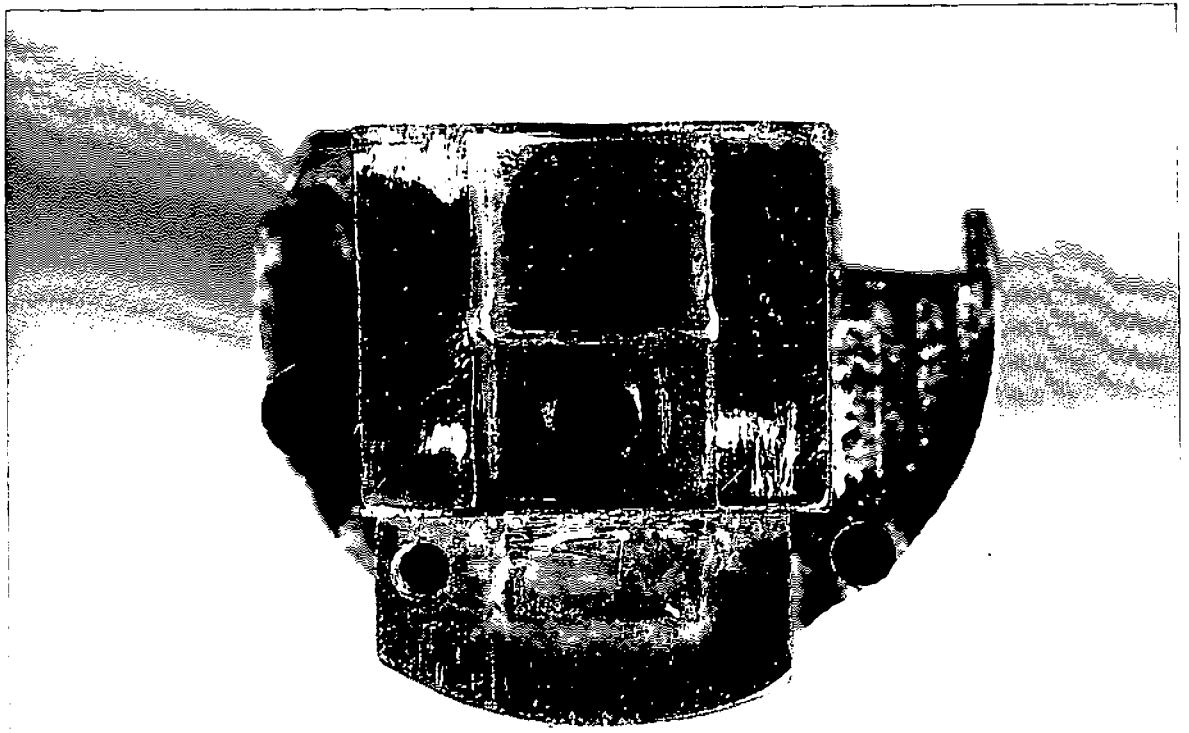

high that the relative populations of levels connected by allowed transitions are governed by the Boltzman distribution.

The ratio $\frac{\Delta}{\delta}$ is $\sim 10^3$, and thus large polarisations may be achieved. Experimentally enhancement ratios (P_2/P_1) of 400-500 have been obtained, corresponding to a polarising efficiency of 60-80%. The magnitude of the failure to reach 100% efficiency was found to depend on crystal purity and quality, and was thus likely to be due to the 'leakage transitions' mentioned earlier. It has been shown by Borghini[59] that the efficiency of the process may be improved by working at higher fields and frequencies. At 18 KG using 4mm microwaves an efficiency of >90% has recently been obtained.

2.3 Target apparatus[60]

The construction of the target cavity finally used is shown in FIGS. 2 and 4. The cavity shape was chosen to be resonant in the TE 012 mode, which gave a region of high oscillating field, suitable for use with a slab target of L.M.N. The static magnetic field of 9.3 Kg is shown, together with the distribution of the oscillating microwave field in FIG.5. The TE 012 mode can be seen to give a good field distribution and enabled us to use a single-mode cavity, thus making it possible to examine the electron paramagnetic resonance behaviour of the spin systems of the target crystal. This would not have been possible if a multi-mode cavity had been used. The microwave circuit is shown in FIG. 8. The klystron stabilisation method is that of George and Teaney[93]. The static magnetic field was provided by a Newport Instrument type D electromagnet, with 11.4 cm. or 12.7 cm. diameter pole tips, and a gap of 3.5 cm. As the line widths observed in electron paramagnetic resonance (E.P.R.)

FIG. 5

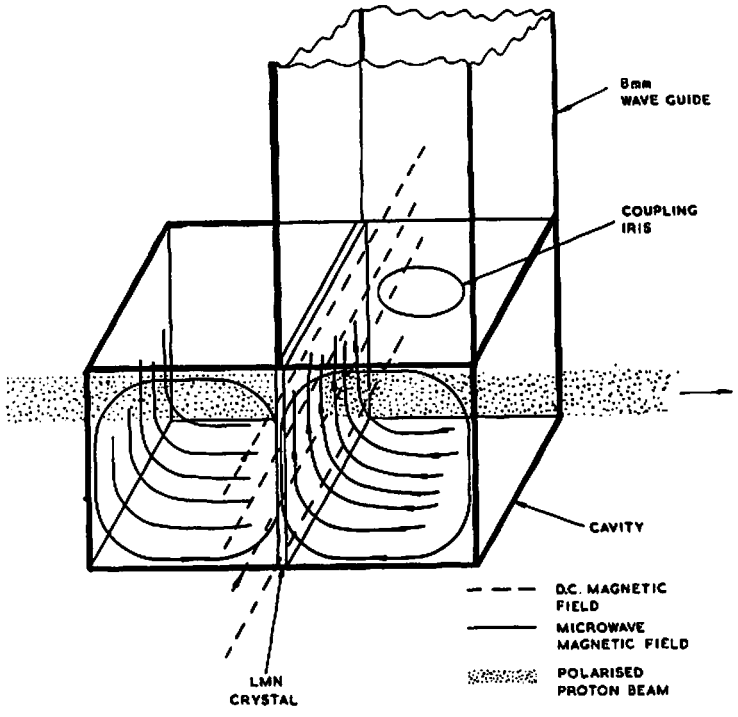

TARGET CAVITY RESONANT IN TE012 MODE AT 35·0 GHz

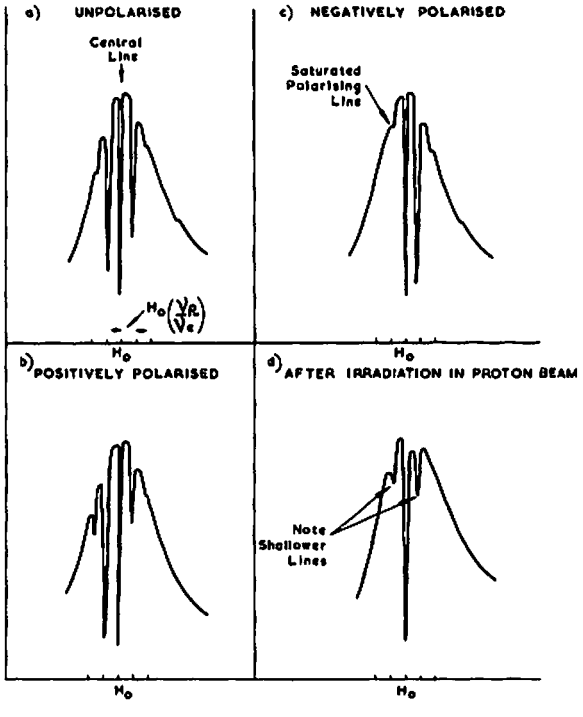

E.P.R. LINE SHAPES

FIG. 6

and in proton magnetic resonance were of the order of a few gauss, a field stability and uniformity of $\pm$ 2 parts in 10^5 was adequate. In the E.P.R. work the magnetic field was varied, and the microwave frequency held constant.

The proton magnetic resonance (P.M.R.) may be measured by applying a weak r.f. field at the resonance frequency of 39.4 MHz, which induces transitions between 1-2, 3-4 (see FIG.3). This field was produced by a single turn of wire wound round the crystal, and led out of the cavity through a microwave choke. The coupling of this coil to the protons in the target crystal was far from uniform.

During preliminary work, a three-turn pickup coil was used, which was more uniformly sensitive to the protons throughout the target crystal. A constant current Q-meter circuit[94] was used to detect the P.M.R. signal. As the static magnetic field was of necessity at a fixed value while polarising the target, the frequency of the r.f. was swept through the resonance. The electronics for this were designed and built by F.N.H.Robinson,[122] and a block diagram of the system is shown in FIG. 7.

A disadvantage of using a P.M.R. system on a polarised target is that the r.f. field induces extra transitions, thus reducing the polarisation of the crystal. The field was kept weak to minimise this effect, and as $\sim$ 8 millivolts across the coil was found to be the upper limit for linear relationship between this voltage and the strength of the resonance signal, this meant working with about 1-2mv of r.f. across the coil. This restriction, combined with the poor filling factor of the coil, gave rather a poor signal to noise ratio for the thermal equilibrium signal.The strength

FIG. 7

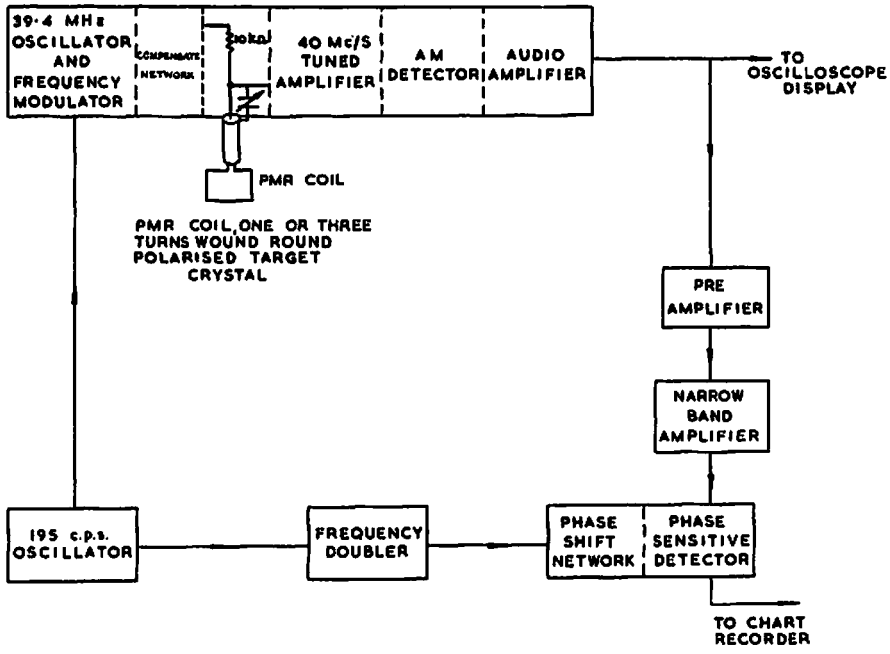

THE PMR SYSTEM

FIG. 7

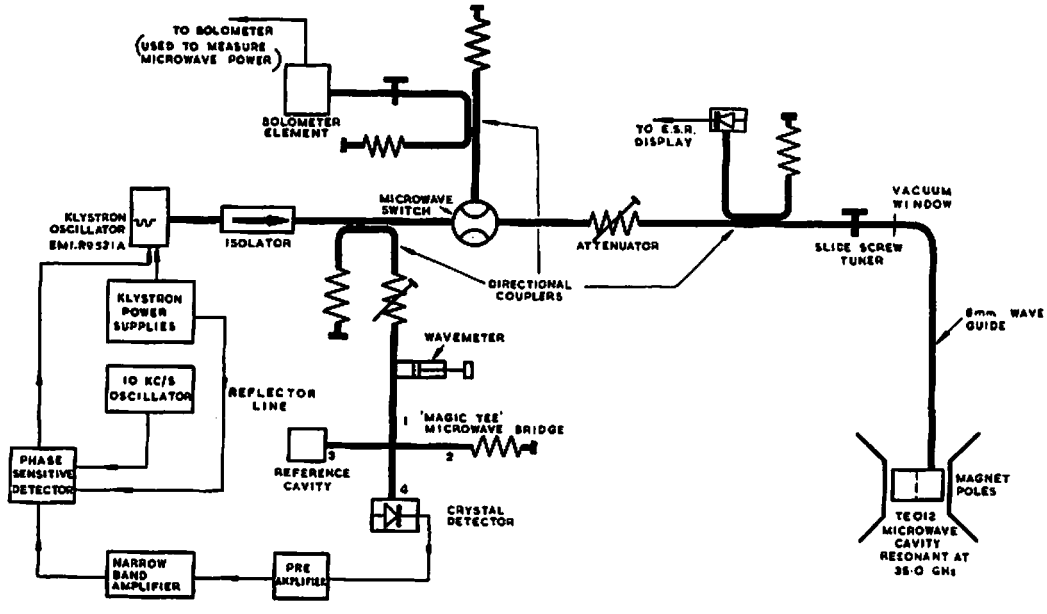

MICROWAVE SYSTEM FOR IRRADIATING THE LMN. CRYSTAL WITH 8MM MICROWAVES

FIG. 8

FIG. 8

of the resonance signal is proportional to the difference in population between the substates with m=1/2 (see FIG.3), a so is proportional to P. The enhancement ratio ε, is defined as the ratio of the signal strengths with microwave power on, to that at thermal equilibrium, and so (see 2.2)

(18) $$P = \varepsilon \tanh (\delta / 2kT)$$

Thus the P.M.R. signal may be used to measure the polarisation of the target. In the more recent targets, notably at CERN,[59] the P.M.R. method has been refined to give values of the polarisation to one or two percent, every few minutes. A Q-meter system capable of this precision is described by Petriček and Odenhal.[94]

For the present experiment the P.M.R. technique was limited in precision to $\sim 10\%$, due to the high signal to noise ratio. The Q-meter used was inherently non-linear, and asymmetric in its response to signals with large positive and negative polarisations. This could be accurately corrected for, and did not cause any difficulty. Neither of these effects affected the suitability of the method for continuously monitoring the polarisation of the target, by means of the large enhanced signal available when the target was polarised; and in preliminary experiments, where a proton beam was not used, the P.M.R. system gave a fairly accurate measurement of the polarisation achieved.

Unfortunately the constructional restrictions on the target cavity for the Cnn work restricted the P.M.R. pickup coil to a single turn round the edge of the crystal (FIG. 4). This arrangement gave a very non-uniform coupling of the coil to the protons throughout the crystal, and the P.M.R. signal could not give the correct average

polarisation of the target. The edge of the crystal was slightly shielded from the proton beam, as the crystal dimensions were 7x6.25x1mm, and a beam collimator 6.5x5.5mm was placed just upstream of the crystal. As the coil was very much more sensitive to the peripheral region, the damaging effect of the proton beam on the target polarisation was not correctly followed. In one proton scattering run, the initial polarisation of the target fell from 0.30 to 0.05 ± 0.025 (measured by nuclear scattering); the P.M.R. signal (normalised to the initial value of 0.30) fell from 0.30 to 0.20.

This led to the abandonment of this method of monitoring the target polarisation, and the level of the E.P.R. signal was used instead, both for setting up the initial polarisation of the target, and for continuous monitoring and maintenance of the polarisation at a maximum value throughout the experiment. The signal monitored was the reflected power from the cavity; when the cavity was on resonance the absorption of microwave power was readily detectable, and by sweeping the static magnetic field through the resonance an E.P.R. spectrum could be obtained. FIG. 6 shows spectra obtained in this way. The vertical scale of the diagram is highly non-linear, and thus the relatively very intense central Nd^{3+} line, corresponding to the sum of transitio 1-3, 2-4, (FIG.3) shows an absorption of power only slightly greater than its main satellites. The deep satellite lines spaced $\pm \frac{\delta}{\Delta} H_o$ on each side of the central line correspond to mutual 'electron'-proton spin-flips i.e. transitions 1-4, 2-3 and the shallow lines spaced at $\pm 2 \frac{\delta}{\Delta} H_o$ on either side of the central line correspond to transitions in which one

electron has reversed its spin direction together with two protons. On good traces the triple spin-flip transitions are visible. Brogden and Butterworth[96] have discussed these multipl spin-flip transitions, and their relative intensities, which were the first observed on a polarised target apparatus.

The liquid helium cryostat was of conventional vertical design. The radiation shield was a tube of 12 gauge silvered copper, cooled by a continuous flow of liquid nitrogen through a single turn of copper tubing soldered to the top of the shield. This used about 50-75 Litres of nitrogen a day, but saved space in the cryostat. The helium capacity was 2 Litres, which fell to 1 Litre while pumping down to 1.3°K. Under working conditions the target had to be refilled with helium at intervals of about 15 hours. The depth of the liquid helium was measured by using a simple dipstick, consisting of a carbon resistor mounted on the end of a stainless steel tube. The drop in resistance of the resistor when reaching the liquid/gas interface was easily identified over the temperature range 1.2°-4.4°K.

2.4 Cooling difficulties

The power input to the cavity when the target was polarised was of the order of 20mW. Not all of this power was dissipated in the target crystal; some was lost in the cavity walls. The problem remained that heat was produced in the crystal which had to be transferred to the helium bath. This cannot be solved by simply allowing helium into the cavit to surround the crystal, as detailed in 2.1. Close attention to this problem is necessary, as the maximum attainable polarisation in the crystal is reduced (see 2.2) by:

$\sim$ (T of crystal unheated + T of crystal when heated).

Also, if the temperature of the crystal is allowed to rise above about $\sim 3.5^{\circ}$ K, the relaxation rates change rapidly, lead to the loss of all polarisation.

The problem was approached in two stages: (1) the remo of heat generated in the target crystal by the incident proton beam and by the polarising microwave power (2) the transfer of the heat in the copper cavity assembly to the helium bath.

To solve problem (1), the thermal contact between the crystal and the cavity walls was improved by using a thin coating of Kel-F, a non-hydrogenous grease made by the Minnes Mining and Manufacturing Company. This has been successful at Saclay,[26)100)] where a larger area of contact can be used.[26)] However Kel-F did not prove good enough, and General Electric 7031 (a low temperature varnish) was used successfully. This varni was a hydrogenous material, and as the P.M.R. coil was firmly constrained to the outer edge of the crystal, in order to retain the high value of cavity Q($\sim$ 5000) obtained at helium temperatures, the P.M.R. signal was now swamped by these new unpolarisable protons. G.E. 7031 exhibited a microwave resonance on cooling down, and was also lossy to microwaves at room temperatures until firmly set. This took several hours, and these effects made the matching of the cavity with the iris a difficult procedure.

Although the use of G.E. 7031 finally removed any possibility of using P.M.R. to full advantage, other solid state methods of measuring the polarisation of the target exist[102)] which are not affected by the presence of the G.E. 7031. Some of these were tried, but with only limited success.

The heat transfer out of the copper depended on

FIG. 9

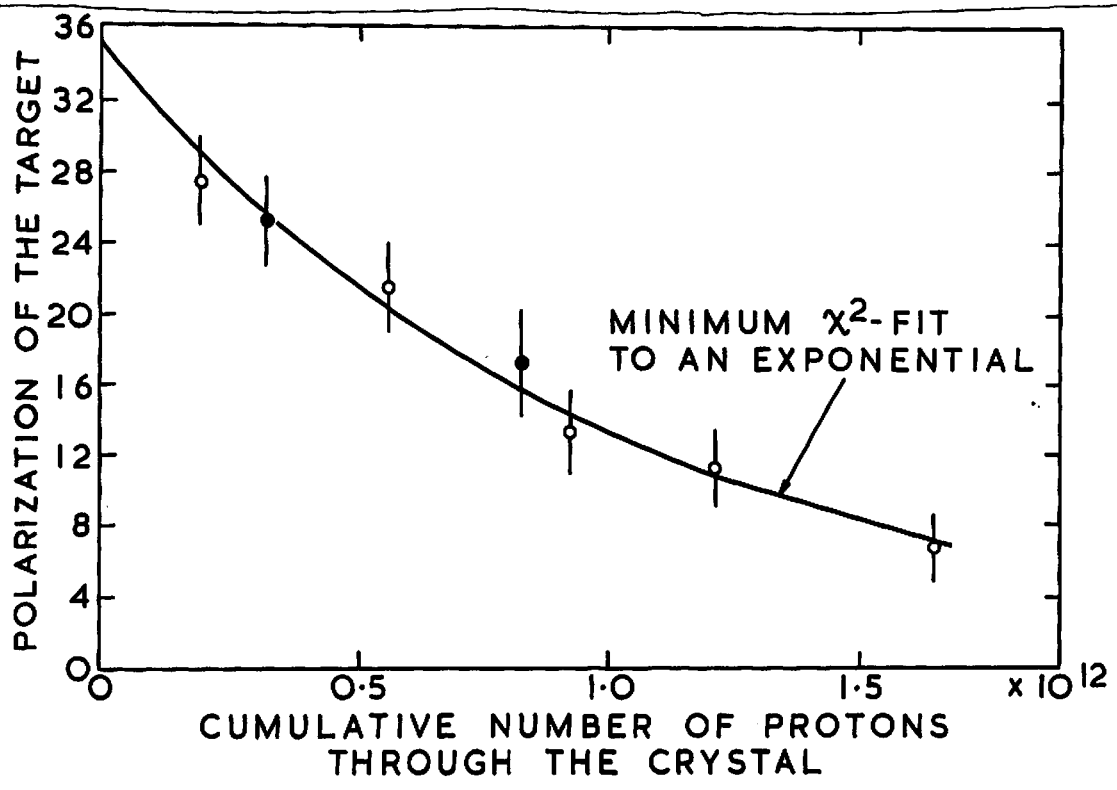

● measured with polarised beam
○ measured with unpolarised beam

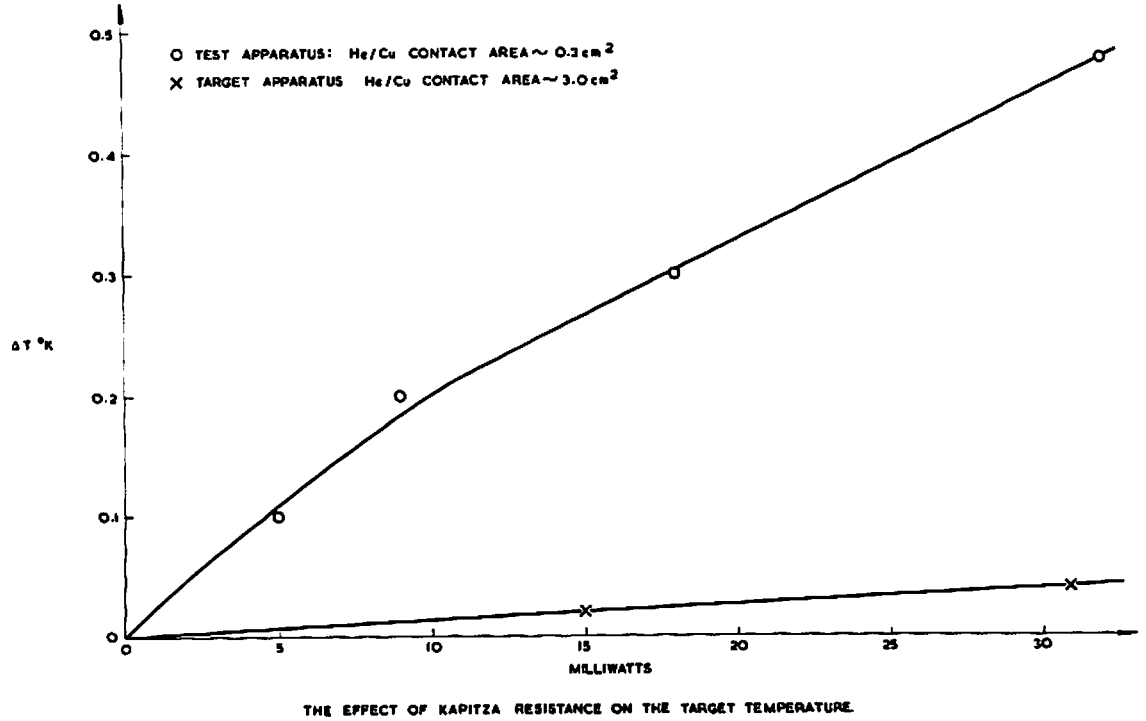

THE EFFECT OF KAPITZA RESISTANCE ON THE TARGET TEMPERATURE.

FIG. 10

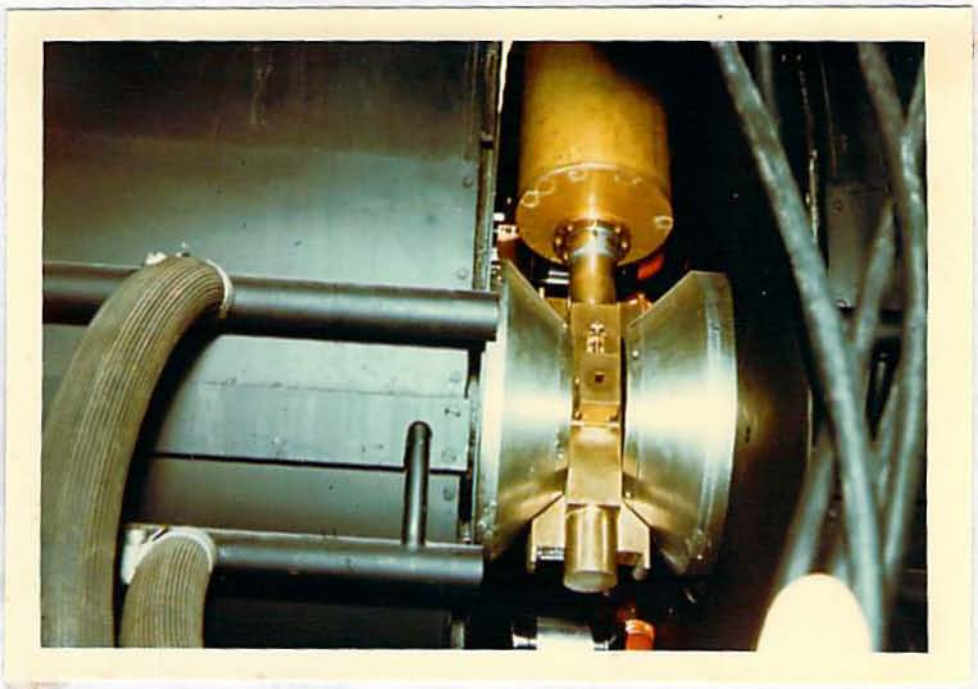

Polarised Proton Target: Final collimation and cryostat tail.

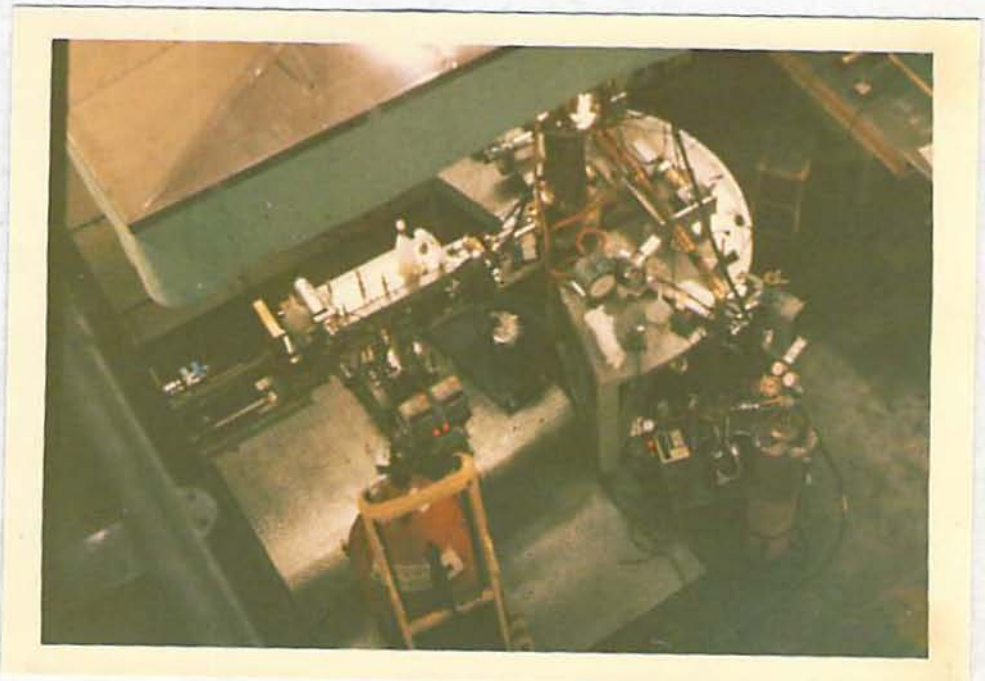

Apparatus used for ~98 Mev P-P Polarisation work.

the thermal conductivity of the copper used, and the heat transfer to the helium from the copper. The conductivity of copper at helium temperatures is strongly dependent on its purity and the amount of work hardening it has undergone. The latter was increased by every cooling down/warming up cycle. "Specpure" copper, supplied by Johnson Matthey Ltd., was used to obtain the highest possible values for thermal and electrical conductivity in the copper. The cavity assembly was designed to have a minimum path between the liquid helium and the cavity walls where the microwave power was dissipated. The lower part of the cavity was made hollow, and the two German silver connecting tubes (see FIGS.2,3) were reconnected each time a crystal was installed. The low melting point solder Cerroseal 35 (a 50:50 mixture of indium and tin) was used with repeated success in avoiding λ-leaks*.

The final stage in the heat transfer was from the copper assembly to the liquid helium. At low temperatures there is a thermal resistance due to an acoustic mis-match between the two materials. This is known as the Kapitza resistance, and has been investigated recently by Challis.[103]

A simple test apparatus was made up to check the magnitude of the Kapitza effect. The temperatures of the helium bath and of a test sample of copper were measured by carbon resistance thermometer, and ohmic heating was

* λ-leak is the term used to describe the losses that occur in liquid helium apparatus below the λ-point ($2.14^{\circ}K$); the helium becomes superfluid, and will leak in significant amounts from holes that are virtually undetectable by other means.

applied to the copper. The data are shown in FIG. 10 and are in fair agreement with Challis[103] results.

By comparison with Challis, it was determined that a factor ~ 10 reduction in the resistance could be achieved by using well annealed and etched "Specpure" copper, and by increasing the contact area between copper and helium from $\sim 0.3 cm^2$ to $\sim 3 cm^2$. This experiment was later repeated, and the results are shown (in FIG.10) to agree with this prediction. An order of magnitude for this effect is given by considering that, under working conditions of ~ 20 mW dissipation, the cavity assembly would be only $0.02^{\circ}K$ above the temperature of the helium bath.

2.5 Radiation damage effects

When the apparatus was used in a proton beam, and the polarisation of the target measured at intervals by the nuclear scattering method described in 2.1, the maximum available polarisation was found to decrease. Approximately half of the initial (unirradiated) polarisation was lost when $\sim 10^{12}$ Mev had been deposited in the crystal by the ionisation produced by $\sim 10^{12}$ protons. Several two-parameter fits to this decay were tried, and an exponential form adopted (FIG.9): the data was not good enough to justify a three-parameter fit, and the exponential was consistently better than a linear form. The damaged crystals annealed out slowly when warmed to room temperature. One crystal recovered to two-thirds the initial polarisation (from about one quarter) in ten days.

This phenomenon complicated the Cnn data analysis considerably, and as it was necessary to assume a definite analytic form for the polarisation falloff with increasing

irradiation dose, extra data on the effect was collected by examining the behaviour of the various solid state parameters accessible to our apparatus, as a function of cumulative irradiation.

The target used for this study was cut from a single crystal of LMN doped with Nd^{146}. The Nd:La ratio in this crystal was found to be 0.10 ± 0.05 % by means of X-ray fluorescence. The crystal dimensions were 7mm × 6.25mm × 1mm, and it was mounted in the cavity (as shown in FIG.2) to utilise $g_{\perp} = 2.70$ for the Nd ions. Throughout this run the temperature of the helium bath was held at 1.32° K, and the microwave frequency at 35.2 GHz.

The E.P.R. spectrum was examined over the range 0-14KG at intervals in the irradiation, and the only changes observed in the E.P.R. spectrum were (1) a gradual decrease in the depths of the first forbidden satellites of the Nd line at 9.3 KG [FIG.6(d)], and (2) the growth of a resonance line at ~ 12 KG.

This resonance line had an approximately Gaussian form, with a width between slope extrema of 20 ± 3 gauss. Fine structure due to N^{14} nuclei could be seen in good resolution consistent with the observations of Bleaney et al[104] on L.M.N. containing radioactive isotopes. To within experimental error, the width did not increase with radiation dose, nor did it vary with temperature in the range of 1.32°-4.2°K. This resonance was due to paramagnetic damage centres associated with the observed falloff of polarisation.

The relaxation of the proton polarisation was measured by observing the level of the pumping satellite of the Nd^{3+} resonance at intervals of about a minute from switching off

FIG. 11

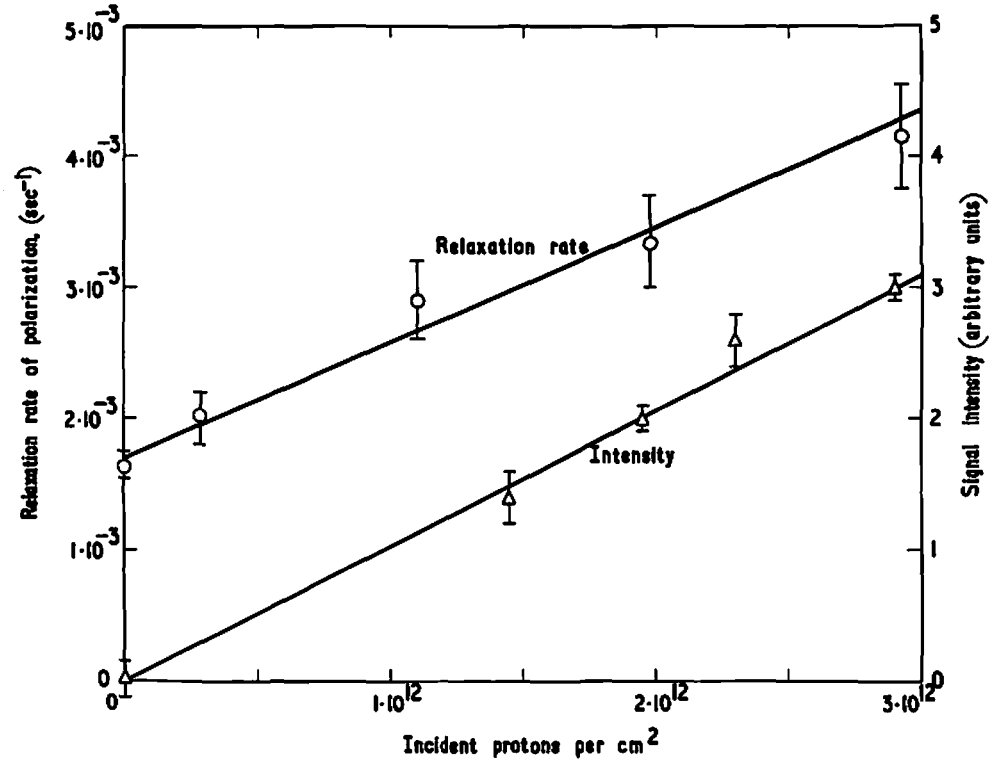
Relaxation rate of polarization, (sec⁻¹)
Signal intensity (arbitrary units)
Relaxation rate
Intensity
Incident protons per cm²
5·10⁻³
4·10⁻³
3·10⁻³
2·10⁻³
1·10⁻³
0
1·10¹²
2·10¹²
3·10¹²
5
4
3
2
1

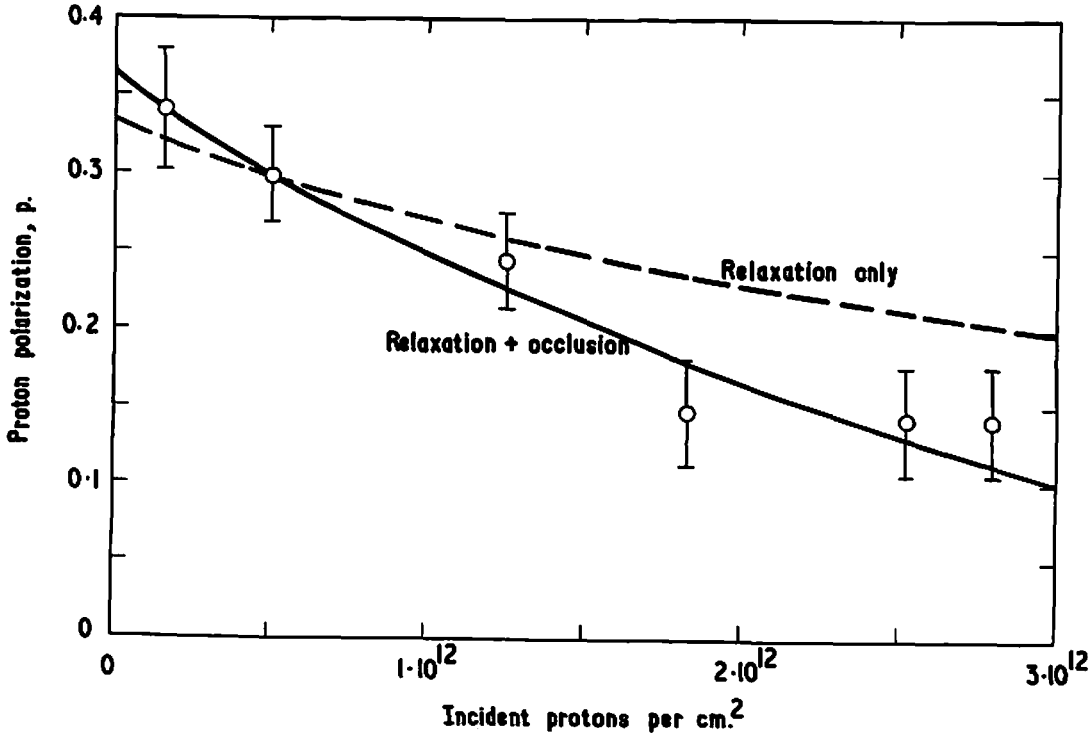
Proton polarization, p.
Relaxation only
Relaxation + occlusion
Incident protons per cm.²
0.4
0.3
0.2
0·1
0
1·10¹²
2·10¹²
3·10¹²

FIG. 12

the microwave pumping power. This method gave results that agreed to better than 10% with the direct observation of the proton relaxation by the P.M.R. output. For all these observations the proton relaxation rate could be characterised by a single exponential rate Rp. Within experimental error, Rp increases linearly with radiation dose. FIG.11 shows these data, and also the variation in the damage centre signal intensity, as a function of radiation dose. The proton energy was 146 Mev, and the thickness of the crystal 1mm, thus the ionisation loss by one proton passing through the crystal was 1 Mev.[105] The average number of damage centres produced per proton was obtained by using a reference signal produced by introducing 400 μ gm of diphenyl-picryl-hydrazyl (DPPH) into the cavity. The value obtained from the comparison of the reference signal and the damage centre signal was $(1.00\pm0.35)10^{6}$ damage centres per proton, thus the average energy needed to produce one damage centre was 1.0 ± 0.4 ev. The g-value of the damage centre resonance was determined to be $2.002\pm.002$, by reference to the g-value of the D.P.P.H.[106] This is sufficiently close to the value of $2.005\pm.002$ found by Bleaney et al[104] to support a common identity. Bleaney et al attribute their line to neutral NO_2 ions. Whatever the identity of the centres responsible for the line, there seems little doubt that they are responsible for the observed decay of the polarisation.

This value of 1ev/damage centre is rather low, and could cause absorption in the optical and near-optical regions. This was investigated, and the following results obtained:

(1) indications of an absorption edge at~ 5ev in the ultraviolet

(2) a general increase in the absorption at the upper end of

the optical band, with no discernible structure.

The deductions from the E.P.R. data are given in ref.95, and will not be repeated in detail here. The decay of the polarisation can be described by two components. The first is due to the increase in Rp, and the second is due to the weak magnetic field of the centres themselves. Liefson and Jeffries[107] have shown that, under rather general conditions, the maximum polarisation attainable is given by:

$$P \simeq \frac{\delta/2}{1 + A\,Rp} \qquad (19)$$

where δ is the Boltzman factor in FIG.3 relating the populations of the Zeeman levels of the Nd ions at thermal equilibrium, and A is constant for a given crystal. In FIG.12. the dotted line shows this form fitted to the polarisation data, using the measured (FIG.10) and calculated values of δ ,Rp. The fitted curve does not represent the data very well, and the disagreement cannot be reduced by varying A.

The second component in the reduction of polarisation is the shift in proton resonance frequency due to the dipolar fields of the damage centres. These fields could reduce the polarisation by inhibiting the transfer of polarisation from the Nd ions to the protons. A simple model may be used to calculate this effect. If we assume that each damage centre completely occludes all the protons within a sphere of radius r, and N is the average density of damage centres in the crystal, then (19) becomes:

$$P \simeq \frac{\delta(1 - 4\pi r^3 N/3)}{2(1 + A\,Rp)} \qquad (20)$$

The values of N, Rp are given in FIG.10, and the constants δ, A can be varied to fit the data. The bold line

in FIG.11 is the result of such a fit, where δ = 16 Å, corresponding to $\sim$ 700 protons being occluded by each centre. This fit is much better than that given by (19) and is good enough to indicate that the decay in P may be attributed entirely to the combined effects of relaxation and occlusion. The effects of overlapping spheres of occlusion are considered in ref. 97, and the conclusion drawn that such effects were detectable in the data.

As we have seen that both N and Rp can be represented by linear forms, we may write: N=x , Rp = b+cx where x is the cumulative number of $\sim$ 146 Mev protons. (20) then becomes:

$$P \simeq \frac{\delta(1 - 4\pi r^3 ax/3)}{2(1 + Ab + Acx)} \qquad (21)$$

which may be represented by P=Aexp(Bx), accurate to second order.

These investigations may also be used to compare various theories put forward by De Gennes[108], Schmugge[109] and Jeffries, and Khutsishvili[110] to describe the process by which the polarising energy is diffused through the lattice. All the models predict a constant value for Rp/N, and the measured and calculated values are compared:

Theoretical and measured values of Rp/N in sec^{-1} cm^3

Measured	0.83×10^{-22}
Khutsishvili's model with d=16 Å	1.2×10^{-22}
Schmugge and Jeffries' model	59×10^{-22}
De Gennes' model	330×10^{-22}

It is relevant to note that Ramakrishna and Robinson[111] also found Khutsishvili's model to offer the best explanation of a transient effect observed in the relaxation of protons in LMN

by Nd^{3+} ions.

There is very little information available on radiation damage effects in LMN targets: the Saclay group[24] find that a similar amount of ionisation energy deposited in the crystal is needed to reduce the polarisation of a crystal to half its initial value.

Laboratory	Energy	Protons/cm^2 for 50% falloff	Mev/cm^3
Harwell	143 Mev	2.8×10^{12}	2.8×10^{13}
Saclay[24,108]	26 Mev	1.25×10^{12}	3.8×10^{13}

Both these figures are subject to variations of ~30%, due to the variability in the falloff of polarisation for different crystals, and indeed a comparison of the fluxes of particles required to reduce the polarisation by half shows almost as good agreement.

Hardy and Shapiro[114] at Saclay have examined the behaviour of Rp when a crystal of LMN was irradiated with electrons from Strontium-90 and Yttrium-90 sources. They observed an increase in relaxation rate with increasing irradiation, and also observed the annealing effect mentioned earlier.

The results reported here shed considerable light on the radiation damage problem encountered in LMN targets used with medium energy charged particle beams at Harwell and Saclay.

2.6 Conclusion

The data gathered here will be useful to those planning low energy polarised target experiments, and may help them to minimise the effects of target damage in this work. The data has also proved to be of interest to solid state physicists, as it provides tests of the various theories concerning dilute paramagnetic centres in solids, and spin diffusion. For the proton-proton work described in the next chapter, the E.P.R.

data lend support to the assumption of a smooth non-linear decay curve for the polarisation as a function of the incident proton flux.

III Spin correlation measurements: 73-143 Mev

3.1 Apparatus

The technique adopted for these measurements of the spin-correlation parameter Cnn requires an incident polarised proton beam, and a polarised proton target. The polarised proton target used in this work has been fully described in the previous chapter, and only the further details of collimation, counting arrangements, and monitoring will be considered here.

Both the polarised and the unpolarised proton beams of the Harwell 280 cm synchrocyclotron* were used. These beams are extracted by scattering from internal targets of aluminium and tungsten respectively, and pass through a magnetic channel. Although the two beams have slightly different energies, giving $\sim$143 and $\sim$146 Mev at the centre of the polarised target crystal, the extraction system is so engineered that the two beams have closely similar paths. The details of the beam handling system and the general arrangement of the experimental apparatus is shown in FIG.13.

A circular collimator, 2.54 cm in diameter, was placed at the beam exit from the cyclotron vacuum tank. The beam then passed through a 3m solenoid. A current of up to $\pm$ 1600 Amps

*In future this accelerator will be referred to as the cyclotron

FIG. 13

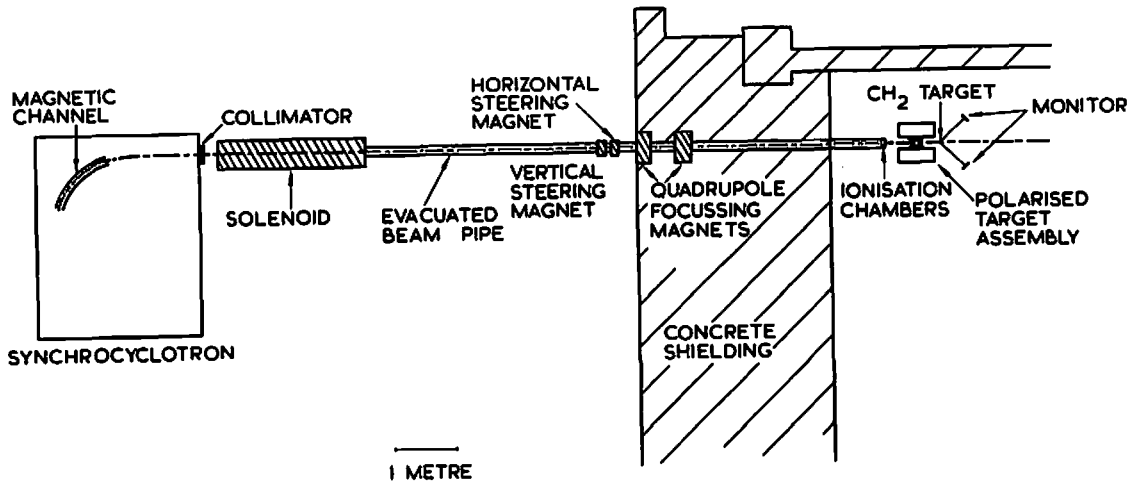

FIG.13 EXPERIMENTAL LAYOUT

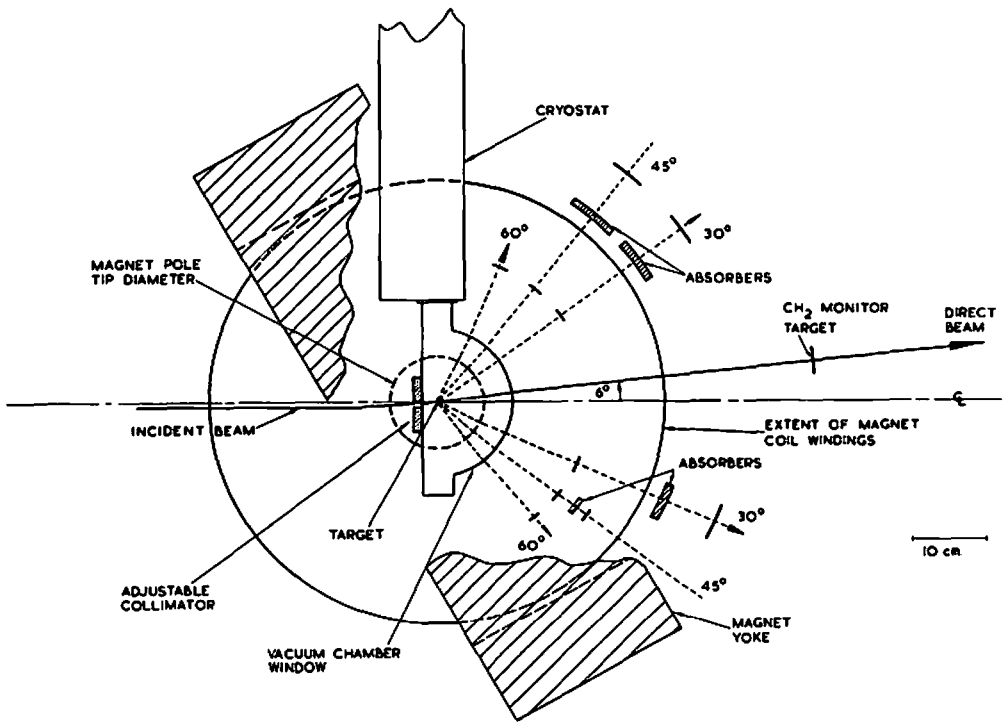

NOTE: TARGET AND BEAM POLARISATIONS ARE NORMAL TO THE SCATTERING PLANE

FIG. 14

FIG. 14

could be used in this solenoid to precess the spin direction of the protons in the polarised beam. This spin precession is described in detail in Appendix 8.9.

The polarisation vector of the beam extracted from the cyclotron lay in the vertical plane, so it was necessary to use the solenoid to precess this polarisation into the horizontal plane. This was required, as the polarised target was designed to give polarisation in the horizontal plane. The requirements of this Cnn experiment are (1) that the polarisation of both target and incident beam be coplanar, and (2) the scattering cross-section be then measured in the plane which is normal to the polarisation vectors of beam and target.

In FIG. 15 the left-to-right asymmetry measured by scattering the beam from a thick carbon target is shown as a function of solenoid current. The two analysing telescopes were in the horizontal plane, and thus the asymmetry measured was due only to the vertical component of the beam polarisation, as it was precessed around the beam axis. As the asymmetry passed accurately through zero at $\pm$ 750A, these two current settings gave the beams required for the Cnn measurement.

A pair of quadrupole magnets was used to focus the beam, and a pair of steering magnets used to alter the beam direction. A pair of differential ionisation chambers[116] was used to fix the beam lines through a known point just upstream of the target assembly, and to maintain the beam spot accurately in this position.

A defining collimator, 0.65 x 0.55 cm, was fixed to the target assembly. This was slightly smaller than the target

FIG. 15

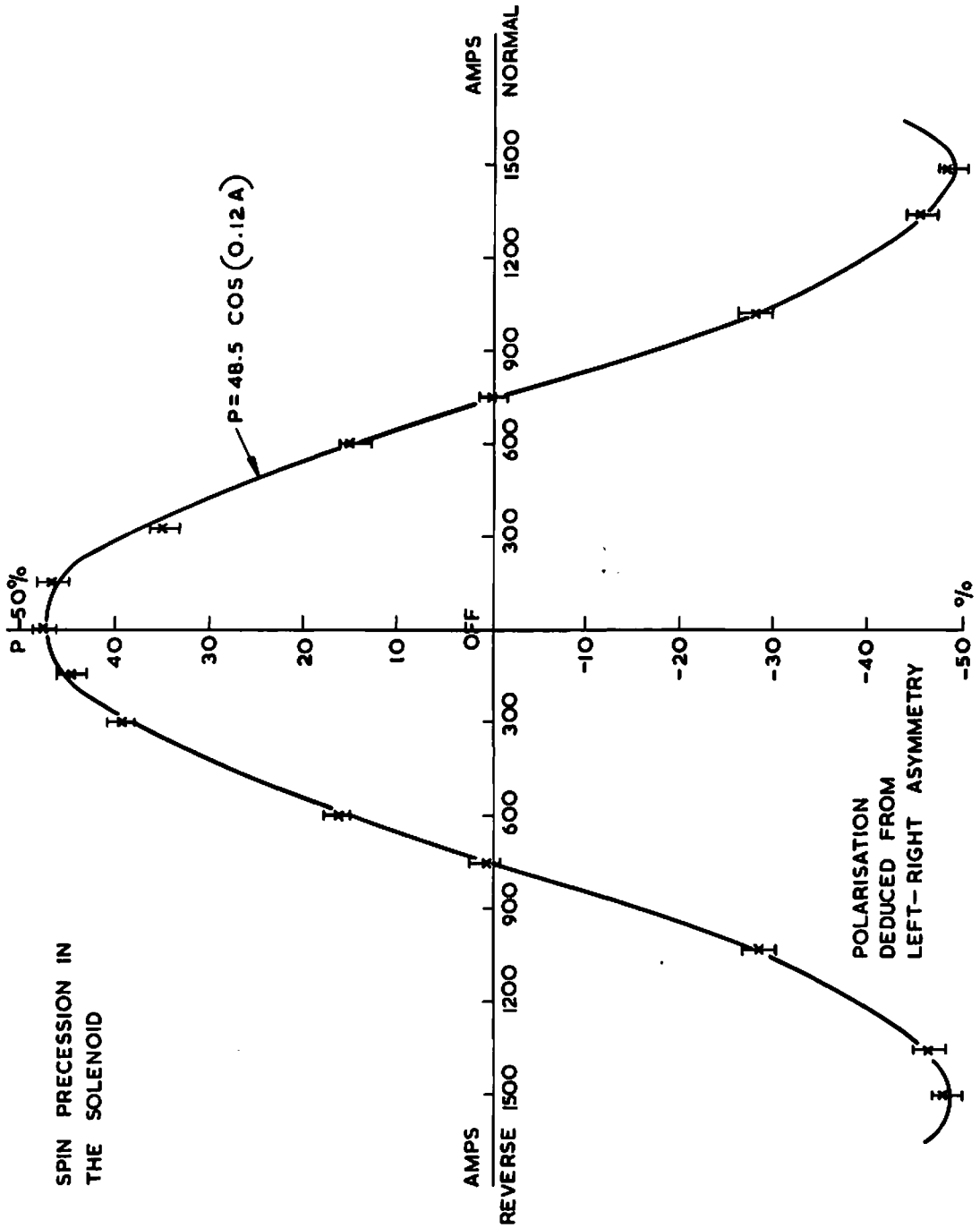
SPIN PRECESSION IN
THE SOLENOID
P=48.5 COS (0.12 A)
P 50%
40
30
20
10
OFF
-10
-20
-30
-40
-50
%
AMPS
REVERSE 1500 1200 900 600 300
AMPS
300 600 900 1200 1500 NORMAL
POLARISATION
DEDUCED FROM
LEFT-RIGHT ASYMMETRY

crystal of LMN, which was 0.70 × 0.625 × 0.10 cm. The focussing of the beam was determined with the aid of a two dimensional sonic spark chamber system[117], which was used to build up a visual record of the shape of the beam spot in a storage oscilloscope. This apparatus simplified the focussing procedure considerably, and it was found possible to get at least 60 % of the beam through the defining collimator.

As the solenoid had a slight focussing effect on the beam, it was necessary to align the solenoid accurately along the beam axis. This was in order to avoid beam shifts when the direction of polarisation of the incident beam was reversed by altering the current flowing in the solenoid.

The material of the target assembly through which the beam passed was one thickness of 0.05 mm Beryllium copper, and two thicknesses of 0.05 mm copper. The exit vacuum window was of 0.12 mm DuPont Mylar .

The beam monitor was composed of two counters set at $\pm 44^{\circ}$ to the beam in the horizontal plane through the beam. These counters detected the scattered and recoil protons from 90° c of m p-p scattering events in a 0.6 cm sheet of polyethylene (CH2) in the beam. The energy resolution was improved by placing 2.08 gm of aluminium absorber in front of each counter. This monitor was independent of the polarisation of the beam, being in the plane of polarisation, and insensitive to the beam spot shape or its position. Double and random coincidences were recorded simultaneously.

The beam then passed into a thick NE102A scintillation counter, which was used to assist in the setting up of the long duty cycle facility[118] of the cyclotron.

FIG. 16

TABLE 1

Dimensions and radial positions for the Cnn counter array.

Angle	Height	Width	Radius
Front Counters			
30 up	1.47 cm	2.05	21.5
45 up	1.52	2.87	21.0
60 up	1.70	3.52	21.5

The above counters define a $\pm 2^{\circ}$ laboratory acceptance angle in the vertical plane.

30 down	2.08	2.64	21.4
45 down	2.02	3.73	21.2
60 down	1.75	4.57	21.4
Back Counters			
30 up	4.55	5.28	41.3
45 up	4.63	7.03	41.3
30 down	5.00	6.10	41.3
45 down	2.75	4.85	26.3

As the static field of the magnet has a maximum value of 9.3 Kgauss, the paths of the protons are significantly curved. The plane of the monitor counter is inclined to take this into account. The computations to decide the position and size of the data-collecting counters are more complicated.

The paths of protons were computed in a step-by-step calculation, using the measured variation of the fringe magnetic field. This is considered in more detail in Appendix 8.1. The counting telescopes are set out to detect the scattered and recoil protons from events in the LMN for angles of 90° and $\pm 61.8^{\circ}$ centre of mass. The layout of the counters is shown in diagram form as FIG.14, and in a photograph as FIG.16. The defining counter sizes were computed for a 4° (lab) acceptance angle in the vertical plane, and for 5.7° in the horizontal plane. The positions, sizes, and setting angles are tabulated in (TABLE 1, TABLE 2).

As can be seen from the figure of Appendix 8.1, it is necessary to shield the counters from the magnetic field. This was done by using perspex light guides to bring the light to the photomultiplier tubes. The tubes were double shielded by steel, and singly by mu-metal: the counter assemblies were mounted on rails fixed to the magnet yoke (FIG. 16).

Copper absorbers were placed as shown in FIG. 14 to reduce the coincidence counting rates from inelastic scattering events from the nuclei of the target. This was most important, as only 3% by weight of the LMN crystal was hydrogen. As a percentage of the hydrogen counting rates, the background was reduced from 30% to 2% by these means. The calculated angular positions for the counters were checked experimentally

Angular Positioning of the Cnn counters

Counter	Relativistic Angle* (Degrees)	Static Field* Effect (Degrees)	Beam Lie* (Degrees)	Angles set on magnet: 143 Mev (Degrees)	98 Mev (Degrees)	74 Mev (Degrees)
60 up	58.2	4.55	-2.1	60.6	-	-
45 up front	44.0	3.02	-2.1	44.9	46.5	48.0
45 up back	44.0	3.58	-2.1	45.5	47.1	48.7
30 up front	30.0	2.48	-2.1	30.4	-	-
30 up back	30.0	2.91	-2.1	30.8	-	-
30 down front	-30.0	2.48	-2.1	-29.6	-	-
30 down back	-30.0	2.91	-2.1	-29.3	-	-
45 down front	-44.0	3.03	-2.1	-43.1	-42.0	-41.1
45 down back	-44.0	3.25	-2.1	-42.9	-41.7	-40.8
60 down	-58.2	4.55	-2.1	-45.8	-	-

*All data correct for 143 Mev beam: the changes for the lower energies are included in the last two columns.

TABLE 2

FIG. 17

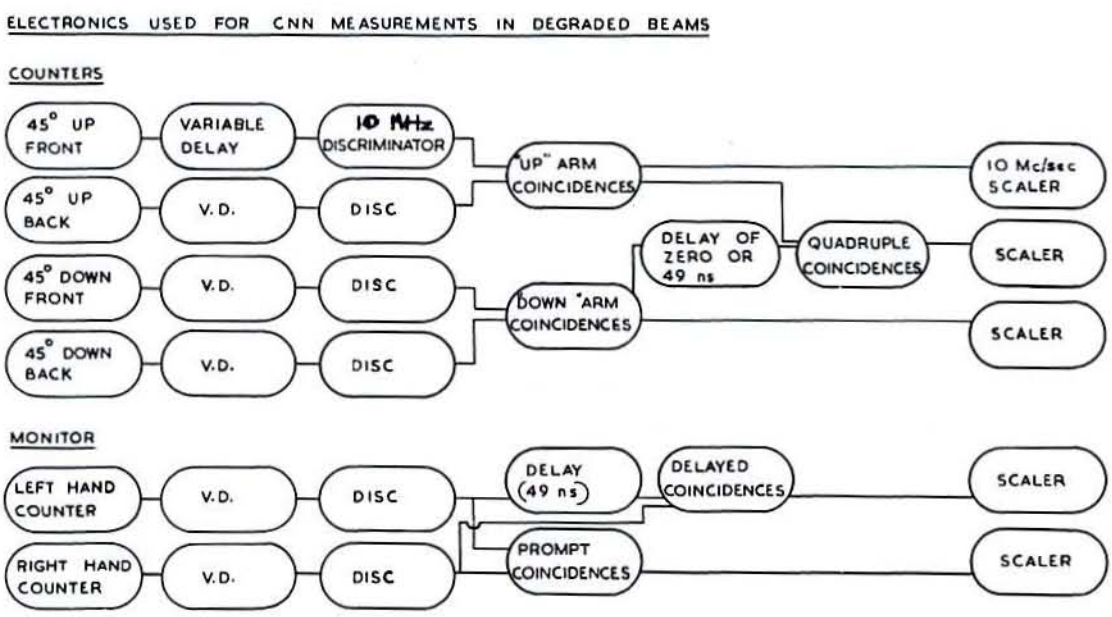
ELECTRONICS USED FOR CNN MEASUREMENTS IN DEGRADED BEAMS
COUNTERS
45° UP FRONT
VARIABLE DELAY
10 MHz DISCRIMINATOR
45° UP BACK
V.D.
DISC
45° DOWN FRONT
V.D.
DISC
45° DOWN BACK
V.D.
DISC
"UP" ARM COINCIDENCES
"DOWN" ARM COINCIDENCES
DELAY OF ZERO OR 49 ns
QUADRUPLE COINCIDENCES
10 Mc/sec SCALER
SCALER
SCALER
MONITOR
LEFT HAND COUNTER
V.D.
DISC
RIGHT HAND COUNTER
V.D.
DISC
DELAY (49 ns)
PROMPT COINCIDENCES
DELAYED COINCIDENCES
SCALER
SCALER

by moving the upper counters and plotting the correlation curves given by the coincidence count rates in the various telescopes. The final values for the absorbers were 1 gm below the knee of each curve. For the 143 Mev work, 9.55 gm/cm^2 Cu were used in the 30° up and down front counters, and 3.50 in both 45° counters.

The unpolarised beam ($\sim 2 \times 10^8$ p.p.s. at 147 Mev) required the use of a long duty cycle ~ 20 %[118], to avoid counting rate effects in the photomultipliers and the counting electronics. The random coincidence rates were then negligible. The unpolarised beam ($\sim 10^7$ p.p.s. at 144 Mev and polarisation $.472 \pm 0.004$[57]) was of too low an intensity to allow the use of "Cee", as this reduces the intensity available by at least a half. For the same reason, counting rate effects were negligible, and random coincidences only ~ 1% of the hydrogen rates. The coincidence counting rates in the three telescopes were all about 5 c.p.s. for the unpolarised beam, and about 1 cps for the polarised beam.

The counting electronics were very simple (as shown in FIG. 17). The photomultiplier outputs were taken directly to 10 MHz discriminators, the outputs of which were fed to the triple (30° U, 30° D) and quadruple (45°) coincidence circuits. Each coincidence circuit fed both a 10 MHz and a 1 MHz scalar, to enable deadtime corrections to be made if necessary (< 0.02 %).

3.2 Experimental work at 143 Mev.

The effects of radiation damage on the polarisation of the first L.M.N. crystal used meant that the desired precision ($\pm$ .05) on Cnn (90°) could not be attained by using only one target crystal. The data taking was thus arranged to take

full advantage of the high (~35%) initial polarisations obtainable from the LMN crystals.

Rewriting equation (9) of 1.3 in a fuller form including ϕ explicitly:

(23) $$I = I_0[1 + (P_I + P_T)P\cos\phi + P_I P_T C_{nn} \cos^2\phi]$$

where $\phi = 0, \pi$ for + or - directions of polarisation of the incident proton beam.

By considering equation (23), we see that information on the target polarisation can be obtained from an unpolarised beam incident on a polarised target, and also from a polarised beam incident on a polarised target. In the second case it is necessary to sum the counts recorded for incident beams polarised in both + and - directions.

The possible measurements from which a Cnn determination can be derived are:

(a) Target unpolarised, Beam unpolarised. $P_I = 0$: $P_T = 0$: useful datum: Target polarisation.

(b) Target polarised, Beam unpolarised. $P_I = 0$: $P_T = -$: useful datum: Target polarisation.

(c) Target polarised, Beam polarised. $P_I = \pm$: $P_T = -$: useful datum: Cnn and target-P_T- data.

(d) Target unpolarised, Beam polarised. $P_I = \pm$: $P_T = 0$: useful datum: p-p polarisation data.

(e) Dummy target (no H_1), Beam unpolarised. $P_I = \pm$: $P_T = N/A$: useful datum: unpolarised background.

(f) Dummy target (no H_1), Beam polarised. $P_I = 0$: $P_T = N/A$: useful datum: polarised background.

Not all of these are required if the target polarisation is estimated from the sum of $P_I = +$ and $P_I = -$ runs of type (c); in FIG.9 the points plotted as solid discs have been

FIG. 18

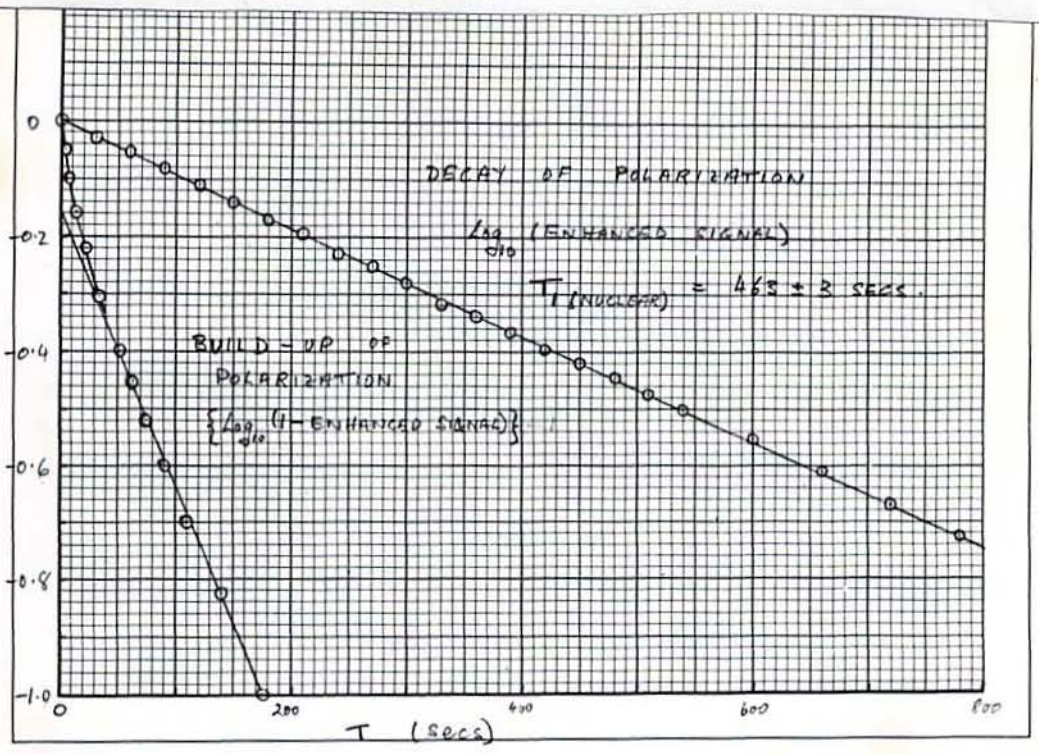

P.M.R. measurements of polarisation build up and decay

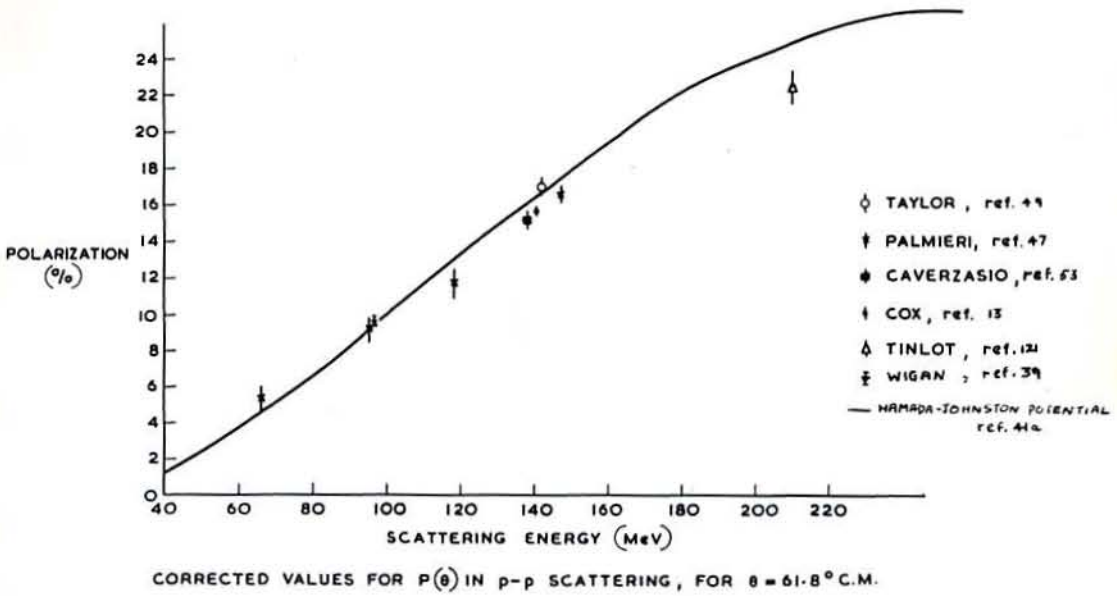

CORRECTED VALUES FOR P(θ) IN p-p SCATTERING, FOR θ = 61·8° C.M.

Polarisation values as renormalised by Jarvis and Rose

FIG. 19

calculated in this way, and the data used to calculate these points also contains information on Cnn (61.8°) at 143.2 Mev. The points derived in this way are of poor precision, as can be seen in FIG.9. The unpolarised beam is $\sim$ x10 more intense than the polarised beam and the open circle points obtained using the unpolarised beam take only about 1/2 hour to get; as compared with $\sim$ 5 hours for the solid circle points.

This time factor is important, as the target had to be refilled with helium every 15 hours, and then pumped down to 1.3° K once more. This procedure took at least two hours, during which only unpolarised target information could be obtained. The polarisation and depolarisation of the target was also time consuming. In FIG.18 the build up and decay of polarisation, as monitored by P.M.R., are shown for a good crystal ($T_{1W} \sim$ 500 seconds for polarisation decay). These data were obtained using an early version of the target, with a P.M.R. coil effectively coupled to the target proton spins. Either polarising or depolarising the target took about 20 minutes to carry out. Depolarisation could be carried out more rapidly by altering the static magnetic field to shift the pumping frequency to the anti-polarity line, and changing the static field once more when $\sim$ zero polarisation had been reached. However it is still necessary to wait several minutes before assuming that the target has reached an unpolarised state, as the polarisation fluctuates about zero before settling down to the thermal equilibrium value[111]. Also, in practice, it was difficult to ensure that the static magnetic field was altered at the instant P_{π} passed through zero.

In view of these time restrictions, and the requirement to measure $P_{\pi} P_{T} Cnn(\theta)$ at the highest possible value of P_{T}

(target polarisation), the scheme illustrated in FIG.9 was most commonly used. A total of eight crystals was used, and the procedures adopted for each were changed slightly, as more understanding of the target and crystal behaviour was gained. The beam polarisation could be changed rapidly from + to -, (by altering the current in the spin precession solenoid: see FIG.15) and the change from unpolarised to polarised beam (or vice versa) took~5 minutes. The split ionisation chambers were found to hold the beams accurately in position; the reproducibility was thoroughly explored during the experiment, and found to be completely satisfactory. It was thus found possible to leave data collection of types (a),(d) (target unpolarised) to the end of the useful life of polarisation of each crystal. The end of a crystal's life was taken to be when the maximum polarisation attainable fell below ~ 0.10.

The counter telescopes had to be removed in order to change the LMN crystal, and this is one of the reasons that the data collected for each crystal were considered as a separate set, with different normalising factors contained in 'I_o' of equation 23.

The experimental data taking at 140 Mev extended over seven months, and the later work at lower energies, including the detailed radiation damage study, were spread over a further three months.

3.3 Experimental procedure at lower energies

The value of Cnn (90°c of m) near 140 Mev was found to be close to unity, but the predictions of the Hamada-Johnston potential suggested that Cnn (90°) would fall off rapidly in value with decreasing energy to become negative

FIG. 20

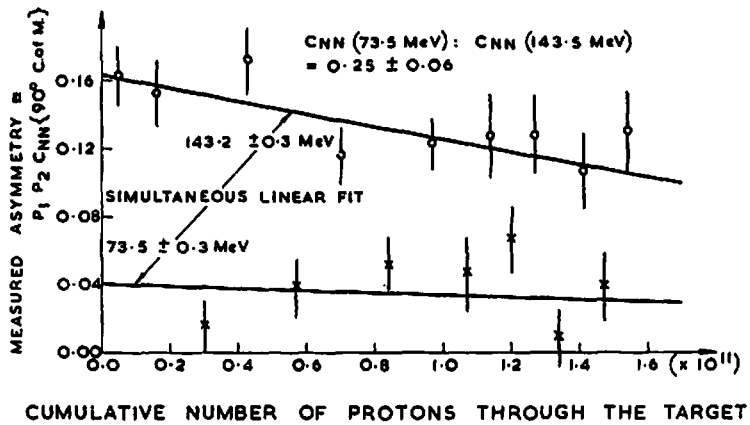
CNN (73·5 MeV) : CNN (143·5 MeV)
= 0·25 ± 0·06
143·2 ±0·3 MeV
SIMULTANEOUS LINEAR FIT
73·5 ± 0·3 MeV
MEASURED ASYMMETRY ≡ P1 P2 CNN(90° C.of M.)
0·16
0·12
0·08
0·04
0·00
0·0
0·2
0·4
0·6
0·8
1·0
1·2
1·4
1·6 (x 10^11)
CUMULATIVE NUMBER OF PROTONS THROUGH THE TARGET

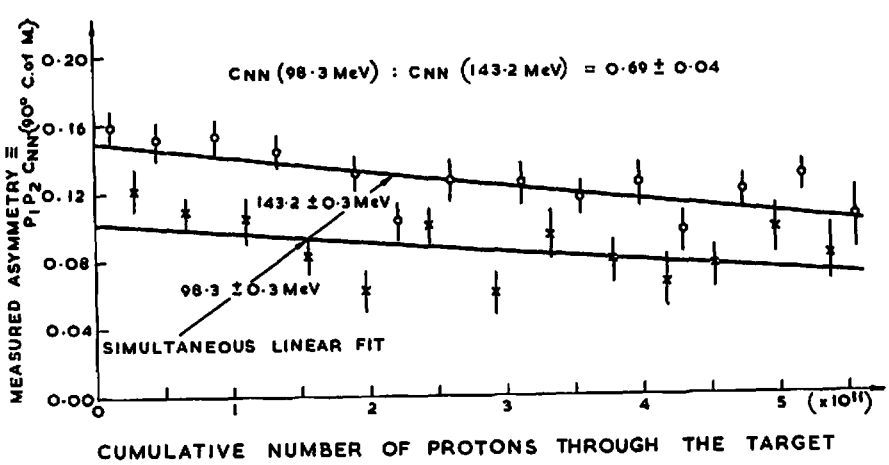
CNN (98·3 MeV) : CNN (143·2 MeV) = 0·69 ± 0·04
143·2 ±0·3 MeV
98·3 ± 0·3 MeV
SIMULTANEOUS LINEAR FIT
MEASURED ASYMMETRY ≡ P1 P2 CNN(90° C.of M.)
0·20
0·16
0·12
0·08
0·04
0·00
0
1
2
3
4
5 (x10^11)
CUMULATIVE NUMBER OF PROTONS THROUGH THE TARGET

FIG. 21

near 50 Mev. In order to examine this falloff a comparison procedure was necessary, as, for energies below ~ 110 Mev, the recoil protons at 61.8° c of m could not escape from the crystal. This meant that only the product $P_I P_T$ Cnn (90°) could be measured, where P_I is incident beam polarisation, and P_T is target polarisation. At 90° c of m P is zero in equation (23), due to the anti-symmetry of polarisation produced in p-p scattering. This point is illustrated by data at 98 [24] and 141 [13] Mev later in this thesis. Thus equation (23) becomes:

$$(24) \qquad I = I_o [1 + (\pm P_I) P_T \ \text{Cnn} \ (90^\circ)]$$

rewriting to show the energy dependence explicitly:

$$(25) \qquad I(E) = I_o(E) \ [1 \pm P_I \ P_T \ \text{Cnn} \ (90^\circ, E)]$$

thus we can calculate the asymmetry $\varepsilon(E, P_T)$ from data taken with the polarised beam at an energy E and with a mean target polarisation of P_T .

$$(26) \qquad \varepsilon(E, P_T) = P_I \ P_T \ \text{Cnn} \ (90^\circ, E)$$

Under continued irradiation, only P_T will vary, Cnn (90°, E) and P_I remaining fixed. If we take alternate measurements at energies E and 143.2 Mev, two curves will be traced out, both with the same shape, the asymmetries on one curve being in a constant ratio to those on the other. Two sets of data collected in this manner for E = 73.5 and 98.3 Mev are shown in FIGS. 20,21.

In addition to the removal of the two 30° (Lab) telescopes, several other changes are required in the 45° telescopes for the lower energy data points. The slower protons are still incident at about 2.1° , as their energy is ~ 140 Mev almost to the target, since the CH_2 degrader used is placed as close to the target collimator as possible. The

beam actually rises a small amount (~ 0.1 mm), which was corrected for by raising the collimator on the target slightly each time a measurement was made at a low energy.

The lower energy of the scattered particles required the angular settings and copper absorbers to be altered each time the energy was changed. The monitor counter was raised to a compromise between the planes of the 143 Mev beam and the lower energy beam, and the absorber changed for each change of energy.

The angular settings used are listed in TABLE 2, and further details follow:

Energy of measurement	Degrader (CH_2)	Cu Absorber in Arms	Al Absorber in monitor
98.3 Mev	9.29 gm/cm**2	1.67 gm/cm**2	1.09 gm/cm**2
73.5 Mev	6.47 gm/cm**2	0. gm/cm**2	0. gm/cm**2

One crystal was used for each of the two lower energies, and data taking was stopped when the polarisation of the target had dropped by about a half.

The counting rates in the telescopes were ~ 1.9 cps at 98 Mev and ~ 1.3 cps at 74 Mev. Both the background coincidence rates and the random coincidence rates were ~ 2% of the total counting rates at both energies. At these rates about an hour was spent counting for one data point at each energy.

3.4 Background measurement

Initial attempts to measure the background coincidence counting rate by using targets of carbon[12], Lanthanum Magnesium Oxide in a can; and nothing in the can; were not successful. Any slight water contamination was found to be detectable, and it was not possible to dry out the target

satisfactorily.

The same difficulties had been encountered with the large polarised target used at the Rutherford Laboratory, and had been resolved by the production of a dummy (hydrogen-free) target material[33]. This material consisted of 66% PTFE* loaded with 26.2 % $BaCo_3$ and 7.8 %MgO, sintered at $\sim 400^{c}$ C to form an easily machined water-free solid. It was not particularly important to reproduce the actual elements in LMN as it was reasonable to consider that neighbouring nuclei would have very similar (p,2p) inelastic cross-sections. Such events were the only ones that could give rise to background coincidences, and as the experimental ratio of background:hydrogen counts was small, this material was used to measure the background. The background counting rate when the target cavity was empty was effectively zero (a B.G:H_2 counting ratio of < 0.01 %).

The density of the dummy target material was 2.45 gm/cm**3 to be compared with 2.08 gm/cm**3 for the LMN target crystals. A dummy target of the same shape and size as the LMN target crystals was used, and the measured background scaled down by 2.08/2.45. This was justifiable as the great majority of the background scattering events occurred in the dummy target. A precise determination of the background rates was not possible, as the LMN target crystals were only determined to be 1.0 ± 0.1 mm. thick. This uncertainty was not serious as the ratio of background: hydrogen count was ~ 2%.

*Polytetrafluoroethylene

Using the unpolarised beam, together with the long duty cycle facility (the Cee)[118], the B.G:H_2 ratio was close to 0.02 for each telescope. Using the polarised beam and using the normal duty cycle, as in the actual experimental data-taking, this ratio was also 0.02, but an asymmetry of -0.05 $\pm$0.04 was measured at 143 Mev. The measured counts were used to correct the 143 Mev data for background although one would expect this asymmetry to be zero, as indeed it was for the lower energy measurements. About threequarters of the background counts recorded using the polarised beam were random coincidences. This could have been reduced by using the long duty cycle beam[118], but only by deviating from the experimental conditions under which the LMN data was collected.

3.5 Energy of the measurements

Recently certain discrepancies have been found between theory and experiment in the range-energy relations commonly used to define the energy at which a scattering experiment has been made. These differences are $\sim$ 1 Mev, and have thus been of small importance in comparison with the precision of p-p data and the energy width of the beams used for p-p measurements. As pointed out by Rose[123] at Williamsberg, such effects are now becoming detectable. For these reasons the material and precise range tables used will be quoted here. FIG. 35 shows the magnitude of the effect near 100 Mev in aluminium, as reported by Portner and Moore[124] for measurements made on the MacGill synchrocyclotron. [(1)(2) in the figure refer to Ref. (127)(128)].

The full energy measurement was made by taking range curves in copper, and using the corrected Sternheimer range tables as quoted in Ref. (105). The value obtained was

Parametrisation of the data used for least squares analysis of 143 Mev data.

Counting rates (C) of the three counter telescopes used for the 143 Mev measurements:

$C(30D:P1\pm:P2-) = T1j.N1(1\pm S)(1\pm P1.P3-P2.P3\mp P1.P2.Cnn(61.8^{c}))$

$C(45 :.. :..) = T2j.N2(1\pm S)(1\mp P1.P2.Cnn(90^{\circ}))$

$C(30U:.. :..) = T3j.N3(1\pm S)(1\mp P1.P3+P2.P3\mp P1.P2.Cnn(61.8^{c}))$

$C(30D:P\pm:P2=0) = T1j.N1(1\pm S)(1\pm P1.P3)$

$C(45 :..:..) = T2j.N2(1\pm S)(1)$

$C(30U:..:..) = T3j.N3(1\pm S)(1\mp P1.P3)$

$C(30D:P1=0:P2-) = T1j.M1(1+P2.P3^{*})$

$C(45 :.. :..) = T2j.M2(1)$

$C(30U:.. :..) = T3j.M3(1-P2.P3^{*})$

$C(30D:P1=P2=0) = M1.T1j$

$C(45 :.. :..) = M2.T2j$

$C(30U:.. :..) = M3.T3j$

Where:30D:45:30U refer to the telescopes defining LAB angles of about 45^{c} and 30^{c} degrees corresponding to $-61.8^{c}:90^{\circ}:+61.8^{\circ}$ in c of m.

Mi:Ni are the normalising factors including solid angle, absorber corrections etc. for each telescope for the Unpolarised and the Polarised beams respectively.

TABLE 3

142.2 ± 0.3 Mev for the polarised beam, and 146.3 ± 0.3 Mev for the unpolarised beam.

At the lower energies, two methods were used to deduce the energy at the target centre. (1) The full energy range in copper was corrected to the incident proton energy after passing through the CH_2 degraders, the range tables of (105) being used for this purpose. This gave:

98.4 ± 0.3 Mev and 73.2 ± 0.3 Mev.

(2) A separate telescope was then used to take range curves in copper for the degraded and undegraded beams and the tables of (105) used to give:

98.2 ± 0.3 Mev and 73.7 ± 0.3 Mev.

As these estimates merely check the consistency of the range tables, the values adopted for the energies at the target centre given by the polarised beam after passing through the CH_2 degraders are 73.5 ± 0.3 Mev 98.3 ± 0.3 Mev; and 143.2 ± 0.3 Mev, for the full energy polarised beam. All these are referred to the copper range tables of (105).

IV Analysis of Cnn data

4.1 Parametrisation

The parameters used for these analyses are tabulated in TABLE 3. The functional forms involving P1, P2, P3 and Cnn (θ) are those given by equation (23) for the various combinations of target and beam polarisation listed on the left hand side of each equation. P1, P2, P3, P3* are the polarisations of beam and target, and in p-p scattering at 61.8° c of m at 143.2 and 146.3 Mev respectively. S is a parameter to allow

for a possible variation in monitoring efficiency dependent on the direction (+ or -) of the incident beam polarisation. M and N are normalising factors including absorber corrections, solid angle factors, detection efficiencies of the telescope arms etc. Two different normalisations (M,N) are used as there is a 3.1 Mev difference in energy between the two beams used, and the slightly differing absorber corrections, beam focus, beam spot shape, and scattered proton trajectories make it unreasonable to expect agreement between N,M for the two beams to the high precision (<0.3%) given by the counting statistics. The second normalising factor Ti applies to data collected using either beam, and is expected to be close to unity. This factor is to allow for slightly differing normalisations to the monitor for the three different telescopes. This might be considered necessary as the occasional movement of the counter telescopes during a run on one crystal could lead to errors of $\leqslant 0.2^{\circ}$ in the resetting of the counter angles. The suffix j of Tj refers to the crystal in use, and the other suffix (shown in Table 3) may be used to refer to each telescope separately instead of considering T to remain the same for all telescopes throughout the data taking for a given crystal. This additional suffix is of doubtful merit (see later), however variations in T between crystals are expected to occur as the entire counting array must be removed in order to replace the target crystal, and must then be replaced and reset. Also the thickness of the target crystals varies, the nominal thickness being 1.0 ± 0.1 mm.

A slight improvement may be made to Table 3 by writing

(27) $$Cnn\ (61.8^{\circ}) = R.Cnn\ (90^{\circ})$$

as the ratio (R) is well-determined independent of the behaviour

of the target polarisation with time.

4.2 Preliminary Analysis at 143 Mev

If the normalising parameters N,M,T are not used, it is still possible to compute values for Cnn. As data is collected for both signs of incident beam polarisation, the techniques of Appendix 3 may be used to obtain values for P2.P3* (from unpolarised beam data), and P1.P3, and P2.P3 (from polarised beam data, by the addition of the first and third equations of Table 3) that are independent of N,M,T and S. Similarly values of the asymmetries P1.P2.Cnn(90°) and P1.P2.Cnn(61.8°) may be obtained. If we take the energy variation of P3(61.8° c of m) from the literature - see FIG.19 - a value of P1.dP3/dE of 0.85%/degree/Mev is obtained, and thus a series of points following the decay of the target polarisation may be found. FIG.9 was obtained in this way. As the protons of 143.2 and 146.3 Mev both lose very close to 1 Mev to ionisation in the target, it is immaterial whether the x-coordinate is the cumulative ionisation produced in the crystal, or the cumulative proton flux through the crystal.

A smooth curve may now be fitted to these data. As discussed earlier, a three-parameter fit could not be justified by the data, and there was little to choose between a linear and an exponential fit by χ^2 tests. As discussed in Chapter II, there are other reasons for using an exponential or other non-linear curve; however both linear and exponential fits were tried. The value of the target polarisation at the x-coordinate corresponding to each P1.P2.Cnn(θ) datum could then be obtained, together with errors that included the effects of correlations between the parameters defining the polarisation decay curve. As P1 for the beam used in this

experiment was known to be 47.2 ± 0.4%,[57] values for Cnn(90°) and Cnn(61.8°) could be derived. The ratio of the two asymmetries P1.P2.Cnn(90°) and P1.P2.Cnn (61.8°) measured simultaneously was evidently independent of the actual value, or indeed the behaviour, of the target polarisation.

Values for Cnn(90°) and R were obtained for the first five crystals. As would be expected, the values of R (see equation 27) agreed well, but the absolute values - i.e. Cnn (90°) - were in poor agreement. The error of the final result was scaled up to allow for the poor χ^2/point before the presentation of these early data, and preliminary analysis at Karlsruhe.[122]

Parameter	Form of decay	Value	Error	χ^2	Degrees of Freedom	Error renormalised for poor χ^2
Cnn(90°)	Exponential	0.89	± 0.02	39.8	12	0.04
	Linear	0.88	± 0.02	34.3	12	0.03
R	Exponential	0.85	± 0.04	12.5	12	
	Linear	0.85	± 0.04	10.4	12	

It was evident that R was reasonably well determined by this procedure, but that for the absolute value of Cnn(90°) further data and closer examination of existing data was required.

It was possible that the target polarisation, as seen by the two beams, might not have been the same. This would not be so if either the intensity distribution of the two beams was the same over the irradiation position of the crystal, or the polarisation of the target crystal was uniform over the same area.

Both these requirements are fairly well satisfied,

throughout the analysis, and identical data reduction and decision procedures applied to both. The good agreement between the results obtained using the two forms was further evidence that the Cnn values finally quoted are not materially dependent on the decay law assumed.

At this stage it should be noted that the decay laws applied to the maximum obtainable polarisation of the target, and drifts in the klystron frequency and the static magnetic field could cause fluctuations in the actual behaviour of the polarisation with time. For this reason as far as possible a continual watch was maintained over the E.P.R. output (on a chart recorder), so that an operator could re-attain the maximum available polarisation as quickly as possible. Fluctuations of this kind were the probable cause of the high (1.4/d.fr.) χ^2 per point finally obtained in the analysis, and also for the necessity to reject a certain number of data points in the course of the analysis.

An initial approach used a functional minimisation routine (due to Powell [34]) that did not require functional derivatives, and used a variable step-length approach to ensure a good convergence rate to the minimum from a poor initial approximation.

The function to be minimised was the sum of the χ^2 contributions from every data point. A typical such contribution is shown below for the case of a datum collected by the 30D telescope when both beam and target were polarised, and an exponential form P2 (x) = Aj.Exp(- x.Bj) was in use, [where x is the cumulative monitor count coordinate corresponding to the cumulative proton flux that had passed through the target up to the midpoint of the count required to collect

experiment was known to be 47.2 ± 0.4%,[57] values for Cnn(90°) and Cnn(61.8°) could be derived. The ratio of the two asymmetries P1.P2.Cnn(90°) and P1.P2.Cnn (61.8°) measured simultaneously was evidently independent of the actual value, or indeed the behaviour, of the target polarisation.

Values for Cnn(90°) and R were obtained for the first five crystals. As would be expected, the values of R (see equation 27) agreed well, but the absolute values - i.e. Cnn (90°) - were in poor agreement. The error of the final result was scaled up to allow for the poor χ^2/point before the presentation of these early data, and preliminary analysis at Karlsruhe.[32]

Parameter	Form of decay	Value	Error	χ^2	Degrees of Freedom	Error renormalised for poor χ^2
Cnn(90°)	Exponential	0.89	± 0.02	39.8	12	0.04
	Linear	0.88	± 0.02	34.3	12	0.03
R	Exponential	0.85	± 0.04	12.5	12	
	Linear	0.85	± 0.04	10.4	12	

It was evident that R was reasonably well determined by this procedure, but that for the absolute value of Cnn(90°) further data and closer examination of existing data was required.

It was possible that the target polarisation, as seen by the two beams, might not have been the same. This would not be so if either the intensity distribution of the two beams was the same over the irradiation position of the crystal, or the polarisation of the target crystal was uniform over the same area.

Both these requirements are fairly well satisfied,

throughout the analysis, and identical data reduction and decision procedures applied to both. The good agreement between the results obtained using the two forms was further evidence that the Cnn values finally quoted are not materially dependent on the decay law assumed.

At this stage it should be noted that the decay laws applied to the maximum obtainable polarisation of the target, and drifts in the klystron frequency and the static magnetic field could cause fluctuations in the actual behaviour of the polarisation with time. For this reason as far as possible a continual watch was maintained over the E.P.R. output (on a chart recorder), so that an operator could re-attain the maximum available polarisation as quickly as possible. Fluctuations of this kind were the probable cause of the high (1.4/d.fr.) χ^2 per point finally obtained in the analysis, and also for the necessity to reject a certain number of data points in the course of the analysis.

An initial approach used a functional minimisation routine (due to Powell [84]) that did not require functional derivatives, and used a variable step-length approach to ensure a good convergence rate to the minimum from a poor initial approximation.

The function to be minimised was the sum of the χ^2 contributions from every data point. A typical such contribution is shown below for the case of a datum collected by the 30D telescope when both beam and target were polarised, and an exponential form P2 (x) = Aj.Exp(- x.Bj) was in use, [where x is the cumulative monitor count coordinate corresponding to the cumulative proton flux that had passed through the target up to the midpoint of the count required to collect

the datum] (28)

$$\Delta\chi^2 = \frac{[C(30D:P1+,P2-)-N1.T1\ (1+S)(1+P1.P3-P2.P3-P1.P2.R.Cnn(90)]^2}{[\sigma\ (C[30D:P1+,P2-])]**2}$$

where the denominator gives the square of the statistical uncertainty relevant to the counting rate C[30D:P1+,P2-] including contributions from the background subtraction, and corrections for random coincidences in both the monitor and the telescopes.

The initial minimisation procedure was used to show that eight of the data were not part of the consistent data set, as the χ^2 contributions for each of these points was >100 for all the possible variations in parametrisation described, and for all starting points tried for the minimisation. These 8 points were then removed from the complete data set of 284 points.

A much faster and more convenient routine was now used. This also was due to M.Powell,[135] and was specialised to the minimisation of sums of squares. The major feature of this technique was the good approximation to the error matrix built up as a function of the minimisation search procedure.

The parametrisation was initially used in the form

(1) Cnn(90°) and Cnn(61.8°) as separate variables

(2) Tij without the suffix i, so that only one common overall normalisation of the monitor was allowed for the three telescopes for a given crystal.

The form Tj was used as this restricted the freedom of the fit as much as possible consistent with known effects. The form Tij was used later to restrict the freedom of the fit as little as possible consistent with known effects.

The parametrisation Tj required 31 variables: Cnn(90°),

Cnn(61.8°), S, P3, (Ni, Mi; i=1,2,3) and (Ti, Ai, Bi, ; i=1 to 7) where Ai, Bi are the parameters defining the exponential or linear forms for P2(x).

(I) Initial Fit : χ^2 for all points <30

This is the result of the fit to the initial data set of (284-8) points:

Fit	Cnn(90°)	Cnn(61.8°)	$\varrho_{90,61}$	S	χ^2/D.Fr.	P3
Exp.	1.03±0.04	0.85±0.03	0.78	0.0008	668/245	0.164±0.002
Lin.	1.01±0.04	0.85±0.03	0.74	0.0008	688/245	0.164±0.002

S is ± 0.0010 in both cases.

Three stages of data reduction were now carried out, identical sets of data being used for both the linear and the exponential fits This gave as a result a set of data for which χ^2<9 for all data points under both hypotheses. All points in the initial data set had been tested to ensure that their rejection was still justified when the 'final' values of the parameters were used to calculate their contributions.

(II) Reduced Set : χ^2 for all points <9

Fit	Cnn(90°)	Cnn(61.8°)	$\varrho_{90,61}$	S	χ^2/D.Fr.	P3
Exp.	1.00±0.04	0.83±0.03	0.77	-0.0000	355/225	0.166±0.002
Lin.	0.99±0.04	0.82±0.03	0.77	+0.0002	370/225	0.166±0.002

S is ± 0.0010 in both cases.

As previously mentioned, the value of the incident beam polarisation had been held constant at the value of 0.472 . A check was now made on the effect of this restriction by repeating the fit using a value of P1 = 0.468 (= 0.472 - quoted error of 0.004) and the same data set. [57]

TABLE 4

Error Matrices from Cnn analysis[+]

Exponential decay law; Analysis (A) using Cnn(90°) and R.

Cnn(90°)	Cnn(61.8°)/Cnn (90°)	P3
$\sigma_1^2 = 1.43.10^{-3}$	$\rho_{12}\sigma_1\sigma_2 = -2.62.10^{-4}$	$\rho_{13}\sigma_1\sigma_3 = 1.80.10^{-5}$
	$\sigma_2^2 = 4.46.10^{-4}$	$\rho_{23}\sigma_2\sigma_3 = 2.91.10^{-5}$
		$\sigma_3^2 = 3.59.10^{-6}$

Thus:

σ[Cnn(90°)] =	$\sigma_1 = 0.038$	$\rho_{12} = -0.33$	Cnn(90°) = 0.9955±0.038*
σ(Ratio) =	$\sigma_2 = 0.021$	$\rho_{23} = 0.73$	Ratio = 0.8279±0.021
σ(P-P-poln.) =	$\sigma_3 = 0.0019$	$\rho_{13} = 0.25$	P3(61.8°) = 0.1656±0.0019**

Exponential decay law; Analysis (B) using Cnn(90°) and Cnn(61.8°) uncoupled.

Cnn(90°)	Cnn(61.8°)	P3
$\sigma_1^2 = 1.56.10^{-3}$	$\rho_{12}\sigma_1\sigma_2 = 1.03.10^{-4}$	$\rho_{13}\sigma_1\sigma_3 = 1.87.10^{-5}$
	$\sigma_2^2 = 1.10.10^{-4}$	$\rho_{23}\sigma_2\sigma_3 = 1.86.10^{-5}$
		$\sigma_3^2 = 3.60.10^{-6}$

Thus:

σ[Cnn(90°)] =	0.039	$\rho_{12} = 0.78$	Cnn(90°) = 0.9959±0.039*
σ[Cnn(61.8°)] =	0.033	$\rho_{23} = -0.30$	Cnn(61.8°) = 0.8245±0.033
σ(P-P poln.) =	0.0019	$\rho_{13} = 0.25$	P3(61.8°) = 0.1656±0.0019**

[+] see 8.2

*,** The stability and repeatability of this solution is shown by the *, **results. Widely differing starting points were used for the minimisations whose results are quoted here.

(III) Test set : P1 displaced by 1 standard deviation

Fit	Cnn(90°)	Cnn(61.8°)	$\rho_{12,01}$	S	χ^2/D.Fr.	P3
Exp.	1.00±0.04	0.825±0.03	0.80	-0.0001	356/225	0.166±0.002
Lin.	1.00±0.04	0.830±0.03	0.78	+0.0002	370/225	0.167±0.002

S is ± 0.0010 in both cases.

This shows that the solution is stable to such displacements, as is necessary for this solution to be at the true minimum.

Although Cnn(90°) and Cnn(61.8°) are the results most easily compared with other work, and assimilated into phase-shift analyses [P.S.A.], the physically distinct parameters determined by this experiment are Cnn(90°), and the ratio (R) of the two Cnn values. R may be incorporated into P.S.A. without undue complications, and the final data set was run with this parametrisation to obtain the correlated error for R and the correlation coefficient ρ^* between Cnn(90°) and R.

(IV) Final Fit : Cnn, R Parametrisation

Fit	Cnn(90°)	R	ρ^*	S	χ^2/D.Fr.	P3
Exp.	1.00±0.04	0.828±0.02	-0.33	-0.0000	355/225	0.1656±0.0019
Lin.	0.99±0.04	0.827±0.02	-0.33	+0.0002	370/225	0.1656±0.0019

S is ± 0.0010 in both cases.

The error matrices for (II) and (IV) are shown in detail in TABLE 4 together with the results obtained for Cnn and P3.

As a final check on these conclusions, the same data set was run using the full Tij normalisation, allowing all three telescopes to have slightly differing efficiencies relative to the monitor for runs on each crystal. This removes the smoothing over possible re-settings of the telescopes made during a set of runs on a crystal, and

and we may consider that both beams do indeed see the same target polarisation. The mean polarisations seen by the two beams can be compared by observing the spread of the points on exponential decay curves fitted to the data. FIG. 9 shows that such a comparison is of necessity of poor precision, but the quality of the overall fit of polarisation falloff data to exponential curves gives a satisfactory χ^2 of 36 for 42 degrees of freedom.

4.3 Least squares analysis at 143 Mev

After the preliminary analysis of 4.2, further data was taken, and an alternative approach to the analysis adopted. The spread of results for Cnn obtained as in 4.1 suggested that fluctuations in the target polarisation or errors such as the missetting of a counter on the magnet had occurred. To distinguish such data from the rest required a least squares analysis that utilised all the data simultaneously. The parametrisation of 4.1 was used in two basic forms. Type A, using Cnn(90°) and Cnn(61.8°) as separate parameters; Type B using Cnn(90°) and the ratio of the two Cnn values, R.

P3 was allowed to vary in the analysis, to provide a check that the mean analysing angle of 30D and 30U telescopes was in fact 61.8° c of m by comparison with other p-p polarisation data. P3* was written as P3 + Δ P3 where Δ P3 was derived from the published data shown in FIG.19 and fixed at that value.

Although the data of Chapter II would have allowed us to use only an exponential form for the behaviour of the target polarisation under continued irradiation, the analysis of that data was not complete until after the χ^2 analysis was run. Thus both linear and exponential forms were used

allows 14 more parameters for the overall fit.

(V) 3-Normalisations/XTal : Cnn(90°) and Cnn(61.8°)

Fit	Cnn(90°)	Cnn(61.8°)	$\rho_{90,61}$	S	χ^2/D.Fr.	P3
Exp.	1.02±0.04	0.85±0.03	0.78	0.0001	293/211	0.166±0.002
Lin.	1.01±0.04	0.85±0.03	0.79	0.0004	310/311	0.166±0.002

Fit	Cnn(90°)	R	ρ^*	S	χ^2/D.Fr.	P3
Exp.	1.02±0.04	0.83±0.04	-0.33	0.0001	293/211	0.166±0.002
Lin.	1.01	0.83	-0.33	0.0004	312/211	0.166

All S values are ± 0.0010.

The conclusions do not vary significantly between the two parametrisations, and the more restrictive fit of (IV) allows sufficient freedom without introducing the additional (and less likely) hypotheses adopted for (V).

The slightly better fit of the exponential decay law, when taken in conjunction with the conclusions of the radiation damage study, leads us to quote only the exponential results of (V). The χ^2/point is still high, and indicates that the scale of errors has been underestimated by using the statistical errors. The fluctuations of the target polarisation are considered to account for this, and the errors quoted in TABLE 5 have been scaled up for the poor χ^2/point. Corrections have also been made for the imposed cutoff at $\chi^2 > 9$, and for the reduction of the data set by 20 points out of an initial 276.

4.4 The Determination of P3

A value for polarisation in p-p scattering at 143.2 Mev at 61.8° c of m is given by this least squares analysis as 0.166 ± 0.003. This value for P3 is correlated to the other variables in the analysis, and is equally affected by changes in the monitoring, counter efficiencies, counter

settings, and the other factors which may have fluctuated during the experiment and so introduced non-statistical errors.

The effects of these fluctuations, and of the consequent data reduction process described in 4.3, can be estimated by calculating the asymmetry P1.P2 directly from the data, by using the equation:

$$(29) \qquad P1.P3 = \frac{r - 1}{r + 1}$$

where: $$r^{**}2 = \frac{C(30D:P1+:P2=0) \cdot C(30U:P1-:P2=0)}{C(30D:P1-:P2=0) \cdot C(30U:P1+:P2=0)}$$

By considering the expression in TABLE 3, it may be seen that this value of P1.P3 is independent of both the beam monitor and the telescope efficiencies. This is fully discussed in 8.3. The value of P3 obtained in this way is 0.165 ± 0.002, which implies that the non-statistical errors other than those associated with the target polarisation were very small.

Although P3 has been considered to be a parameter to be determined by the experiment, good experimental data exists. Cox et al[13] have used the same polarised beam to determine the angular variation of P3 using a liquid hydrogen target. Using the known variation of P3 with energy [ref. 50 and FIG.19], we obtain P3(61.8° c of m, 143.2 Mev) = 0.162 $\pm$ 0.003 from a smoothed curve (based on Perring's[137] phase-shift analysis) through the data points. This result does not include uncertainties in P1, and is in good agreement with the results of this experiment.

If the Cox value of P3 were used directly in the analysis, the error matrices quoted in TABLE 4 predict values

of Cnn(90°) and R of 0.98 ± 0.05 and 0.80 ± 0.03 respectively.

This was not done for several reasons The result quoted for P3(61.8°) from this analysis was derived without reference to the beam energy or to the scattering angle, and also has been shown to be very insensitive to the precise value assumed for P1. Thus, apart from the small corrections for the energy dependence of P3(61.8°c of m), all the results are insensitive to all other available data and may therefore be used directly in phase-shift analyses without introducing further error correlations. This would not be the case if the value of Cox et al were to be used.

The datum P3(61.8°) is a data point of equal precision to that of Cox et al, and therefore may be used in one of two ways; firstly it may be taken to confirm the consistency of the analysis procedure, and also, by reference to other data, the mean setting angle for the 30° Lab telescopes; or secondly, as a subsidiary result from the experiment. We quote P3(61.8°, 143.2 Mev) = 0.166 ± 0.003 as one of the results of this experiment.

4.5 Analyses at 73.5 and 98.3 Mev

The method used to obtain data on Cnn(90° c of m) at 73.5 and 98.3 Mev has been described in 3.3. Data was taken at 143.2 Mev and (say) 98 Mev alternately, using only the polarised beam and the 90° c of m telescopes. Both directions ($\pm$) of the incident beam polarisation were used and the target was polarised all the time. By reference to TABLE 3, it can be seen that an asymmetry ε may be measured at each energy , of the form (see TABLE 3):

$$\varepsilon = \frac{C(45:P1+:P2-) - C(45:P1-:P2-)}{C(45:P1+:P2-) + C(45:P1-:P2-)} \qquad (30)$$

$$\varepsilon = \frac{P1.P2.Cnn(90^\circ) - S}{1 - S.P1.P2.Cnn(90^\circ)}$$

From the least squares analysis at 143.2 Mev, we may write $S = 0.0000 \pm 0.0010$, thus $\varepsilon = P1.P2.Cnn(90^\circ)$. If we plot ε against the cumulative proton flux through the crystal - or total ionisation energy left in the crystal - the two curves will be traced out as P2 varies FIG.20,21. These two curves are related by the ratio of $Cnn(90^\circ)$ at the two energies being used. A least squares fitting procedure may thus be used to fit all the ε data to a smooth curve, the 143.2 Mev asymmetries being multiplied by a parameter

$$R^* = \frac{Cnn(90^\circ) \text{ at low energy}}{Cnn(90^\circ) \text{ at } 143.2 \text{ Mev}}.$$

The polarisation falloff seen in FIG.20,21 may be described (as for 143 Mev analysis) by a straight line, an exponential, or any other smoothly varying curve. The x-coordinate may be in terms of cumulative energy deposited in the crystal, or in terms of cumulative proton flux through the target crystal. All these possible descriptions of the decay gave sensibly the same results for the values of R*. Second order terms giving a third parameter for the polarisation falloff were found to be unjustified by the data.

The errors quoted are derived from the error matrix of the least squares solution in each case:

73.5 ± 0.3 Mev

x-coordinate	R*	P2 law used	χ^2/D.Fr.
Cumulative	0.690±0.041	Exponential	21.7/24
number of protons	0.689±0.043	Linear	22.5/24
Cumulative ionisation	0.688±0.042	Exponential	22.6/24
deposited in crystal	0.689±0.038	Linear	23.3/24

Results and predictions for Cnn measurements

Parameter	Experiment	Breit (Ypp4)(1967)	Arndt(1966)	Perring(1966)	Perring(1967)
$Cnn(90^\circ, 143.2)$	1.00 ± 0.05	0.98	0.97	0.97*	0.97*
$\frac{Cnn(61.8^\circ, 143.2)}{Cnn(90^\circ, 143.2)}$	0.83 ± 0.03	0.84	0.87	0.85*	0.85*
$\frac{Cnn(90^\circ, 98.3)}{Cnn(90^\circ, 143.2)}$	0.69 ± 0.04	0.70	0.71	-	0.77***
$\frac{Cnn(90^\circ, 73.5)}{Cnn(90^\circ, 143.2)}$	0.25 ± 0.06	0.33	0.32	-	0.36
$P(61.8^\circ, 143.2)$	0.166 ± 0.003	0.163**	-	0.162*	0.163*

*Includes these results for Cnn at 143 Mev, and the recent (1966) Harwell data on polarisation and differential cross-section at 140.7 and 144.1 Mev.

**Breit (YRB1(Ko))(1966)

***This fit includes this Cnn value, 93 and 98 Mev (1967) Harwell polarisations and 99 Mev Harwell (1967) cross-section.

TABLE 5

98.3 ± 0.3 Mev

x-coordinate	R*	P2 law used	χ^2/D.Fr.
Protons	0.253±0.055	Exponential	12.6/13
	0.252±0.059	Linear	12.7/13
Ionisation	0.252±0.056	Exponential	12.6/13
	0.251±0.059	Linear	12.6/13

The results adopted were, as in 4.3, those for the exponential law, and the cumulative number of protons.

i.e. $Cnn(90^\circ; 73.5 \text{ Mev})/Cnn(90^\circ; 143.2 \text{ Mev}) = 0.253 \pm 0.055$

$Cnn(90^\circ; 98.3 \text{ Mev})/Cnn(90^\circ; 143.2 \text{ Mev} = 0.690 \pm 0.041$

4.6 Conclusion

The values of the exponential quantities in this experiment have been determined by χ^2 minimisation procedures. Error matrices have been calculated, and the quoted errors in TABLE 5 allow for correlations.

The right hand columns in TABLE 5 refer to the predictions and fits of various modern phase-shift analyses. Both the Yale[134] communications (YRB 1(Ko) and Ypp-IV) are predictions, so also are Perring's 1966[137] analysis and the Livermore[16] energy dependent analysis. The later Perring[137] analyses include the data in this thesis, and are therefore fits.

V Apparatus for 98 Mev proton scattering experiments

5.1 Liquid hydrogen degrader

The external proton beams of the Harwell 280 cm synchrocyclotron are at a mean energy of about 140 Mev, and have an energy spread of about 2 to 3 Mev (F.W.H.M.). The intensity available is fairly low, $\sim 10^8$ pps unpolarised protons, and $\sim 10^7$ pps polarised protons.

In order to produce a beam with an energy of about 100 Mev, it is necessary to degrade the energy of the beam in some material. In order to retain a reasonably small energy spread in the degraded beam a material of low atomic number must be used. As the intensity of the beam is already low, it is necessary to minimise the multiple scattering in the degrading material to give a reasonably small beam spot at the target with a minimum of further collimation. As the beam divergence introduced by multiple scattering increases as the square of the atomic number of the material used, a low atomic number is again necessary.

The best solution is to use liquid hydrogen to degrade the mean energy of the beam. This minimises multiple scattering and straggling, and removes the possibility of contamination of the low energy beam from inelastic collisions in the degrader.

To make best use of these properties of hydrogen, very thin plastic windows were used along the beam path through the hydrogen cryostat. The techniques developed to contain hydrogen behind windows of material of 0.005 cm thickness and of low atomic number are described in 5.2.

The degrader cryostat was made from stainless steel and was continuously pumped by a 7.6 cm Genevac oil diffusion

FIG. 22

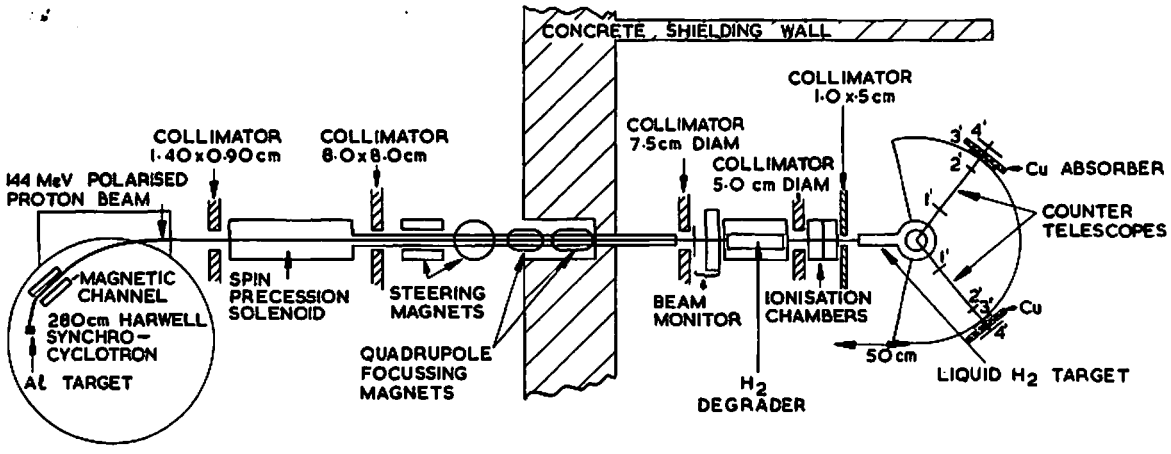

EXPERIMENTAL LAYOUT FOR ~95 MeV P-P: P(θ)

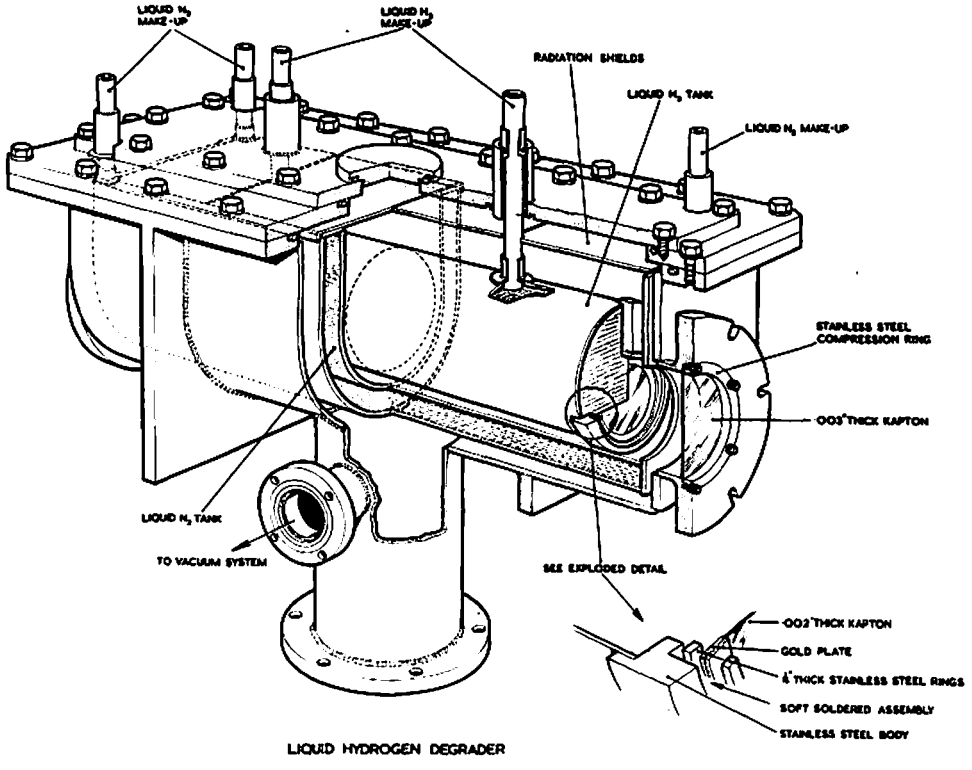

LIQUID HYDROGEN DEGRADER

FIG. 23

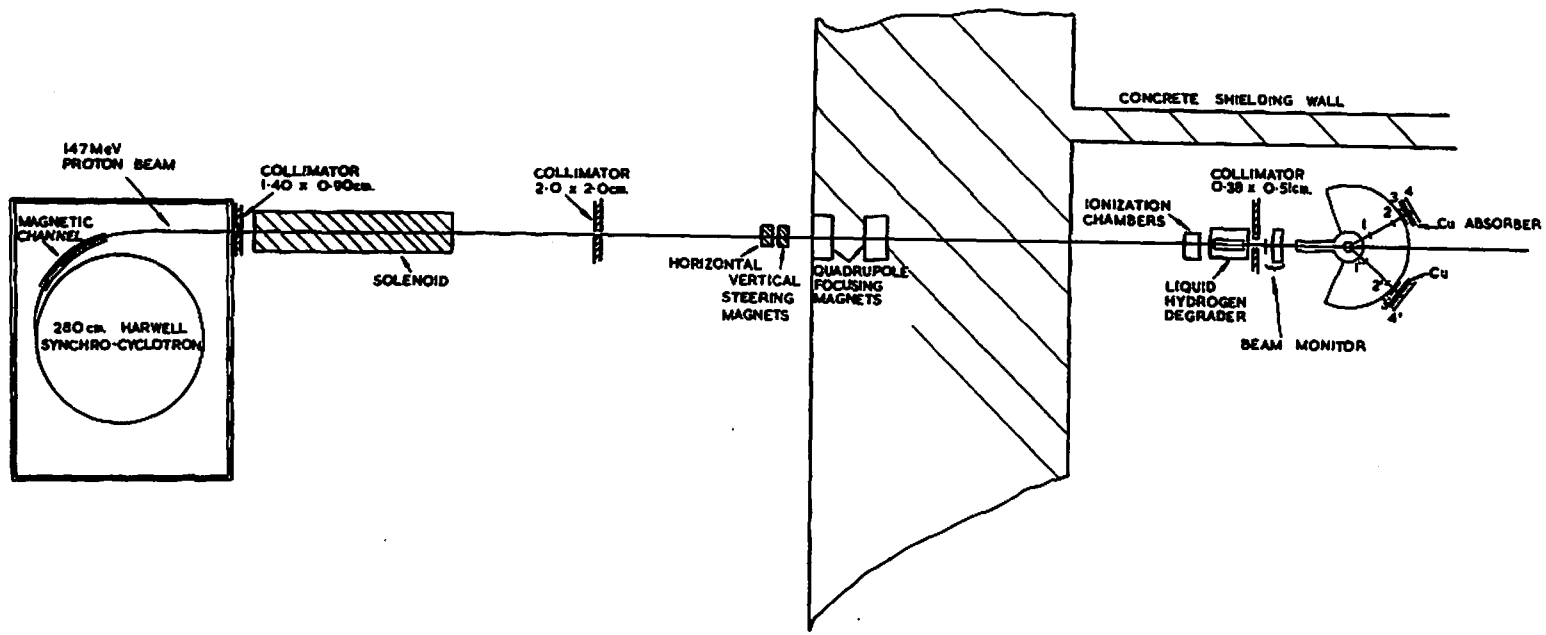
147MeV
PROTON BEAM
MAGNETIC
CHANNEL
280cm. HARWELL
SYNCHRO-CYCLOTRON
COLLIMATOR
1·40 x 0·90cm.
SOLENOID
COLLIMATOR
2·0 x 2·0cm.
HORIZONTAL
VERTICAL
STEERING
MAGNETS
QUADRUPOLE
FOCUSING
MAGNETS
CONCRETE SHIELDING WALL
IONIZATION
CHAMBERS
COLLIMATOR
0·38 x 0·51cm.
LIQUID
HYDROGEN
DEGRADER
BEAM MONITOR
1
2
3
4
Cu ABSORBER
Cu

SCHEMATIC [illegible]

pump. A sectional drawing is shown in FIG. 23. The hydrogen was in a cylinder of stainless steel suspended directly from two 15 cm lengths of thin wall (0.010 cm) cryogenic stainless steel tubing. A steel saddle tank containing liquid nitrogen shielded the bottom and sides of the hydrogen vessel from radiation losses. The top radiation shields were sheets of silver plated copper, which were allowed to touch the suspension tubes of the H_2 vessel in order to reduce the heat input to the liquid hydrogen by tying the tubes to the temperature of liquid nitrogen at this point. The end radiation shields were of 0.006 mm Al foil, with a vertical slit, to make it possible to see the level of the H_2 in the inner container through the transparent plastic windows.

The overall length of the cryostat was 60 cm, however several different inner containers were used with window sizes varying from 4 to 6 cm. In the final stages of development, the level of the liquid hydrogen dropped by less than ~ 5 cm in 30 hours.

5.2 Thin Film Windows for Liquid Hydrogen Containment [40]

An ideal window for use on a liquid hydrogen degrader would have the properties of:

(i) transparency, to make alignment and hydrogen level determination as simple as possible.

(ii) being unaffected by radiation.

(iii) low atomic number.

(iv) being readily demountable (or replaceable) when required.

(v) minimal thickness consistent with adequate strength.

Several techniques are known which fulfil some of these requirements. Methods based on the use of epoxy resins

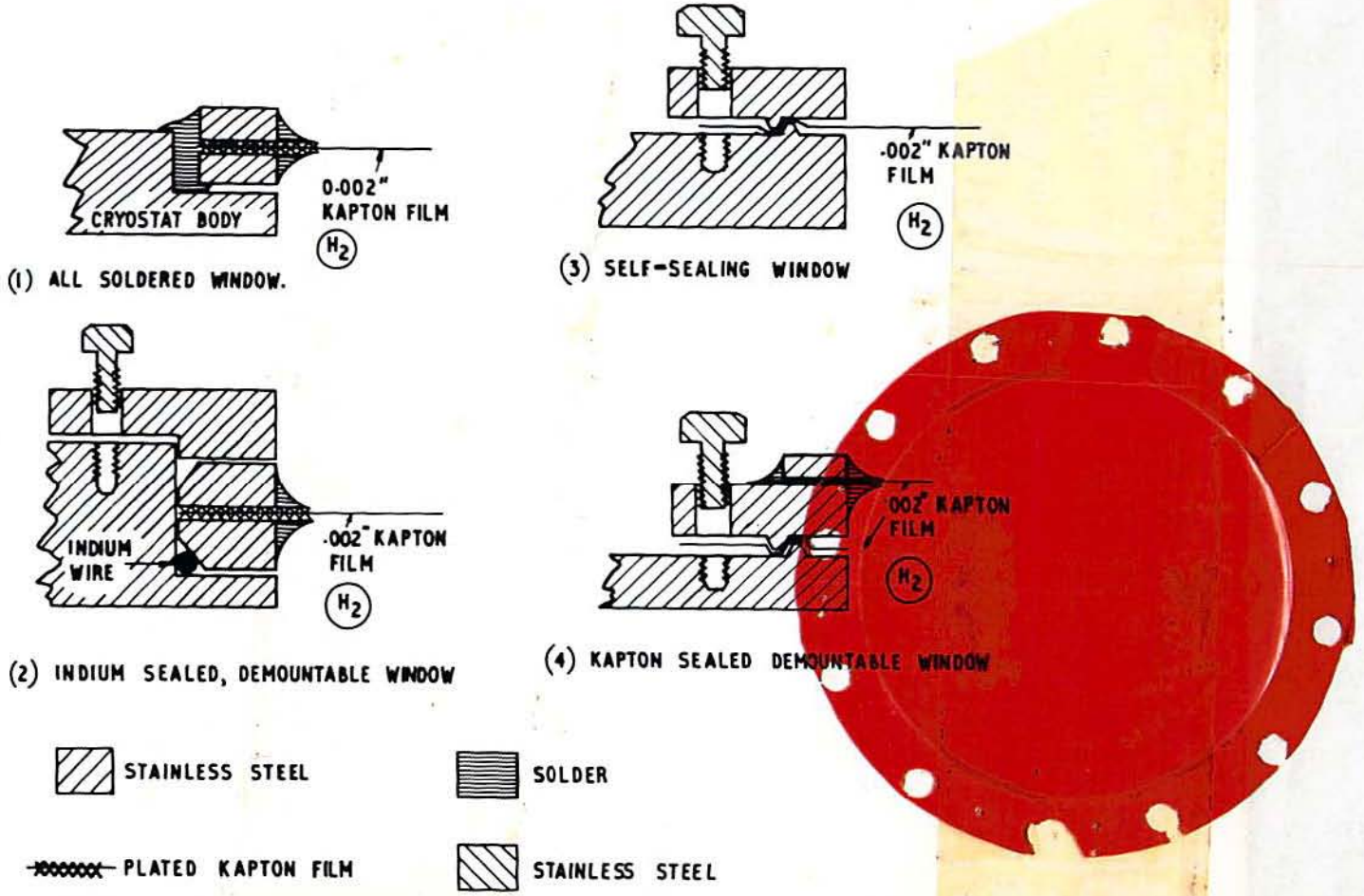

WINDOW SEALING METHODS USED FOR LIQUID HYDROGEN CONTAINMENT.

FIG. 24

have been published by several writers. Mylar has been used to construct liquid helium vessels,[140] and for direct attachment to a metal liquid helium container.[141]

It is not easy to make a demountable or easily replaceable window in this way. An alternative approach is to use a mechanical seal. Warschauer has described[142] a demountable window of this type, where an 0.013 cm sheet of polyethylene is used. The sheet is held onto a flat greased surface on a vessel by a metal collar, which is drawn down onto the sheet by bolts. Astrov[143] has described a similar technique for sealing a solid brass disc to a brass liquid helium container.

Mylar loses its mechanical strength under continued irradiation and a better material has been developed by Du-Pont. This is known as Kapton H-film, and is a polyamide of chemical composition[144] $[C_{22}\ H_{10}\ N_2\ O_4]n$. The mechanical strength of unirradiated Kapton exceeds that of Mylar at all temperatures,[145] and retains a degree of flexibility even at liquid helium temperatures.

Unlike Mylar, Kapton initially increases in strength under irradiation. Tests have been made to measure the effect of radiation[144] on the mechanical strength of Kapton and Mylar, and it has been found that Kapton is $\sim$50 $\times$ less sensitive to radiation than Mylar.

Several different techniques have been tried using Kapton windows to enclose liquid hydrogen. These are illustrated in FIG.24. FIG.24 (3) is a mechanical seal, using the same Kapton to act as both gasket and window. Two mating rims of truncated triangular section are cut onto the faces of the steel hydrogen vessel and a steel retaining collar, and the seal made by bolting the collar down onto the Kapton. This

technique has been found successful, but the use of 0.005 cm film is hazardous, as the mating rims tend to cut into the surface of the film. When using 0.013 cm film no such cutting was observed. This window is easily demountable, and fulfils requirements (i) - (iv). It is necessary to use comparatively thick Kapton, and this is the main disadvantage of the technique.

In order to reduce the thickness of Kapton required, the window sealing was achieved in two stages, the first being the seal between the Kapton and a mounting ring and the second the seal between this mounting ring and the hydrogen vessel. The technique adopted was to solder the metal-coated Kapton to stainless steel rings or collars, and then attach the steel mountings to the hydrogen vessel.

Tests were carried out by the Optical and Electrical Coatings Co. of Reigate, Surrey. They showed that it was possible to evaporate a thin layer of metal onto 0.005 cm Kapton without damage. Mylar of the same thickness was found to suffer damage. Attempts to deposit a layer of solder directly onto the Kapton were not successful, as the adhesion of the evaporated layer was low. Satisfactory adhesion was obtained by evaporating a Nickel-Chromium alloy as a substratum and coating this layer with evaporated gold. The total thickness of metal deposited on each side of the Kapton was $\sim 6.10^{-5}$ cm. Transparent areas were retained by suitable masking during the evaporation. The coating separated from the Kapton at $\sim 250^{\circ}$ C, but prolonged heating at $\sim 150^{\circ}$ C and above could also cause separation. By using a layer of gold over the Ni/Cr it was found possible to solder the metallised film

to stainless steel rings and collars. This could be done rapidly by using orthophosphoric acid as flux and 62 % Sn/ 38 % Pb Binary Eutectic solder. This solder was supplied by Enthoven Solders Ltd. to the American specification QQs 571D.

The window shown in FIG.24 (1) was made by soldering stainless steel rings 3 mm wide, 1 mm thick, and 4 cm in diameter to both sides of a piece of metallised 0.005 cm Kapton. This assembly was then soldered onto the hydrogen vessel using the same flux and solder. A vessel using this type of window has been cycled $\sim$30 times between the temperatures of room and liquid hydrogen with no degradation of the seals. This type of window may be removed intact although with some difficulty, and re-used.

The most difficult seal to make is that between Kapton and the rings, and a more readily removed window may be made by using an indium compression seal between rings and the vessel. Such a seal is shown in FIG.24 (2), and has been found to be still satisfactory after 3 cycles between room and liquid hydrogen temperatures. This type of window is rapidly reassembled, unlike Type (1), but the indium tends to hold rings and vessel firmly together after a few cooling cycles. This frequently makes it necessary to break the Kapton window in order to remove the window assembly when replacement is desired.

The best features of the window sealing methods described are combined in the design of FIG.24 (4). Here the load bearing seals are soldered joints, and the gasket seal is Kapton. The large thermal capacity of the collar shown in FIG.24 (4) makes it difficult to solder the metallised Kapton to the collar without the metallic layer separating from the

Kapton. The design illustrated has been found to work, but it may be improved in several ways. A first improvement would be to use 0.013 cm Kapton for the mounting gasket, as the thickness of the gasket is not important. A second improvement would be to use the layout of FIG.24 (2) to apply the sealing pressure, which then allows the use of thin rings of low thermal capacity.

The four types of window discussed have differing advantages and disadvantages, however the Type (4) window incorporating the suggested improvements should be suitable for most applications.

All the types shown in FIG.24 have been used successfully in experimental runs.

5.3 Liquid hydrogen target

The liquid hydrogen target used for the 98 Mev experiments was a cryostat of conventional vertical design. A 1.5 litre hydrogen container was suspended inside a radiation shield containing liquid nitrogen. The shield was attached to the hydrogen vessel suspension tube to reduce the heat input to the liquid hydrogen. The liquid hydrogen used to scatter the proton beam was contained in an 8 cm diameter right cylinder of 0.005 cm Kapton fixed to a brass frame by a Ciba epoxy resin [Ax 111, Ay 111].

The vacuum region is extended by an 8 cm diameter tube to a distance of 50 cm upstream from the centre of the scattering chamber. A mechanical seal is used to attach a 0.005 cm Kapton window to the end of this tube. The scattered beam exit window in the brass is 8 cm high, and extends round the lower part of the cryostat to $\pm 90^{\circ}$ on each side of the beam line. A window of 0.005 cm Kapton is fixed to the outside of

the cryostat by [Ax 111, Ay 111] epoxy resin.

5.4 Experimental Layout

The layout of the experimental apparatus used for scattering experiments with a polarised beam is shown in FIG. 22. The 144 Mev polarised proton beam is produced by scattering at 10.8° [57] from an aluminium target inside the cyclotron. It is then extracted through a magnetic channel which, in conjunction with a collimator at the exit from the vacuum vessel, passes a beam with an energy width of about 2 Mev (F.W.H.M.). For these experiments a spin precession solenoid (as described in chapter III) was used to precess the plane of the incident polarisation vector.

Quadrupole magnets were used to focus the beam, and steering magnets used to position the beam spot at the required position. The beam monitor detected coincidences of scattered and recoil particles from elastic scattering events at 90° c of m in a 0.5 mm sheet of CH_2 . Aluminium absorbers were used to reduce the background and random coincidences. The polarisation vector of the incident beam was in the vertical plane for these experiments. The monitor was also in a vertical plane, and was therefore unaffected by reversals of direction of the incident beam polarisation.

A low (but constant) background counting rate (~0.7 counts/min.) was recorded by cosmic rays coming vertically downward, causing coincidences between the counters.

The liquid hydrogen degrader was placed downstream of the beam monitor, and a pair of differential ionisation chambers [116] positioned immediately after the degrader. These chambers were used to hold the centre of gravity of the beam at a stable and repeatable position, to a precision of <0.1 mm.

The defining collimator was mounted after the ionisation chambers, 3 cm from the forward extension of the hydrogen target vacuum chamber.

The hydrogen target was mounted over the centre of curvature of a 94 cm radius scattering table which was marked out at intervals of 1^{o} round the circumference. Eight scintillation counters were used, four on each of two movable arms pivoted under the target mounting plate. E.M.I CV2316 photomultiplier tubes were used with short perspex light guides and NE102A plastic scintillatiors. There were two defining scintillators (2,3) on each arm, one (2) subtending about half the solid angle of the other (3). A front counter (1) was used to limit the counter telescopes to seeing only the region near the target. In order to reduce counting losses in the arms, 0.05 cm NE102A plastic scintillation material was used for counters 1-3 on each arm. A large counter (4) of 0.25 cm NE102A was mounted after the two defining counters (2 and 3). Energy discrimination was obtained by requiring triple coincidences 1 2 4 and 1 3 4, and placing copper absorbers between 3 and 4.

The angular settings of the counter telescope arms were made by using a set square against a standard position on each arm, and referring to the angular scale machined into the scattering table. The set square was attached to a block engraved with a matching angular scale, subdivided at intervals of $1/20^{o}$ and $1/50^{o}$. It was found possible to set and reset the angular position of the arms to $\pm 0.02^{o}$ when using this method of defining their position.

The counting electronics were very simple, and are shown in FIG.25. The photomultiplier output pulses were fed

FIG. 25

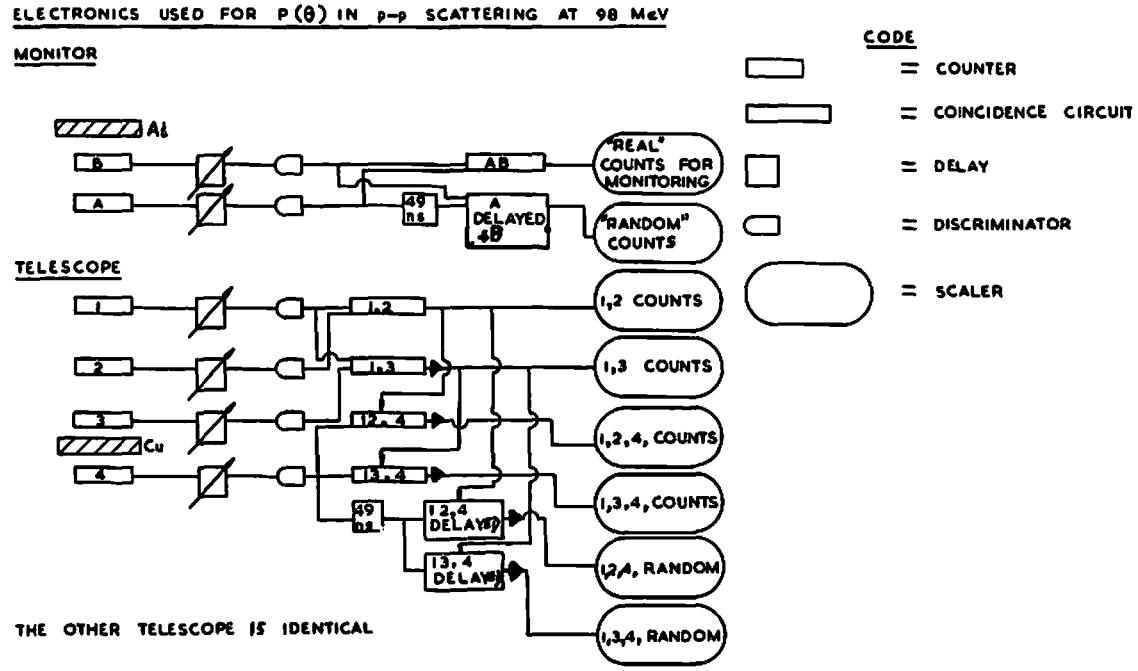
ELECTRONICS USED FOR P(θ) IN p–p SCATTERING AT 98 MeV
MONITOR
Al
b
A
AB
49 ns
A DELAYED 4θ
"REAL" COUNTS FOR MONITORING
"RANDOM" COUNTS
TELESCOPE
1
2
3
Cu
4
1,2
1,3
2,4
3,4
49 ns
1,2,4 DELAYED
1,3,4 DELAYED
1,2 COUNTS
1,3 COUNTS
1,2,4, COUNTS
1,3,4, COUNTS
1,2,4, RANDOM
1,3,4, RANDOM
THE OTHER TELESCOPE IS IDENTICAL
CODE
= COUNTER
= COINCIDENCE CIRCUIT
= DELAY
= DISCRIMINATOR
= SCALER

to 10 MHz discriminators, and then to fast coincidence circuits with a resolving time of $\sim$18 ns. the random triple coincidence rate was estimated by recording triple coincidences with 4 delayed by an extra 49 ns, the time interval of the fine structure of the proton beam.

VI Experimental methods and results at $\sim$ 98 Mev

6.1 Experimental method for polarisation work

The technique used for these polarisation measurements has been referred to in 1.3, 2.1, 3.1, and 4.4; and is described in detail in 8.3. The two essential features of the method are:

(1) To collect data simultaneously at equal scattering angles on each side of the beam.

(2) To collect data using both signs of the incident polarisation alternately.

It is shown in 8.3 that (1) and (2) combined make it possible to measure a scattering asymmetry $\varepsilon(\theta)$ independently of the efficiency of the counter telescopes, of the monitor, and to a certain degree the beam zero angle assumed. θ refers to the opening angle between the arms. The experimental counts are combined to give a quantity r, where:

(31) $$r^2 = [LU.RD]/[LD.RU]$$

and for example, LU refers to the coincidence counting rate recorded in the arm set at θ_L° on proton left, and taken with positive (UP) incident beam polarisation. Then:

(32) $$[(\theta_L + \theta_R)/2] = [r-1]/[r+1] \pm [1-\varepsilon^2]/\ N$$

where N = the sum of the four counts LU etc. [see 8.4]

A solenoid was used to reverse the direction of the incident polarisation vector ($\underline{P}$). The precession effect is described in 8.9. The current through the solenoid required to reverse $\underline{P}$ was found experimentally.

A thick (~ 2 gm/cm^2) carbon^{12} target was placed over the pivot of the scattering table, and the liquid hydrogen degrader and final collimation removed from the beam line. The two scattering arms were then set at equal angles (θ_L , θ_R) to the beam zero. The asymmetry:

$$\varepsilon(\theta) = \frac{1 - N(\theta_L) / N(\theta_R)}{1 + N(\theta_L) / N(\theta_R)} \qquad (33)$$

may then be measured as a function of solenoid current (I) when ε (I) will be equal to $\underline{P}$ (I) . $\underline{P}$ [$= P_\perp P\cos(\theta)$] where P is the polarisation produced in p-C^{12} scattering. The graph of ε v I will be a cosine curve, with maximum values when the polarisation vector $\underline{P}$ has been precessed by zero or π . The results of this measurement are shown in FIG. 15, and the required currents for this experiment are zero and 1500 Amps. The current in the solenoid was held constant to within 25 Amps which corresponds to a negligible variation in the measured asymmetries. The measurement was repeated at $\sim$ 100 Mev with the final collimation in place, before each experimental run as a check on the correct functioning of the solenoid.

The solenoid technique for measuring asymmetries is sensitive to only one main source of systematic error. This is the possibility of shifts in beam position (and to a lesser degree, shape) between the settings OFF and 1500 Amps . The effects are considered in detail in 8.5. Any effects due to beam spot shape changes were minimised by

TABLE 6

Counter Telescopes for ~ 100 Mev scattering

Counter	Thickness	Width	Height	Radial Distance Wide Angles	Radial Distance Small Angles
1	0.05 cm	6.36	7.12	49.5	-
	0.05 cm	3.55	7.11	-	100.3
1'	0.05 cm	6.33	7.11	49.5	-
	0.05 cm	3.55	7.10	-	100.3
2	0.05 cm	2.170	4.437	100.2±0.2	248.0±0.4
2'	0.05 cm	2.160	4.445	100.4±0.2	247.6±0.4
3	0.05 cm	3.580	7.168	110.4±0.2	258.1±0.4
3'	0.05 cm	3.544	7.086	110.5±0.2	257.8±0.4
4	0.25 cm	7.6	11.2	114.0	264
4'	0.25 cm	7.6	11.2	114.0	264

Dimensions of 2, 2' measured to ± 0.005 cm.

3, 3' measured to ± 0.020 cm.

TABLE 7

Zero angles deduced from angle scans

Telescope	Solenoid	Arms	Hydrogen target	Zero Angle°
Primed	1500 Normal	Wide	Empty	23.126 ± 0.0025
Unprimed	1500 N	Wide	Empty	23.157 ± 0.0025
Unprimed	Off	Wide	Empty	23.152 ± 0.0025
Unprimed	1500 N	Small	Full	23.080 ± 0.0033
Primed	1500 N	Small	Full	23.115 ± 0.0025

Beam shift between solenoid ON and OFF: -0.005 ± 0.003°

FIG. 26

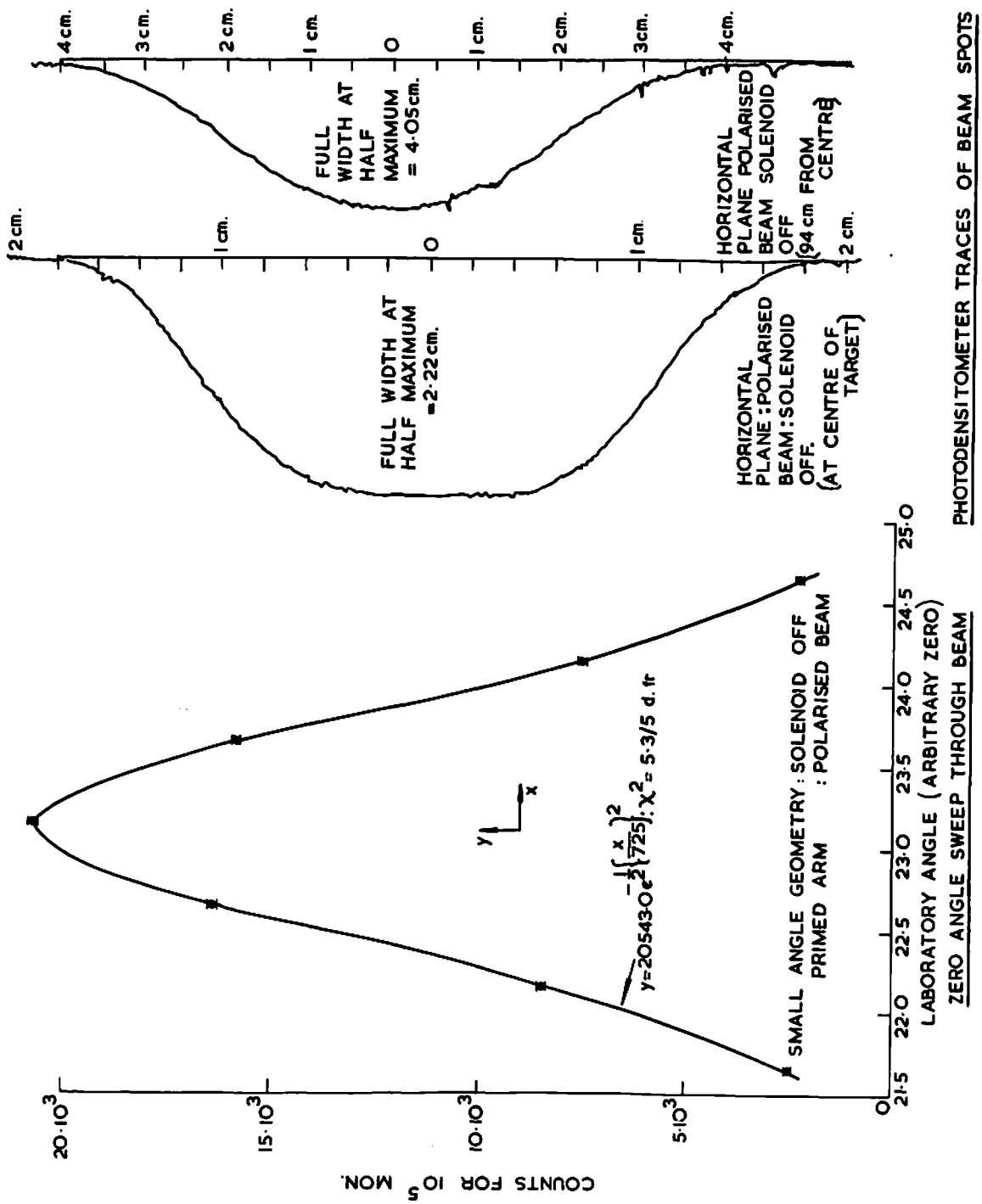
4 cm.
3 cm.
2 cm.
1 cm.
0
1 cm.
2 cm.
3 cm.
4 cm.
FULL WIDTH AT HALF MAXIMUM = 4·05cm.
HORIZONTAL PLANE POLARISED BEAM SOLENOID OFF (94 cm FROM CENTRE)
2 cm.
1 cm.
0
1 cm.
2 cm.
FULL WIDTH AT HALF MAXIMUM =2·22 cm.
HORIZONTAL PLANE: POLARISED BEAM: SOLENOID OFF. (AT CENTRE OF TARGET)
PHOTODENSITOMETER TRACES OF BEAM SPOTS
COUNTS FOR 10^5 MON.
20·10^3
15·10^3
10·10^3
5·10^3
0
21·5
22·0
22·5
23·0
23·5
24·0
24·5
25·0
LABORATORY ANGLE (ARBITRARY ZERO)
ZERO ANGLE SWEEP THROUGH BEAM
SMALL ANGLE GEOMETRY: SOLENOID OFF
PRIMED ARM : POLARISED BEAM
y=20543 e^{-½[x/725]^2}: χ^2 = 5·3/5 d.fr
y
x

the use of a final collimator, that defined the beam spot. The shapes of beam spot for solenoid OFF and 1500 Amps were measured by taking photodensitiometer traces from X-ray films exposed in each of the two beams. The shapes were identical, and therefore only the traces from films taken with the solenoid off are shown in FIG. 26. The beam shifts between the two solenoid settings were reduced by aligning the solenoid accurately along the beam line, to less than 0.5 mm at the position of the scattering target for $\sim$100 Mev beams.

The beam zero positions for each of the two counter telescopes were found by scanning the curves through the direct beam (much reduced in intensity) using a single counter as a monitor. The dimensions and radial positions of the counter telescopes used for $\sim$100 Mev measurements are listed in TABLE 6, and the zero angles measured in the above manner in TABLE 7. A plot of the beam profile detected by counter 3 in this measurement is shown in FIG 26. The beam profiles were also measured by taking X-ray photographs at the target position and also near the position of counter 3. The trapezoidal shape at the target centre becomes a good Gaussian due to air scattering before reaching counter 3. When the finite size of counter 3 is included, the Gaussian form given by the angle scan is obtained.

The energy spectrum of the beam incident on the target was examined using a lithium drifted germanium counter, loaned by C.Whitehead. This counter was $\sim$5 cm deep, and could stop protons of up to $\sim$ 120 Mev in the active region. The pulse height distribution obtained with the counter is shown in FIG. 27. The variation of the pulse height with energy

FIG. 27

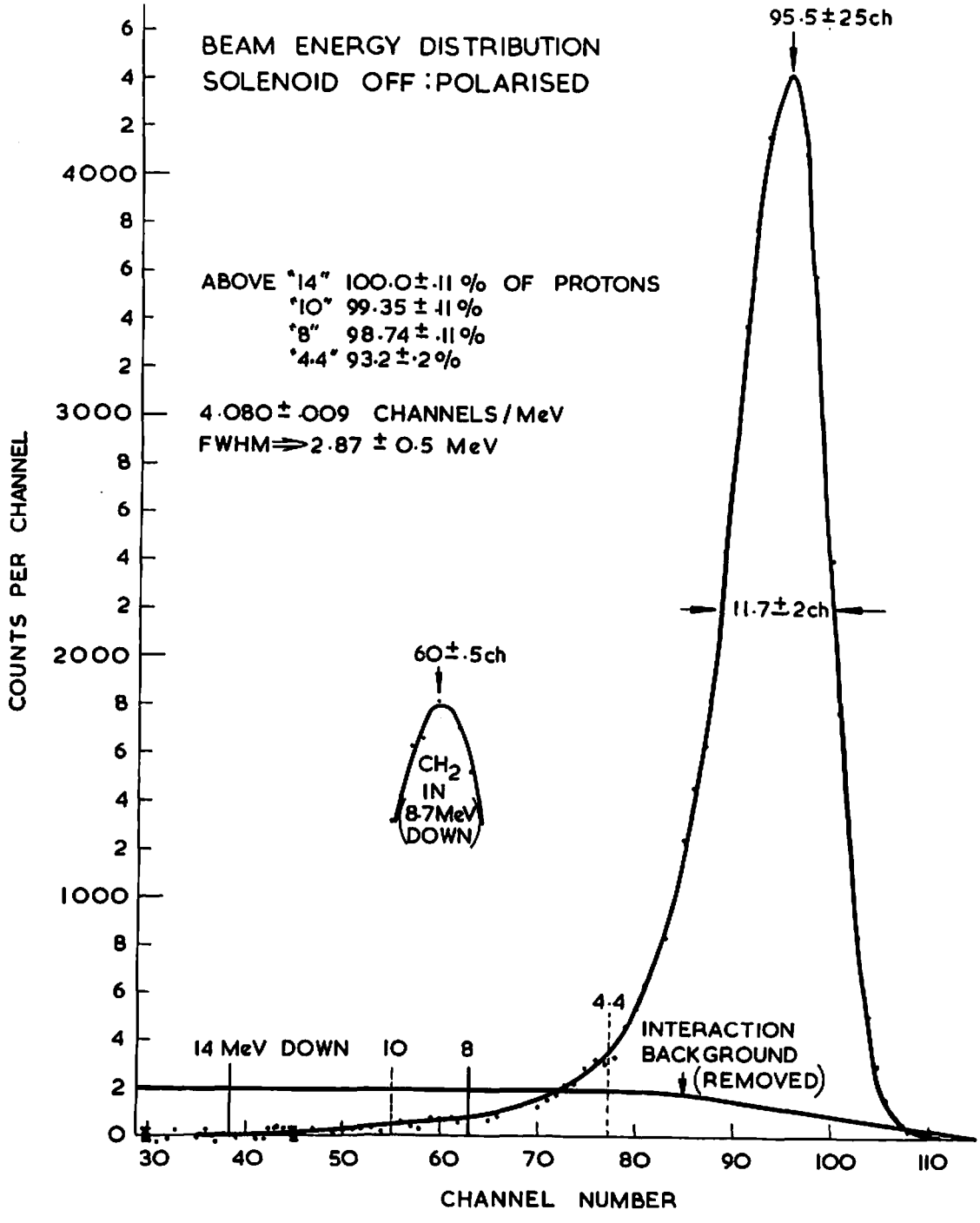

PROTON ENERGY DISTRIBUTION IN DEGRADED BEAM.

was determined by adding a CH_2 shim of accurately known surface density after the final collimator. The interaction background was estimated by considering the constant distribution of pulse height below channel 30 to be all background. It was assumed that the size of the interaction background at a given energy would depend on the number of protons in the beam of higher energy. These assumptions were used to subtract background effects. These estimates are not precise, and the quoted percentages of protons in the beam below a given energy are subject to errors from this source in addition to those quoted.

The spectrum shown is that obtained for the beam used for 98 Mev p-p polarisation measurements; FIGS.26,27 both refer to this beam. For p-C^{12} measurements, a slightly longer degrader was used, which gave an incident beam a few Mev less in energy. The shapes and spectra obtained using this second degrader were not appreciably different.

When making measurements of the asymmetry after scattering from a target, it is necessary to correct for the effect of asymmetries arising from other material in the path of the beam, as is also seen by the telescopes [see 8.6]. As these background asymmetries are measured with the scattering material (hydrogen or carbon) in the target chamber removed, they are necessarily measured at a higher energy than that at which the correction must be applied. Extra absorber is used to select the same scattered protons, but the extra absorption in this copper is negligible. The energy dependence of the measured background asymmetry and its magnitude is taken to be that found in p-C^{12} scattering. About two thirds of the material in the beam that gives

TABLE 8

Background Fractions for 98 Mev P(θ)

Lab. Angle°	Arms	Measured %	Calculated % from C'' data	Fr. of background from downstream of target(X)
8	Small	30	29	0.88±0.03
10	Small	22	21	0.86±0.03
12.5	Small	15	14	0.83±0.03
	Wide	20	17	0.86±0.015
15	Small	9	10	0.82±0.03
	Wide	12	12	0.85±0.015
17.5	Wide	8	8	0.835±0.015
20	Wide	4	6	0.82±0.015
22.5	Wide	3	4	0.81±0.015
25.4	Wide	1.9	2.0	0.80±0.015
27.5	Wide	1.5	1.3	0.79±0.015
30				0.79±0.015
35				0.77±0.015
40				0.75±0.015
45				0.75±0.015

rise to background effects is carbon[12], however the remainder is made up of the oxygen and nitrogen in the air and Kapton and the 0.0007cm aluminium radiation shields. Although the aluminium gives rise to less than 5% of the background, and oxygen and nitrogen are expected to behave in a manner reasonably similar to that of carbon[12], it is somewhat surprising that both the magnitude (TABLE 8) and the asymmetry (FIG.29) observed in the background are similar to that expected if all the material were carbon.

6.2 Carbon data for background corrections

In FIG. 30 the data of Dickson and Salter[129] (as renormalised by Jarvis and Rose[50]) is compared with the background asymmetries measured using the empty hydrogen target. The Copper absorbers were set to strongly attenuate protons 17.5 Mev down in energy from the mean energy of the incident beam.

In TABLE 8, the data of Mark et al[130] - shown in FIG.28 - is used to calculate the ratio of counts from the empty hydrogen target to the counts from hydrogen only. In order to make this estimate (which is of poor precision), the proportion (x) of the total background which originates downstream of the hydrogen (and thus at a lower energy than that at which the background is measured) must be found. This was done by measuring the simulated effect on the background counting rate of the various pieces of Kapton and aluminium in the target at one angle for both of the two counter geometries used, and calculating the angular variation of x. This makes some allowance for the effect of finite beam size, although the extra angular divergence produced by the target is not negligible.

The corrected values of the background asymmetry

FIG. 28

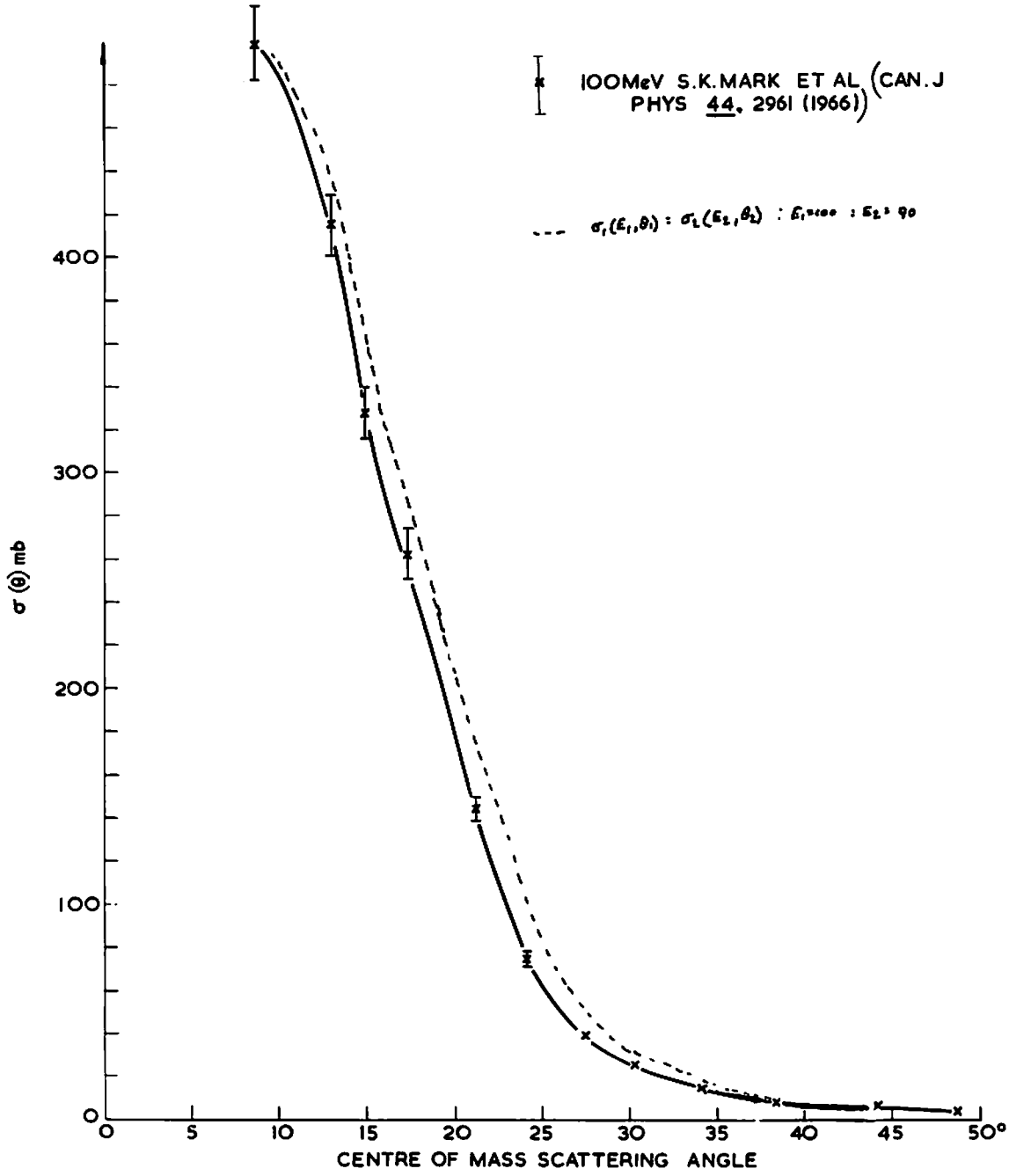

DIFFERENTIAL CROSS SECTION OF P - C^{12} SCATTERING INCLUDING 4·4, 7·6, 9·6 MeV LEVELS

and background fraction (f)* for any given angle (θ) are:

(33) $f' = f(1 + x [(1/\sigma).(d\sigma/dE)] \Delta E)$

(34) $\epsilon'_{CH} = \epsilon (1 + x [(1/P).(dP/dE)] \Delta E)$

where ΔE is the energy thickness of the target, x is the proportion of the background requiring correction, and σ and P are the differential cross-section and polarisation of carbon at the angle (θ).

Several different ways of estimating

$[(1/\sigma).(d\sigma/dE)]$(=d) and $[(1/P).(dP/dE)]$(=e)

are possible. The data of Dickson and Salter at 95 and 135 Mev[129] are on the same absolute scales, and the values of both d and e may be obtained to a reasonable precision. The angular range of this data is limited, especially at 95 Mev. In order to bridge these gaps, other p-C^{12} data is used, together with some new measurements.

The recent precise 100 Mev data of Mark et al[130] is used to estimate d. The inelastic levels up to 10 Mev are included. Given the value of the cross-section (σ) at an energy E, and angle θ, the optical model may be invoked to estimate the cross-section at an angle θ' and an energy E' by considering the shrinking of the diffraction peak. The relation is:[150]

(35) $\sigma (E , \theta) = \sigma (E' , \theta')$ where $\theta \sqrt{E} = \theta' \sqrt{E'}$

This relation has been used to estimate the variation of cross-section with angle at 90 Mev. These two curves are plotted on FIG.28, and the values of d obtained listed in TABLE 10 at the end of the section.

The poorly determined absolute scale of the Dickson and Salter polarisation data, together with the poor precision of the relative data at 95 Mev, makes it inadvisable

*see 8.6

to use these data in conjunction with the data of Rolland [131] et al to derive values of e for all angles.

The polarisation in elastic proton scattering from C^{12} was therefore remeasured at 93.7 ± 0.3 Mev.

A target of pile graphite, 1.050 gm/cm^2 thick, was used with an early form of H_2 degrader. This gave an energy of 93.7 ± 0.3 Mev at the centre of the carbon. This energy was deduced from a range curve taken in copper in conjunction with the revised Sternheimer range tables of Ref. (105).

It was necessary to use accurately calculated thicknesses of copper as absorbers to attenuate the 4.4 Mev inelastic level of C^{12}. A computer programme (described in 8.8) was used to calculate the required copper absorbers, taking into account the finite size of the beam spot, the intensity distribution across the beam, the energy losses in air etc. and their variation with angle.

The data was taken in the manner described in 6.1. The lower vacuum chamber of the hydrogen target was used with 0.005 cm Kapton windows. The wide angle geometry was used but the front counters (1,1') were replaced with the 3.55 cm counters (1, 1')from the small angle arms to reduce background coincidences to a minimum. The value of x was 1.00, and the background fraction did not exceed 2% at even 9° Lab. Due to the consistency of the background with previous carbon data and the agreement between the background and C^{12} asymmetries, no background correction was required. Allowance was made for the small errors introduced by this assumption.

Two corrections were made that have not previously been discussed here. The finite size of the scintillator

FIG. 29

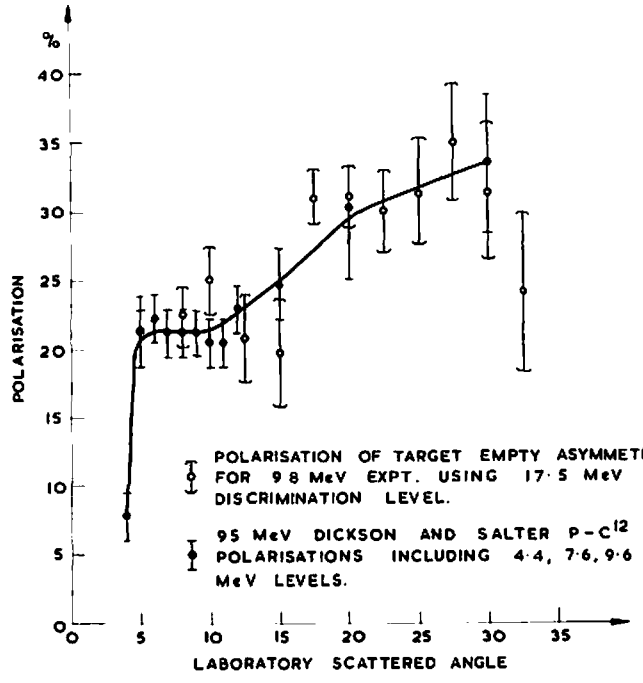

COMPARISON OF BACKGROUND ASYMMETRY WITH P-CARBON DATA.

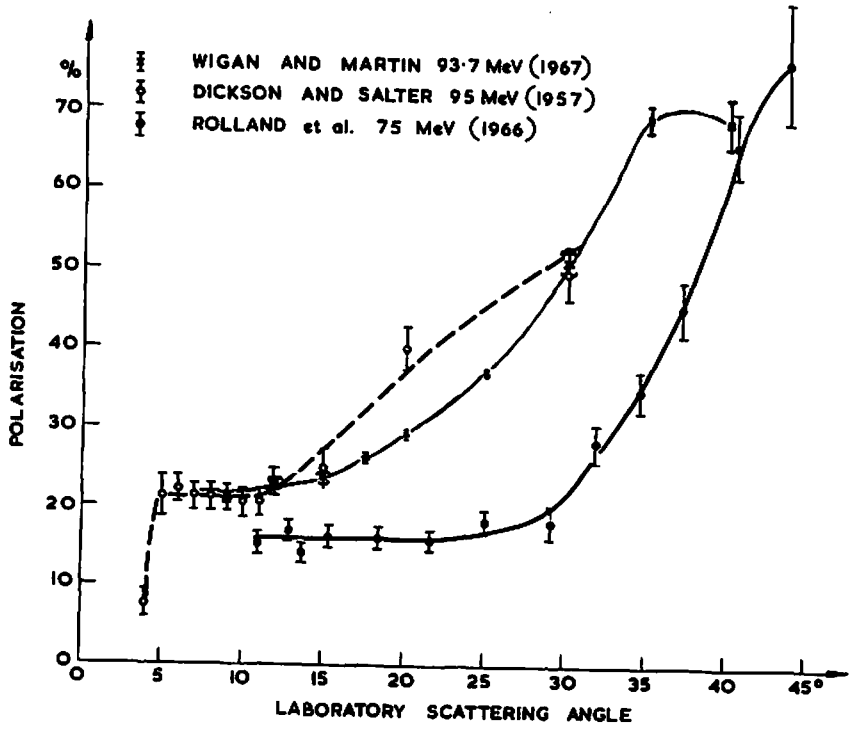

POLARISATION IN ELASTIC P-C12 SCATTERING : 75-95 MeV.

FIG. 30

dilutes the measured polarisation, as scattering events out of the horizontal plane may be recorded. This correction is discussed in 8.7.

The multiple coulomb scattering in the carbon target also dilutes the polarisation. The amount of this multiple scattering was calculated using the method described by Cormack[148] and the correction for the measured asymmetries deduced. An arbitrary error of 50% was ascribed to this calculation.

The results are shown in FIG. 30, and a tabulation of the data, main corrections, and results is listed in TABLE 9. The agreement with Dickson and Salter (as renormalised by Jarvis and Rose) is fairly good. The precision of the data, together with the 0.85% precision of the absolute scale of the polarisation, is adequate to use in conjunction with the Rolland data to calculate e(= [1/P].[dP/dE]). The points labelled 'Rolland' in FIG. 30 are the results of combining published data over ranges of 1^{o}.

The various estimates of d and e are tabulated in TABLE 10 together with the values adopted for the correction of the 98 Mev p-p polarisation data. An arbitrary 50% error is associated with these estimates of e and d.

6.3 Preliminary measurements of p-p polarisation at 93.2 ± 0.3 Mev

The same apparatus used for p-C^{12} polarisation measurements was used to examine the problems expected to arise in the measurement of p-p polarisation. The asymmetries to be measured were ~ 0.040, compared with a minimum value of ~ 0.110 for p-C^{12} elastic scattering.

The wide angle geometry, with the small angle counters

Asymmetries in elastic p-C^{12} scattering at 93.7 ± 0.3 Mev

Lab Angle°	Raw Asymmetry	Beam Shift	Finite Size	Multiple Scattering	Result	Polarisation* %
9	0.1025±0.0014	0.000	0.0007	0.0044±0.0022	0.108±0.0026	21.2±0.55
12	0.105 ±0.0019	0.0003	0.0005	0.0025±0.0012	0.108±0.0023	22.9±0.5
15	0.110 ±0.0028	0.0003	0.0003	0.0017±0.0009	0.112±0.0030	23.7±0.6
17.5	0.1215±0.0033	0.0004	0.0003	0.0015±0.0008	0.124±0.0033	26.3±0.7
20	0.1358±0.0027	0.0006	0.0002	0.0012±0.0006	0.138±0.0028	29.2±0.6
25	0.172 ±0.0023	0.0007	0.0002	0.0010±0.0005	0.174±0.0024	36.9±0.5
30	0.237 ±0.0067	0.0010	0.0002	0.0010±0.0005	0.240±0.0067	50.8±1.4
35	0.323 ±0.0081	0.0006	0.0002	0.0010±0.0005	0.325±0.0081	68.9±1.7
40	0.321 ±0.0148	0.0007	0.0001	0.0008±0.0004	0.323±0.145	68.4±3.1

*relative errors only: an absolute error of 0.85 % on the polarisation is not included here.

(109)

TABLE 9

Energy dependent corrections to asymmetries

$\Delta\varepsilon = \frac{1}{\varepsilon}\frac{d\varepsilon}{dE}$ is the fractional change in b.g. asymmetry/Mev

$\Delta\sigma = \frac{1}{\sigma}\frac{d\sigma}{dE}$ is the fractional change in b.g. fraction/Mev

Lab Angle°	Dickson and Salter		Mark+ $\alpha\sqrt{E}$	Rolland + Wigan, Martin	Values adopted with arbitrary 50% errors	
	$\Delta\varepsilon$ *	$\Delta\sigma$ *	$\Delta\sigma$ *	$\Delta\varepsilon$	$\Delta\sigma$ *	$\Delta\varepsilon$
8	-0.022	0.0054	-	-0.016	0.0054	-0.016
10	-0.028	0.0073	-	-0.016	0.0073	-0.016
12.5	-0.025	0.011	0.0094	-0.017	0.0094	-0.017
15	-0.028	0.012	0.0102	-0.019	0.0102	-0.019
17.5	-	-	0.0103	-0.022	0.0103	-0.022
20	-0.021	0.016	0.0165	-0.025	0.0165	-0.025
22.5	-	-	0.029	-0.027	0.029	-0.029
25.4	-	-	0.024	-0.027	0.024	-0.027
27.5	-	-	0.037	-0.031	0.037	-0.031

TABLE 10

Lab Angle°	Dickson and Salter		Mark+ $\delta\sqrt{E'}$	Rolland + Wigan, Martin	Values adopted with arbitrary 50% errors	
	$\Delta\varepsilon$ *	$\Delta\sigma$ *	$\Delta\sigma$ *	$\Delta\varepsilon$	$\Delta\sigma$ *	$\Delta\varepsilon$
30	-0.023	0.016	0.028	-0.031	0.028	-0.031

^{12}C(p,p) data used here

Dickson and Salter from ref. (129) at 95 and 135 Mev.

Mark et al from ref. (130) at 100 Mev.

Rolland et al refers to data shown in FIG. 29 at 75 Mev. [Ref. 131]

Wigan and Martin refers to measurement shown in FIG. 29 at 94 Mev. [Ref. 147]

* refers to data where the inelastic levels in p-^{12}C scattering have been included.

TABLE 10 continued

(1, 1′), was used to give a high counting rate. The background was minimised by this restriction on the region from which the telescopes could detect coincidences. The region of interest was restricted to angles of less than $\sim 20^{\circ}$. Beyond this angle the counter telescopes could not see all the hydrogen. Under these conditions the background coincidences were held to below 25% at 10° (Lab).

The effect of energy discrimination was studied by using copper absorbers to define two energy discrimination levels. These levels were set to remove protons that were 4.4 and 10 Mev down from the mean energy of the beam at the centre of the target. These levels were set close to the mean energy of the beam to test the consistency of the background estimation. The 4.4 level removed events from $\sim 7\%$ (see FIG. 28) of the protons in the incident beam.

The mean energy at the centre of the target was determined to be 93.2 ± 0.3 Mev by taking a range curve in copper, and using the revised Sternheimer range tables of Ref.(105). The mean thickness of the target was similarly determined to be 8.7 ± 0.3 Mev.

The experimental data was collected as described in 6.1. Measurements of the asymmetry were made when the target was full, and also when it was empty and evacuated.

The measured background fractions (f) and asymmetries (ε_{Bj}) were corrected by using equations (33) and (34). The energy dependence of f and ε_{Bj} were taken from TABLE 10.

It may be seen from TABLE 11 that the background corrected (hydrogen) asymmetries obtained using 4.4 and 10 Mev levels are in good agreement, but the background fraction for 4.4 level was found to be greater than that for 10 Mev.

P-P polarisation at 93.2 ± 0.3 Mev

Lab Angle° (centre of mass°)	(Target Full)	(Target Empty)	(corr. for B.G)	pooled	Polarisation %
10°(20.48°)	*0.05951 ± 0.0027	0.112 ± 0.005	0.0395 ± 0.0036	0.0388 ± 0.0025	8.22 ± 0.53
	**0.0524 ± 0.0023	0.098 ± 0.007	0.0376 ± 0.0033		
12°(24.57°)	*0.0534 ± 0.0017	0.102 ± 0.006	0.0443 ± 0.0021	0.0446 ± 0.0021	9.45 ± 0.44
15°(30.70°)	*0.0553 ± 0.0018	0.118 ± 0.008	0.0472 ± 0.0021	0.0476 ± 0.0027	10.08 ± 0.36
	**0.0551 ± 0.0023	0.112 ± 0.011	0.0476 ± 0.0028		
17°(34.78°)	*0.0575 ± 0.0025	0.126 ± 0.010	0.0517 ± 0.0027	0.0518 ± 0.0027	10.98 ± 0.57
17°.5(35.80°)	*0.0553 ± 0.0025	0.132 ± 0.010	0.0498 ± 0.0026	0.0519 ± 0.0 19	10.99 ± 0.40
	**0.0583 ± 0.0024	0.118 ± 0.014	0.0536 ± 0.0027		
17.25°(35.29°)	-	-	-	17 AND 17.5 COMBINED	[10.99 ± 0.31]
20°(40.90°)	*0.0578 ± 0.0025	0.149 ± 0.013	0.0535 ± 0.0016	0.536 ± 0.0015	11.36 ± 0.32
	**0.0567 ± 0.0025	0.130 ± 0.050	0.0535 ± 0.0034		

Also including multiple scattering, beam shift and finite counter size corrections.

Relative errors only, the absolute scale uncertainty of 0.85 is not included.

* = 4.4 level. ** = 10 level

TABLE 11

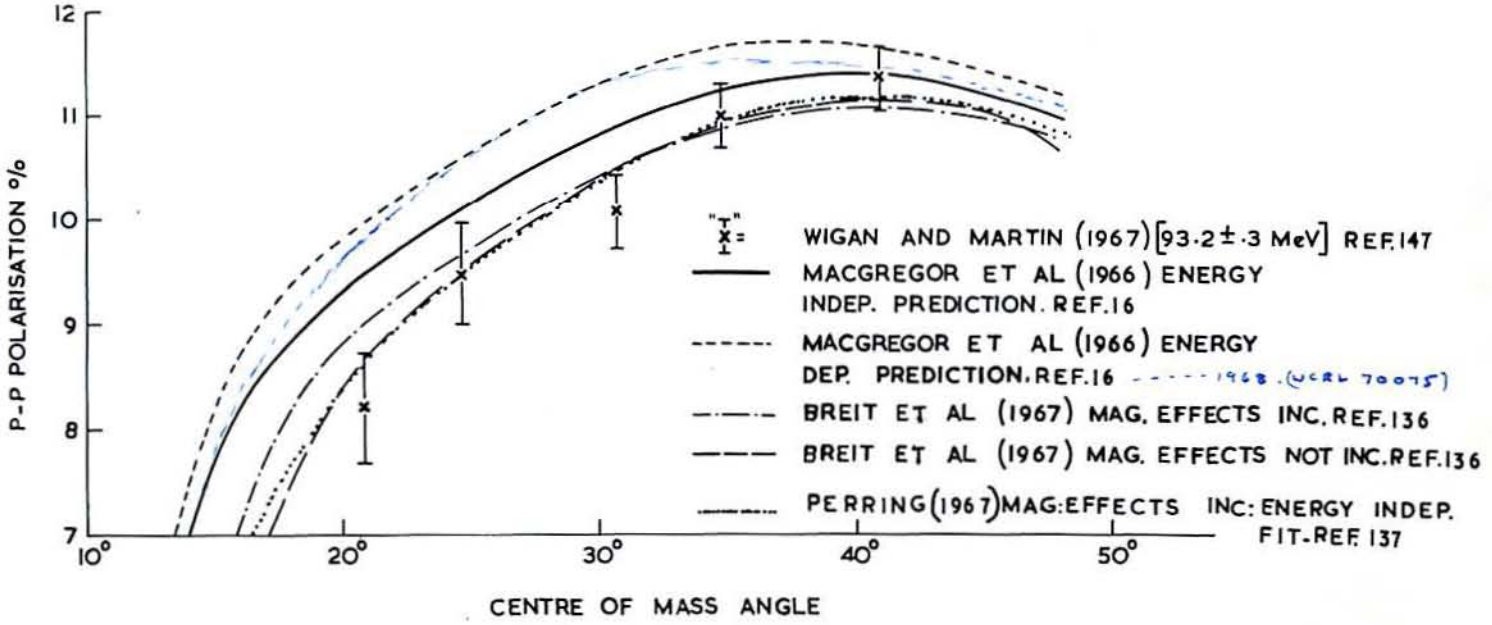
P-P POLARISATION %
12
11
10
9
8
7
10°
20°
30°
40°
50°
CENTRE OF MASS ANGLE
WIGAN AND MARTIN (1967) [93.2 ± .3 MeV] REF. 147
MACGREGOR ET AL (1966) ENERGY INDEP. PREDICTION. REF. 16
MACGREGOR ET AL (1966) ENERGY DEP. PREDICTION. REF. 16 ----- 1968. (UCRL 70075)
BREIT ET AL (1967) MAG. EFFECTS INC. REF. 136
BREIT ET AL (1967) MAG. EFFECTS NOT INC. REF. 136
PERRING (1967) MAG: EFFECTS INC: ENERGY INDEP. FIT-REF. 137

FIG. 31

In later experiments the levels were reduced to 8 and 7.5 Mev. The data for the two levels are then combined and the small corrections applied for the finite size of the scintillators, for multiple scattering in the hydrogen, and for the small shift in the beam between solenoid 'OFF' and '1500 Amps'. These results are in the 'pooled' column in TABLE 11. The results are plotted in FIG. 31, together with the phase-shift predictions of MacGregor[16] and Breit[136]. The fit of Perring[33] includes this data.

The conclusions drawn from this preliminary work were that (i) the telescopes should be able to see all the hydrogen at all angles, (ii) that the background at small angles would be very high unless a second set of more restricted telescopes were used, (iii) that energy discrimination so close to the mean energy of the beam was unnecessary.

6.4 P-P Polarisation measurement at 97.7 ± 0.3 Mev

The measurement of polarisation has been discussed several times, and only changes in the procedure will be described.

The mean energy of the proton beam at the centre of the hydrogen target was 97.7 ± 0.3 Mev, and the thickness of this target was 8.4 ± 0.3 Mev. These were determined by range curves in copper and the revised Sternheimer range tables of Ref. (105). The two telescopes are detailed in TABLE 6, and their ranges of application overlapped by 5°. Two energy discrimination levels were used to eliminate protons in the beam, 8 and 17.5 Mev below the mean beam energy.

In order to estimate the background as accurately as possible two methods of measurement and calculation were

TABLE 12

Basic Asymmetry Data at 98 Mev

Small Angle Arms

Lab. Angle:	Discrimination Level:	Target Full:	Target Empty:	Target Empty: CH_2 Shim in:
8	17.5	0.0509±0.0018	0.1 6±0.010	0.080±0.008
10	17.5	0.0575±0.0018	0.118±0.012	0.091±0.010
12.5	17.5	0.0546±0.0018	0.098±0.015	0.099±0.013
15	17.5	0.0564±0.0019	0.093±0.019	0.082±0.016
Wide Angle Arms				
12.5	8	0.0581±0.0022	0.127±0.008	
15	8	0.0612±0.0022	0.110±0.012	
17.5	8	0.0613±0.0022	0.128±0.012	
20	8	0.0619±0.0023	0.137±0.018	
22.5	8	0.0567±0.0023	0.186±0.025	
25.4	8	0.0530±0.0024	0.178±0.031	
30	8	0.0469±0.0020	0.1[illegible]2±0.041	
35	8	0.0336±0.0026	0.138±0.047	0.082±0.039
40	8	0.0154±0.0028	0.1[illegible]7±0.059	0.071±0.047
45	8	-.0066 ±0.0031	0.081±0.069	0.034±0.048
17.5	17.5	0.0612±0.0013	0.146±0.008	0.101±0.008
20	17.5	0.0608±0.0013	0.146±0.009	
22.5	17.5	0.0565±0.0013	0.140±0.014	
25.4	17.5	0.0559±0.0012	0.148±0.018	
27.5	17.5	0.0511±0.0014	0.165±0.020	
30	17.5	0.0444±0.0014	0.148±0.023	
35	17.5	0.0304±0.0 15	0.114±0.027	0.1[illegible]4±0.021
40	17.5	0.0155±0.0015	0.076±0.049	0.031±0.036
45	17.5	-0.0019±0.0017	0.073±0.061	-0.009±0.042

used. The 'target empty' asymmetry was measured in the usual way, with the correct additional copper absorber in the arms, to give $\varepsilon''_{\beta\zeta}$ and f'' [background asymmetry and fraction]. The asymmetry measured in this way is at the correct energy for background originating from upstream of the target, and as all the background is assumed to have the same energy variation as carbon, this is the correct asymmetry for the fraction of background (1 - x) originating upstream of the hydrogen. The background fraction is measured partly (1 - x) at the correct energy, and partly (x) at an energy too high by 8.4 Mev, as there is no hydrogen in the target. The beam divergence and beam spots are now too small, and f'' is thus an underestimate of the background.

If a CH_2 shim, 8.4 Mev thick, is placed just upstream of the target, and the absorbers set at the same value as for hydrogen scattering, then the asymmetry ($\varepsilon'_{\beta\zeta}$) measured will be at the correct energy for (x) of the background, and too low for (1 - x). The part of the background fraction ($f^{\llcorner}$) originating downstream will be at the correct energy, but will be overestimated, due to the larger beam divergence.

The background data $\varepsilon''_{\beta\zeta}$, $\varepsilon'_{\beta\zeta}$, f'', $f^{\llcorner}$ may be used in two ways:

(I) $\varepsilon''_{\beta\zeta}$, $\varepsilon'_{\beta\zeta}$ may be combined by assuming that all the background is composed of the same material, when the corrected value will be:

(36) $$\varepsilon_{H\llcorner} = \varepsilon''_{\beta\zeta} \cdot (1 - x) + \varepsilon'_{\beta\zeta} \cdot x$$

A second estimate of ε_{-} may be made using equation (34)

(37) $$\varepsilon' = \varepsilon''_{\beta\zeta} (1 + x\ (1/P)(dP/dE)\,\Delta E)$$

and the mean ($\bar{\varepsilon}$) of these two values of $\varepsilon'_{\beta\zeta}$ may then be used as in 8.6, together with equation (33):

TABLE 13

Corrections to 98 Mev Hydrogen Asymmetries

Lab. Angle °	Finite Size of counter	Beam Shift effect	Multiple Scattering Correction factor	Multiple Scattering Correction
8.0	0.00006small	-0.00004	1.0088	0.00034
10.0	0.00005small	-0.00011	1.0055	0.00026
12.5	0.00003small 0.00019wide	-0.00005	1.0036	0.00018
15.0	0.00001small 0.00007wide	-0.00003	1.0025	0.00014
17.5	0.00001small 0.00005wide	-0.00001	1.0019	0.00011
20.0	0.00004wide	-	1.0015	0.00009
22.5	-	0.00005	1.0012	0.00007
25.4	-	0.00007	1.0010	0.00005
27.5	-	0.00008	1.0008	0.00004
30.0	-	0.00009	1.0007	0.00003
35.0	-	0.00004	1.0006	0.00002
40.0	-	0.00004	1.0004	0.00001
45.0	-	-	1.0003	-

98 Mev Hydrogen Asymmetries

Lab. Angle°	Energy Cutoff	Pooled ($\varepsilon_{\phi\zeta}$) value	Pooled $\Delta\varepsilon$ value	Quoted result
8 small	17.5 Mev	0.0381±0.0025	0.0387±0.0023	0.0384±0.0024
10 s	17.5	0.0464±0.0022	0.0483±0.0022	0.0473±0.0022
12.5 s	17.5	0.0493±0.0022	0.0490±0.0019	0.0491±0.0019
*12.5 wide	8	-	-	0.0471±0.0030
15 s	17.5	0.0536±0.0020	0.0542±0.0020	0.0539±0.0020
*15 w	8	-	-	0.0553±0.0046
17.5 w	17.5	0.0576±0.0014	0.0575±0.0014	0.0575±0.0014
17.5 s	8	-	-	0.0582±0.0024
*20 w	17.5	-	-	0.0584±0.0015
*20 w	8	-	-	0.0603±0.0024
*22.5 w	17.5	-	-	0.0547±0.0013
*22.5 w	8	-	-	0.0543±0.0025
*25.4 w	17.5	-	-	0.0548±0.0012
*25.4 w	8	-	-	0.0517±0.0024

*Background data from shim not taken

TABLE 14

Lab. Angle°	Energy Cutoff	Pooled (ε_{α_5}) value	Pooled $\Delta\epsilon$ value	Quoted result
*27.5	17.5	-	-	0.0498±0.0014
*30 w	17.5	-	-	0.0436±0.0021
*30 w	8	-	-	0.0466±0.0020
*35 w	17.5	-	-	0.0291±0.0015
*35 w	8	-	-	0.0312±0.0026
*40 w	17.5	-	-	0.0153±0.0016
*40 w	8	-	-	0.0150±0.0029
*45 w	17.5	-	-	-0.0021±0.0017
*45 w	8	-	-	-0.0071±0.0031

TABLE 14 cont.

(38) $f'_H = f_H(1 + x\ (1/\sigma)(d\sigma/dE)\Delta E)$

to give the correction ($\Delta\varepsilon$) to the measured target full asymmetry, where:

(39) $\Delta\varepsilon = \varepsilon$ (measured) $- f'_H\ [\ \varepsilon$(measured) $- \varepsilon'\ ]$

(II) We may use (38), (37) to obtain a value for $\Delta\varepsilon$, and combine this value of $\Delta\varepsilon$ with the value obtained by combining all the f_H, f_L, $\varepsilon''_{0\varsigma}$, $\varepsilon'_{0\varsigma}$ data simultaneously.

(39) $\Delta\varepsilon = \varepsilon$(measured)$(1 - f'_H) + (1 - x)\ f_H \varepsilon_H + x\ f_L \varepsilon_L$

We may then pool the two values of $\Delta\varepsilon$. The values of x used in both these calculations are tabulated in TABLE 8. x was measured at 8° (small angle arms) and 17.5° (wide angle arms) by measuring the effect of parts of the hydrogen target simulated by Kapton and aluminium foil.

In TABLE 12 are listed the asymmetries measured under the three experimental conditions and with the two counter telescopes and two energy discrimination levels.

In TABLE 13 are listed the corrections applied for the finite size of the defining counters (3, 3'), the beam shift between the two solenoid settings, and the multiple Coulomb scattering in the hydrogen. The first two corrections are discussed further in 8.7 and 8.5.

These corrections are applied to give [TABLE 14] the hydrogen asymmetries corrected for background in one [or both] of the two ways described. The weighted mean of the two estimates of the background correction is used to calculate the result. The 'error' on the final estimate of the background correction is found by extracting the common errors, pooling the two values of the 'error', and reinserting the common errors. The agreement between the two methods is

TABLE 15

Mean Angle Correction to 98 Mev P(θ)

Lab. Angle°	30	35	40	45
% loss of protons for 17.5 Mev level				
Proton Right	0.0	3.9±0.4	11.4±1.0	18.3±2.0
Proton Left	0.0	0.0±0.5	3.1±0.5	6.4±1.0
% loss of protons for 8 Mev level				
Proton Right	0.0	3.1±1.0	10.2±2.0	18.3±2.0
Proton Left	0.0	0.0±0.5	2.2±1.0	6.4±1.0
Change in mean Angle° 17.5 Mev	0.0	0.01	0.08±0.05	0.18±0.05
8 Mev	0.0	0.01	0.08±0.04	0.18±0.05

satisfactory, in view of the large beam width, thick target, and high backgrounds (~ 30% at 8° Lab- see TABLE 8.).

The liquid hydrogen container used for this experiment had a 1 cm wide strut on proton right of the beam. This strut occluded some of the scattered protons although it was well away from the fringes of the main beam. A percentage of the total number of protons scattered to proton right is occluded at the wider angles (>35%).

This percentage may be calculated from the geometry of the beam and the telescopes. The only effect of this occlusion is to shift the mean angle of scattering, by displacing the mean effective centre of the target downstream. This is because the discrimination levels 17.5 and 8 Mev are sufficiently high to completely exclude any scattered proton that has been through the brass. The mean angle corrections are listed in TABLE 15, and the corresponding centre of mass angles are included in the table of results, TABLE 16.

The results are plotted in FIG. 32, together with the data of Taylor et al [47] and Palmieri et al [49], at neighbouring energies. The smooth curves are all derived from the energy independent phase-shift analysis of MacGregor and Arndt at 95 Mev. This analysis represents the previous data, and does not include the measurements of Cnn reported in this thesis.

The data are also plotted on FIG. 33, together with the predictions of the phase-shift analysis of Breit and MacGregor [16]. The fit of Perring [134] includes this data.

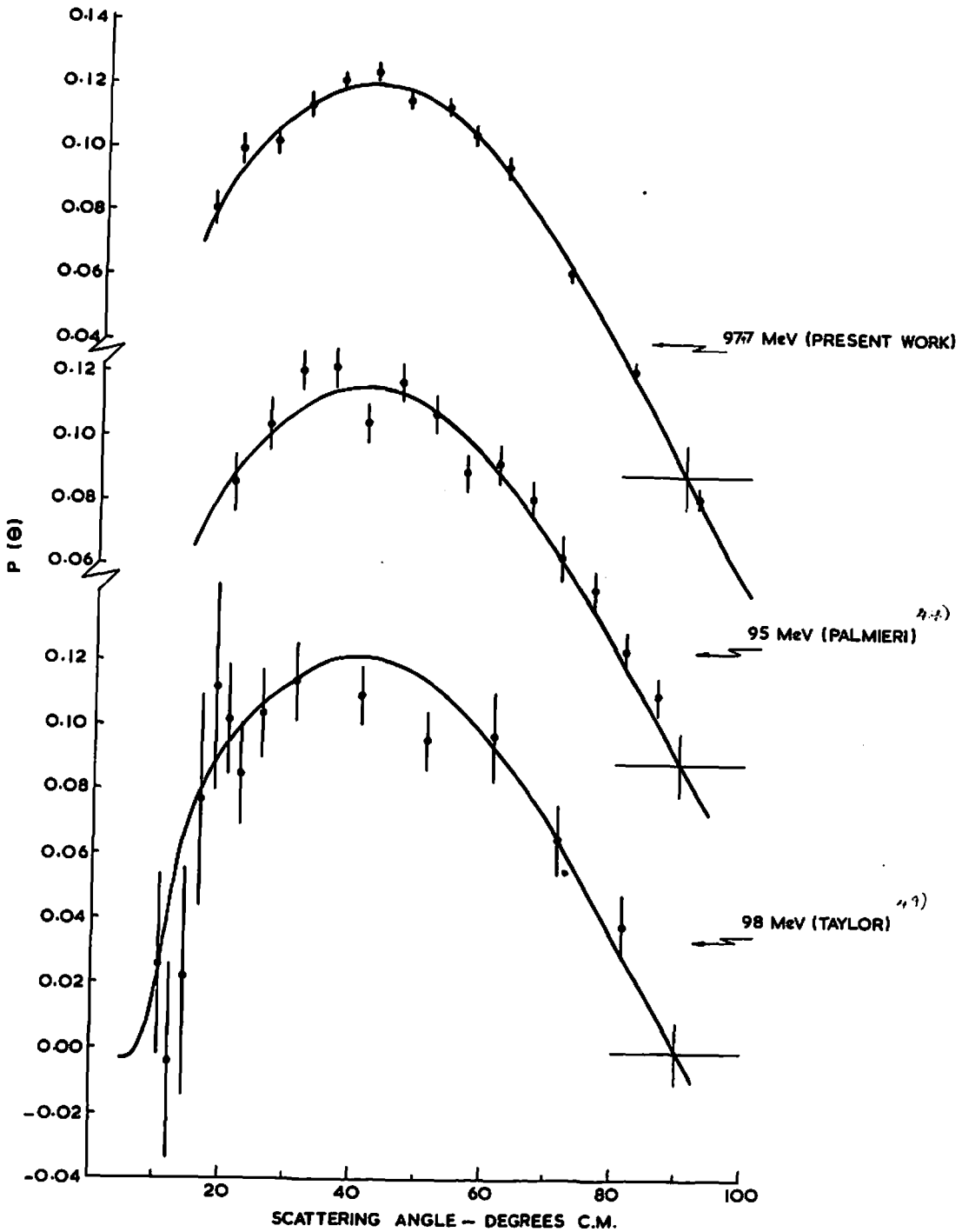

FINAL RESULTS (1966) : V'S AVERAGE [illegible]
V DERRIN [illegible]

FIG. 32

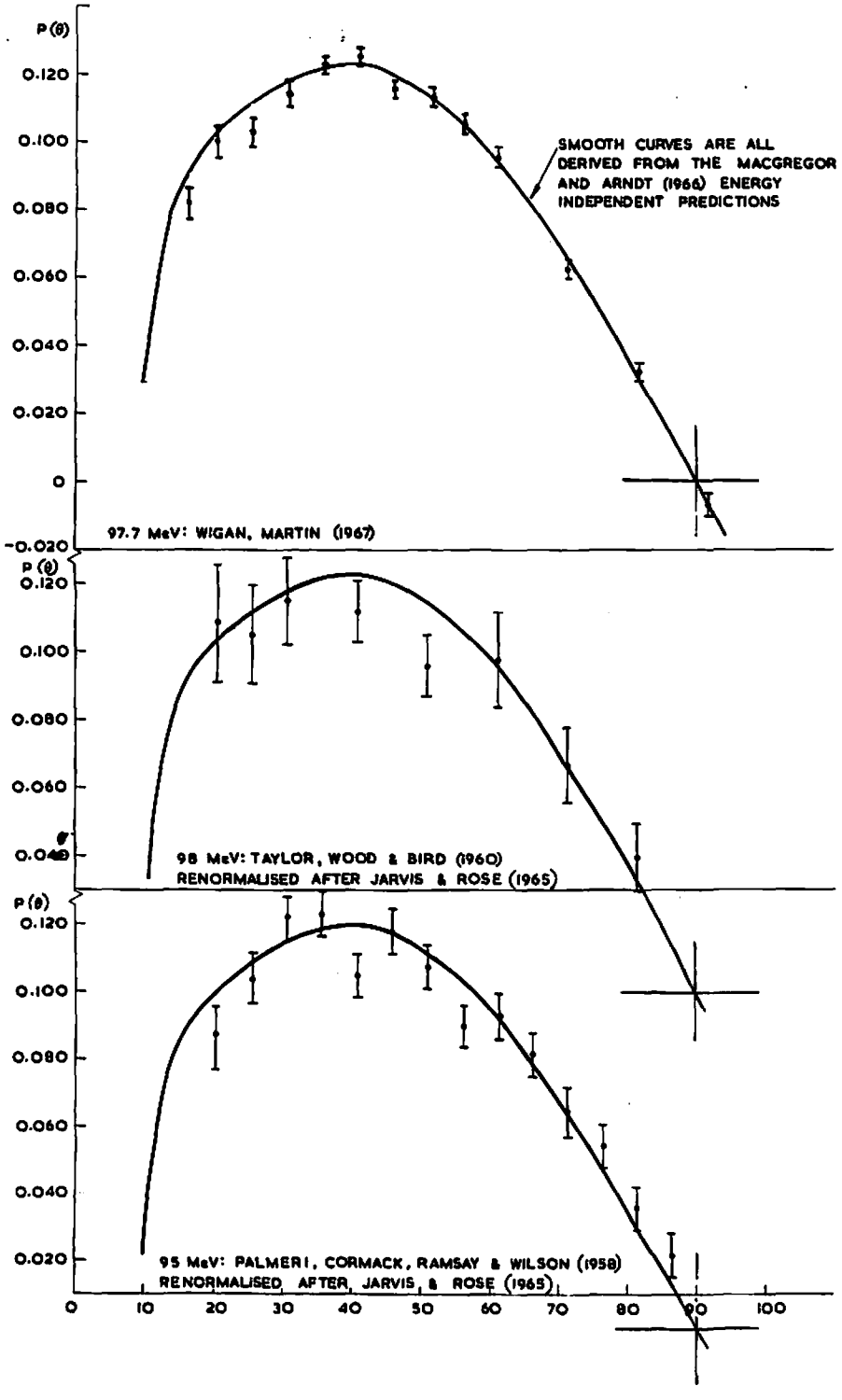
P(θ)
0.120
0.100
0.080
0.060
0.040
0.020
0
-0.020
SMOOTH CURVES ARE ALL DERIVED FROM THE MACGREGOR AND ARNDT (1966) ENERGY INDEPENDENT PREDICTIONS
97.7 MeV: WIGAN, MARTIN (1967)
98 MeV: TAYLOR, WOOD & BIRD (1960)
RENORMALISED AFTER JARVIS & ROSE (1965)
95 MeV: PALMERI, CORMACK, RAMSAY & WILSON (1958)
RENORMALISED AFTER JARVIS & ROSE (1965)
0
10
20
30
40
50
60
70
80
90
100

TABLE 16

Polarisation Results at 97.7+ 0.3 Mev

Centre of mass angle °	Asymmetry	Polarisation* %
16.41	0.0384±0.0024	8.14 ± 0.51
20.50	0.0473±0.0025	10.02 ± 0.47
25.62	0.0485±0.0020	10.28 ± 0.42
30.73	0.0541±0.0019	11.46 ± 0.40
35.84	0.0578±0.0012	12.25 ± 0.25
40.94	0.0589±0.0013	12.49 ± 0.27
46.04	0.0548±0.0012	11.61 ± 0.25
51.90	0.0539±0.0013	11.42 ± 0.27
56.20	0.0498±0.0014	10.56 ± 0.30
61.27	0.0452±0.00145	9.58 ± 0.31
71.39	0.0296±0.0013	6.27 ± 0.27
81.60	0.0153±0.0014	3.24 ± 0.29
91.81	-0.0032±0.0015	-0.68 ± 0.32

*The absolute scale error of 0.85 % has not been included here.

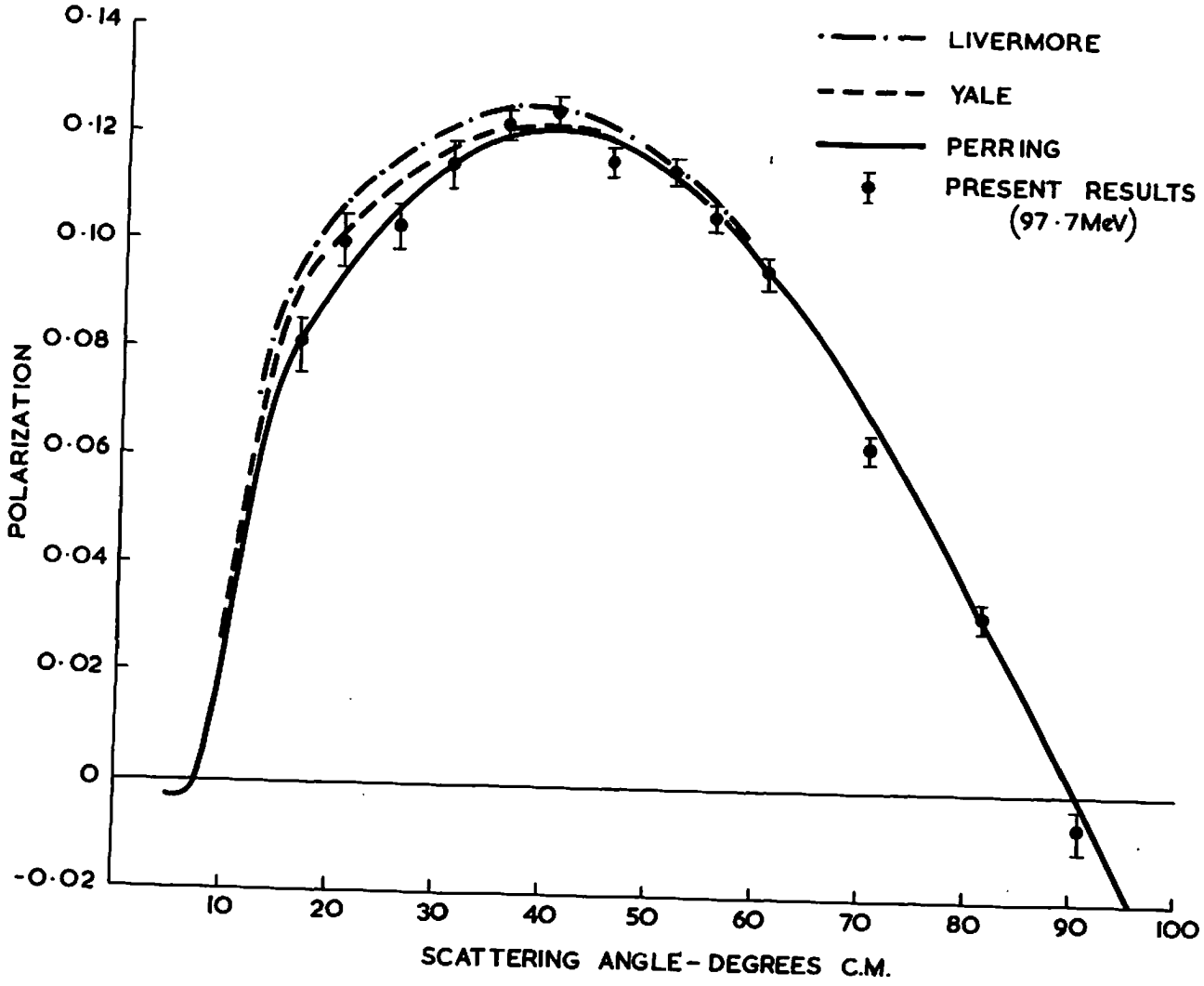

FINAL RESULTS (1968) : LIVERMORE IS UCRL-70075 (1967) PREDICTION

FIG. 33

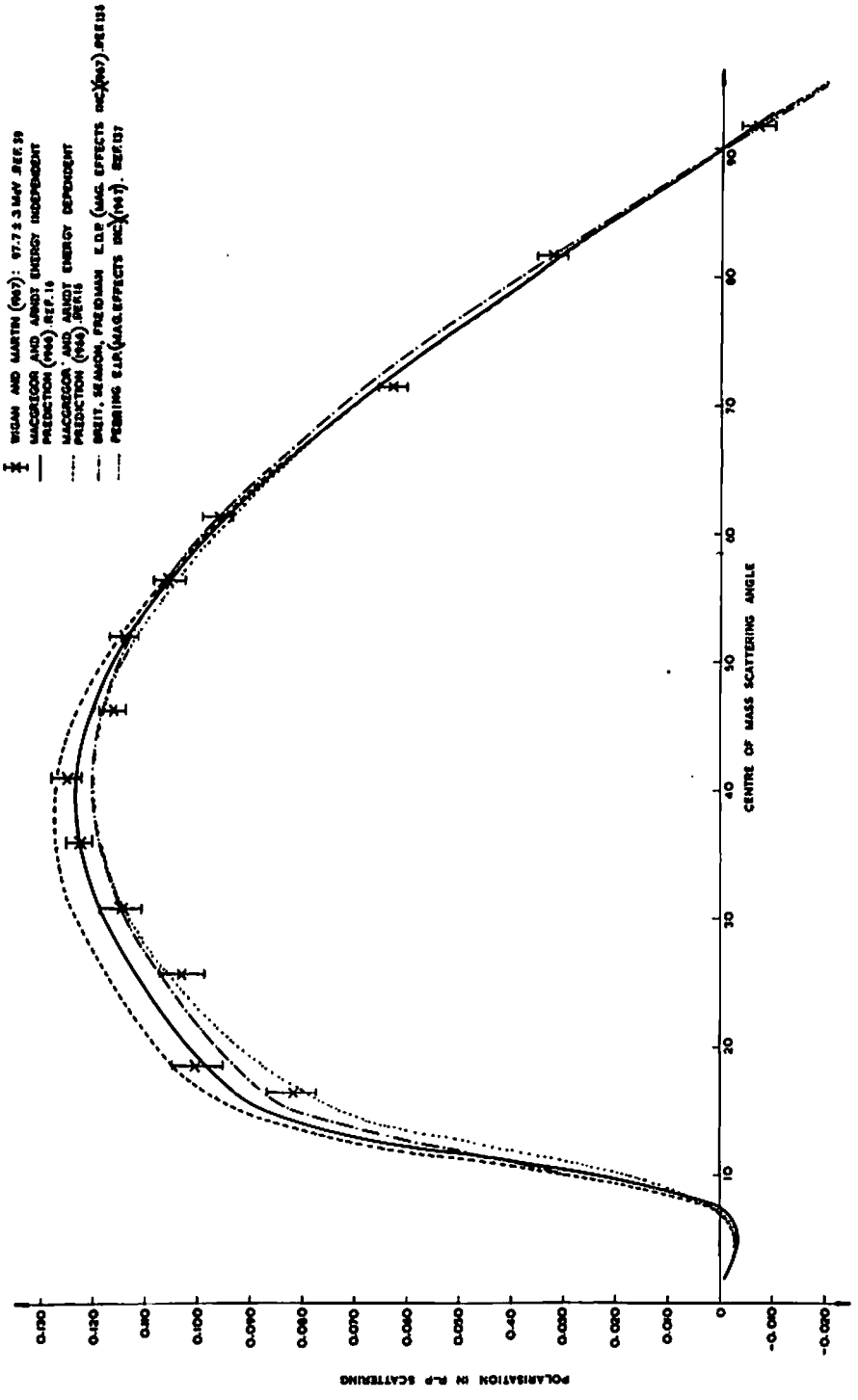
BIGAN AND MARTIN (1967): 97.7 ± 3 MeV. REF. 39
MACGREGOR AND ARNDT ENERGY INDEPENDENT PREDICTION (1966). REF. 16
MACGREGOR AND ARNDT ENERGY DEPENDENT PREDICTION (1966). REF. 15
BRETT, SEAMON, FRIEDMAN E.D.E (MAG. EFFECTS INC.) (1967). REF. 38
PERRING E.I.R (MAG. EFFECTS INC.) (1967). REF. 37
POLARISATION IN P-P SCATTERING
CENTRE OF MASS SCATTERING ANGLE
0.150
0.130
0.120
0.110
0.100
0.090
0.080
0.070
0.060
0.050
0.040
0.030
0.020
0.010
0
-0.010
-0.020
0
10
20
30
40
50
60
70
80
90

VII Discussion of the p-p scattering results in the 70-140 Mev region

7.1 Results obtained

A summary of the p-p data reported in this thesis is required before further discussion.

(a) Cnn at 73.5, 98.3, 143.2 Mev

(b) $P(\theta)$ at 93.2, 97.7 Mev

(c) $\sigma(\theta)$ at 97.8 Mev (absolute)

Only the preliminary data is available for (c) at this time, however, as the data is used in the phase-shift analysis at 95 Mev, this preliminary data is listed in TABLE 17. The experimental techniques used were similar to those of Jarvis et al (Ref.13), and some details of the measurement are included in 8.10.

Several phase-shift analyses have been reported recently without the data reported here, notably the energy dependent and energy independent analyses of MacGregor and Arndt at Livermore[16], and the Yale[136] series of analyses YRBI (Ko) and Ypp-IV. The later Yale analyses (Ypp-IV) are presented in two forms, one including magnetic moment effects on the F-waves and above, and one not including this refinement. These analyses have been used to make predictions for the data of this thesis, based on all previous work. The various predictions are compared with the new data in FIG. 31, 33, 34.

Perring[137] has carried out a set of analyses using data sets including the new data. These allow for the magnetic moment effects on F-waves and above, and are also plotted in FIGS. 31, 33, 34.

TABLE 17

Preliminary cross-section data at 98.8 ± 0.3 Mev

Centre of mass angle°	Cross-section (mb)*
20.51	4.548 ± 0.083
22.56	4.497 ± 0.094
24.50	4.588 ± 0.065
26.65	4.749 ± 0.075
28.70	4.839 ± 0.077
30.74	4.824 ± 0.074
32.79	4.884 ± 0.072
35.85	4.789 ± 0.059
40.95	4.856 ± 0.048
46.05	4.781 ± 0.038
57.64	4.760 ± 0.035
61.28	4.735 ± 0.031
66.39	4.691 ± 0.034
71.39	4.634 ± 0.021
76.42	4.624 ± 0.030
81.45	4.583 ± 0.059
86.47	4.61 ± 0.035
91.47	4.602 ± 0.036
96.46	4.613 ± 0.035

* These are absolute cross-sections, with relative errors; the absolute normalisation factor is 1.0000 ± 0.0082

'Total' cross-section (integrated from 12°-90° c of m) = 29.1 ± 0.3 mb.

FIG. 34

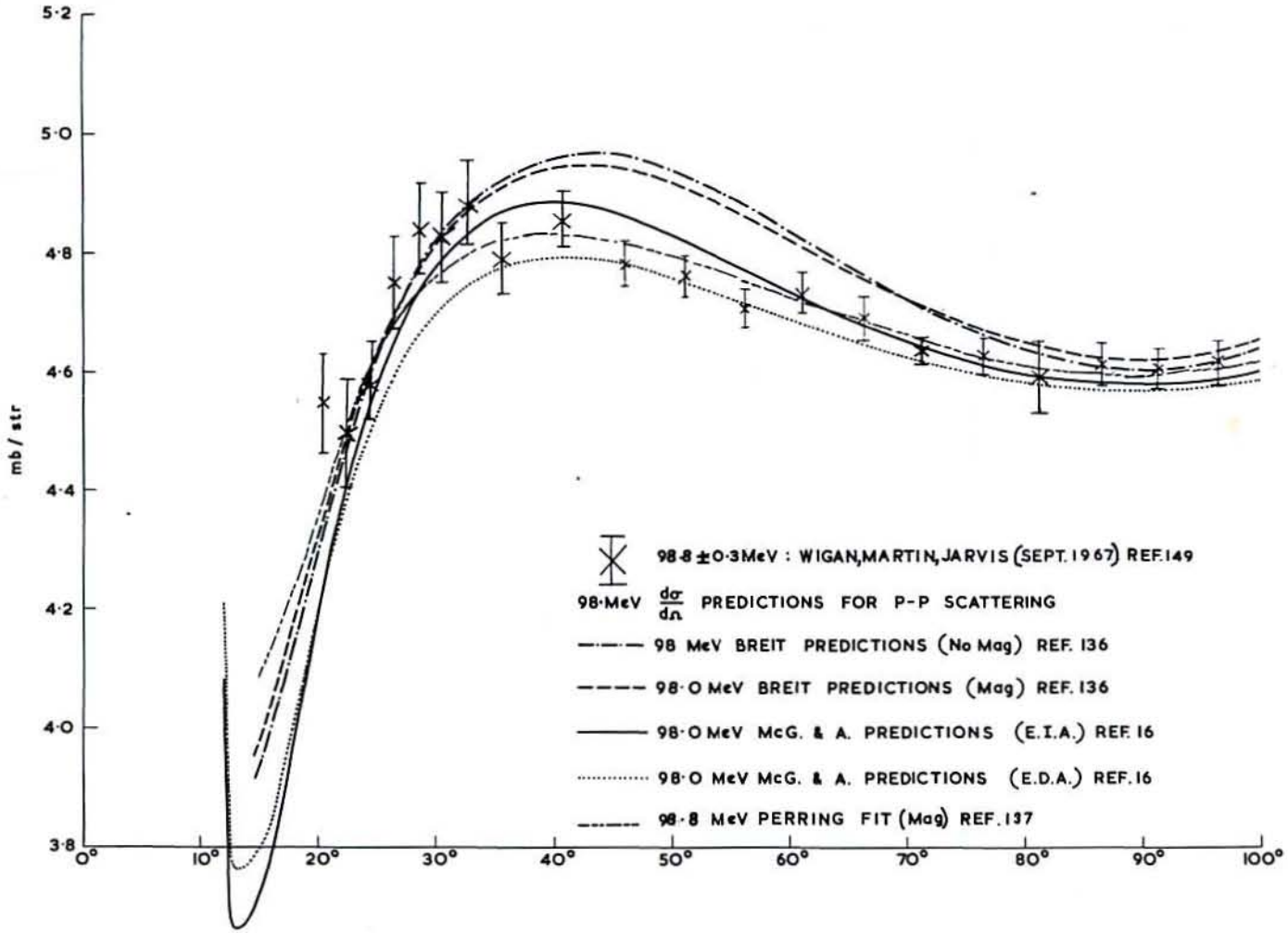

DIFFERENTIAL CROSS-SECTION IN P-P SCATTERING NEAR 98 MeV

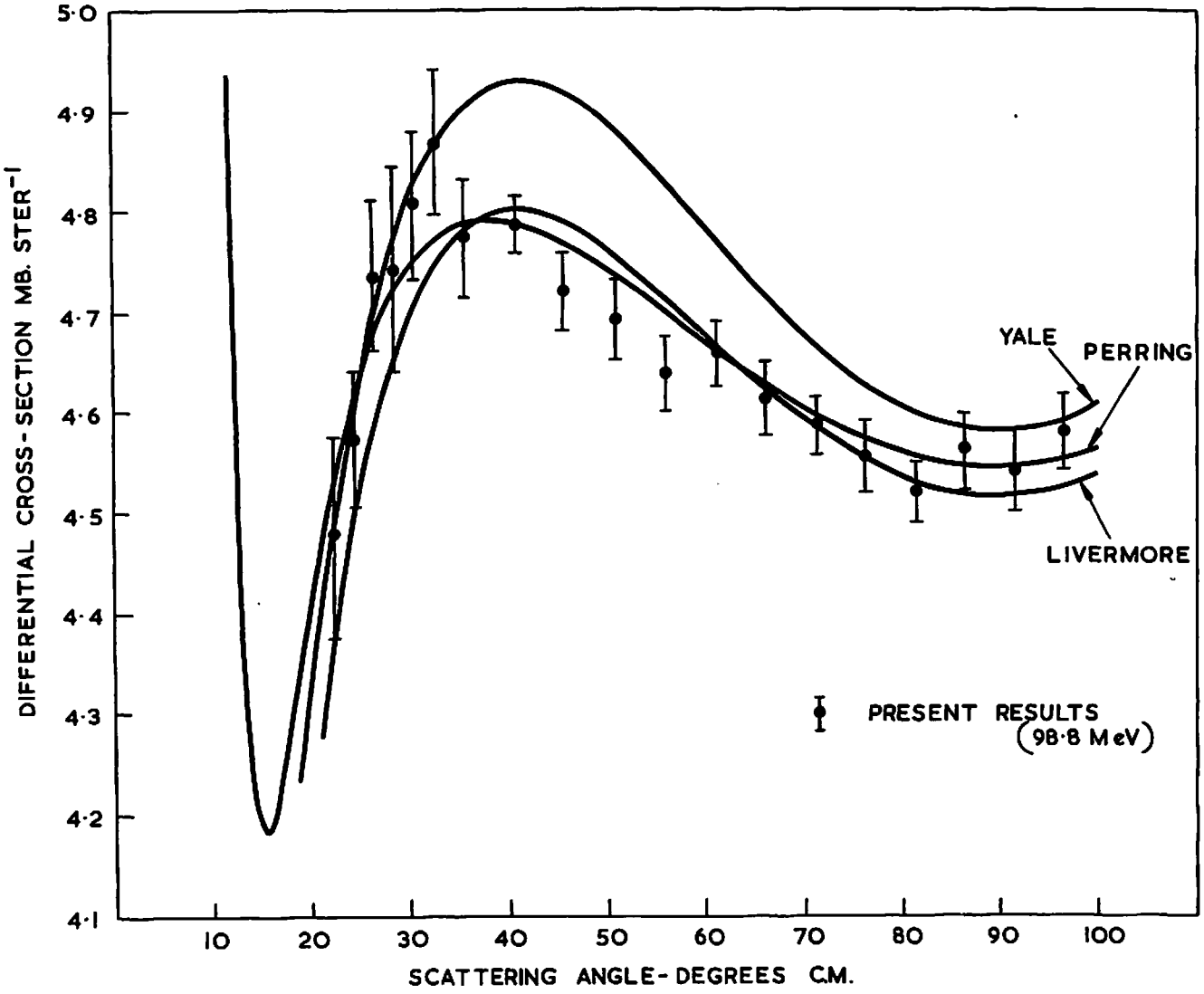

FINAL RESULTS (1968) : LIVERMORE IS UCRL-70075 (1967) PREDICTION

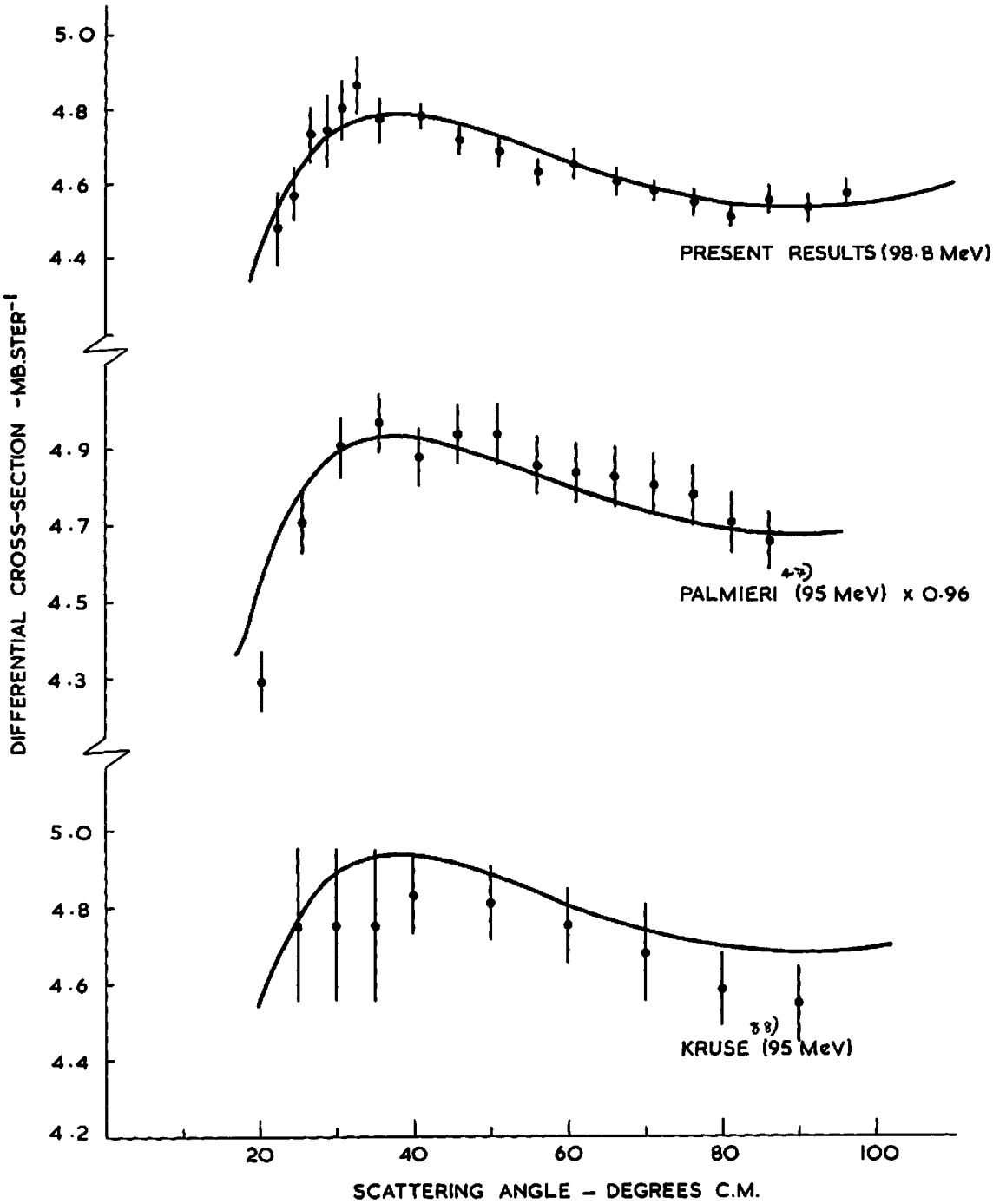

FINAL RESULTS (1968) • PERRING FITS (1967)

7.2 The determination of the energies of the measurements

In all cases the energy quoted for a measurement is referred to a range curve taken in copper, and interpreted using the revised Sternheimer tables listed in Ref.105.

The precision of the data is such that an error of 1 Mev would be of some concern, and this is the order of magnitude of the disagreements between theory and experiment found at McGill[124] near 100 Mev as is shown in FIG.35. For these reasons all the energies quoted are referred to ranges in the same material, interpreted in the same way.

7.3 Comparisons with other data

The polarisation data near 95 Mev is shown in FIG.32 together with the Harvard and previous Harwell measurements. It is evident that both these earlier data sets contain unresolved systematic errors, as is shown by their failure to extrapolate to zero polarisation at 90^{0} c of m. This fault was also present in $\sim$140 Mev polarisation until the recent Cox et al[13] values were obtained (FIG.37).

The normalisations for polarisation data were in considerable disagreement until Jarvis and Rose[50] showed that polarisations of some of the beams used had been referred to an incorrect value for the polarisation in p-C^{12} scattering measured at Harwell in 1957. The renormalised results for the maximum polarisation in p-p scattering are shown in FIG. 38 over a wide range of energies. A smooth curve may now be drawn between $\sim$60 and $\sim$600 Mev, and the 93, 98 and 141 Mev (1967) Harwell values lie on this curve. The polarisation data at 93, 98 Mev fit in well with the data at other energies, and are of adequate precision to provide the stronger constraints on the phase-shift analyses required by

FIG. 35

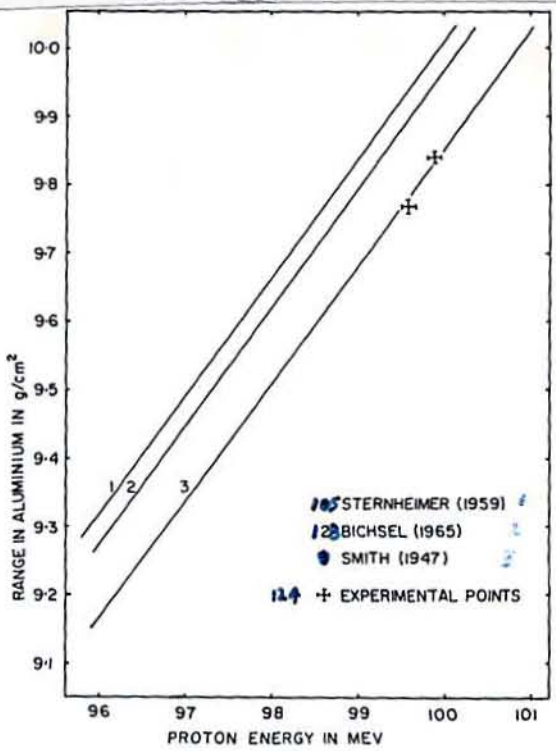

FIG. 35. Comparison between present experimental range–energy values and theoretical range–energy curves.

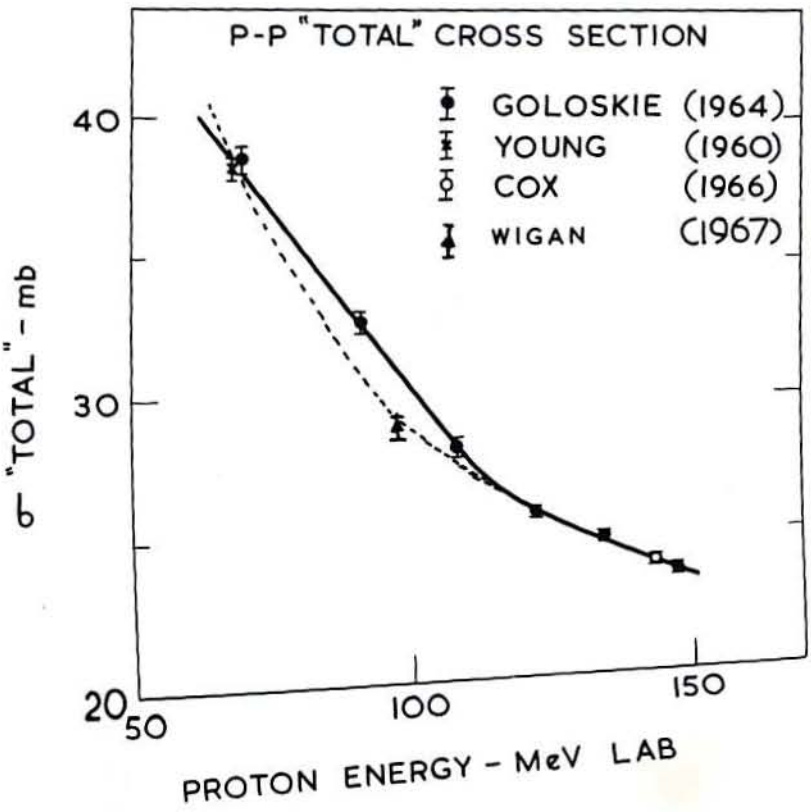

FIG. 36

MacGregor et al (16).

The cross-section [149] is the only absolute measurement in this energy region, other than that of Kruse [88] [to ± 5%]. The relative values are also a significant improvement on the previous data. The integrated 'total' cross-section [from 12° -90° c of m] is shown on FIG.36, together with the results of Goloskie [50], Cox, [13] and Young. [54] The Goloskie point at 90 Mev is in disagreement with the new value at 99 Mev, which favours a smooth variation of σ_{total} with energy. The kink required to draw a smooth line through all the Goloskie points has previously been criticised, [91] although this is the first experimental disagreement.

The Cnn (90° c of m) measurements are shown as a function of energy in FIG.39, where the smooth curve is the prediction of the Hamada-Johnston [41] potential model, which fits remarkably well. The references listed on the figure are to be found under Ref. 151. At 140 Mev the Cnn data do not contribute much new information, as the concurrently measured σ, P results of FIG.37 were analysed and used first to closely define the phase-shift solution. At 98 and 74 Mev the Cnn results are valuable, but it is advisable to make some allowance for the possible ± 0.3 Mev error in the mean energies of the measurements. This is made necessary by the rapid variation of Cnn(90°) with energy, (see FIG.39).

7.4 Phase-shift analyses

In TABLE 18 the results of the Perring analyses for T=1 phase shifts are tabulated together with the Livermore (1966) results. The Livermore analyses represent the previous data, and include both n-p and p-p information in the data sets. The Perring data sets contain solely p-p information.

FIG. 37

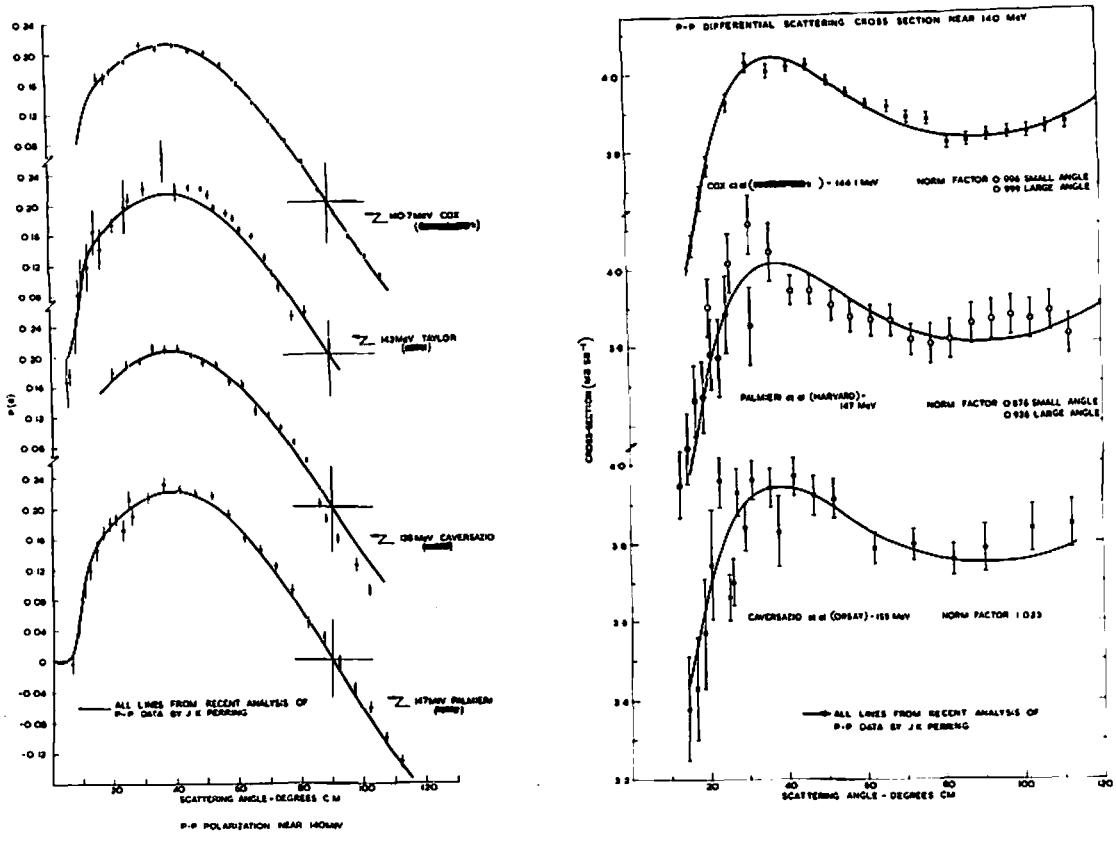

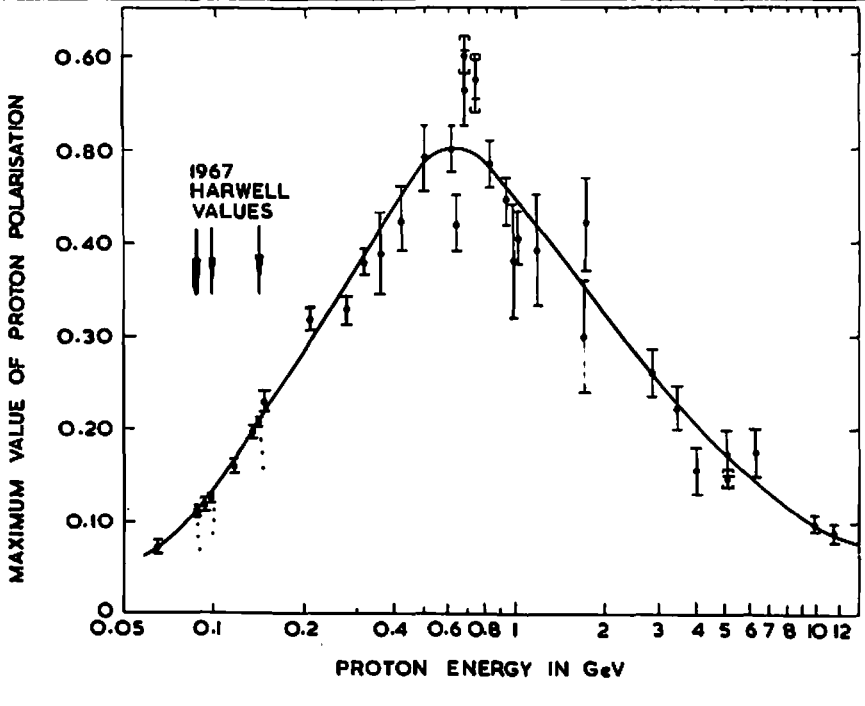

MAXIMUM POLARISATION IN P-P SCATTERING

FIG. 38

FIG. 39

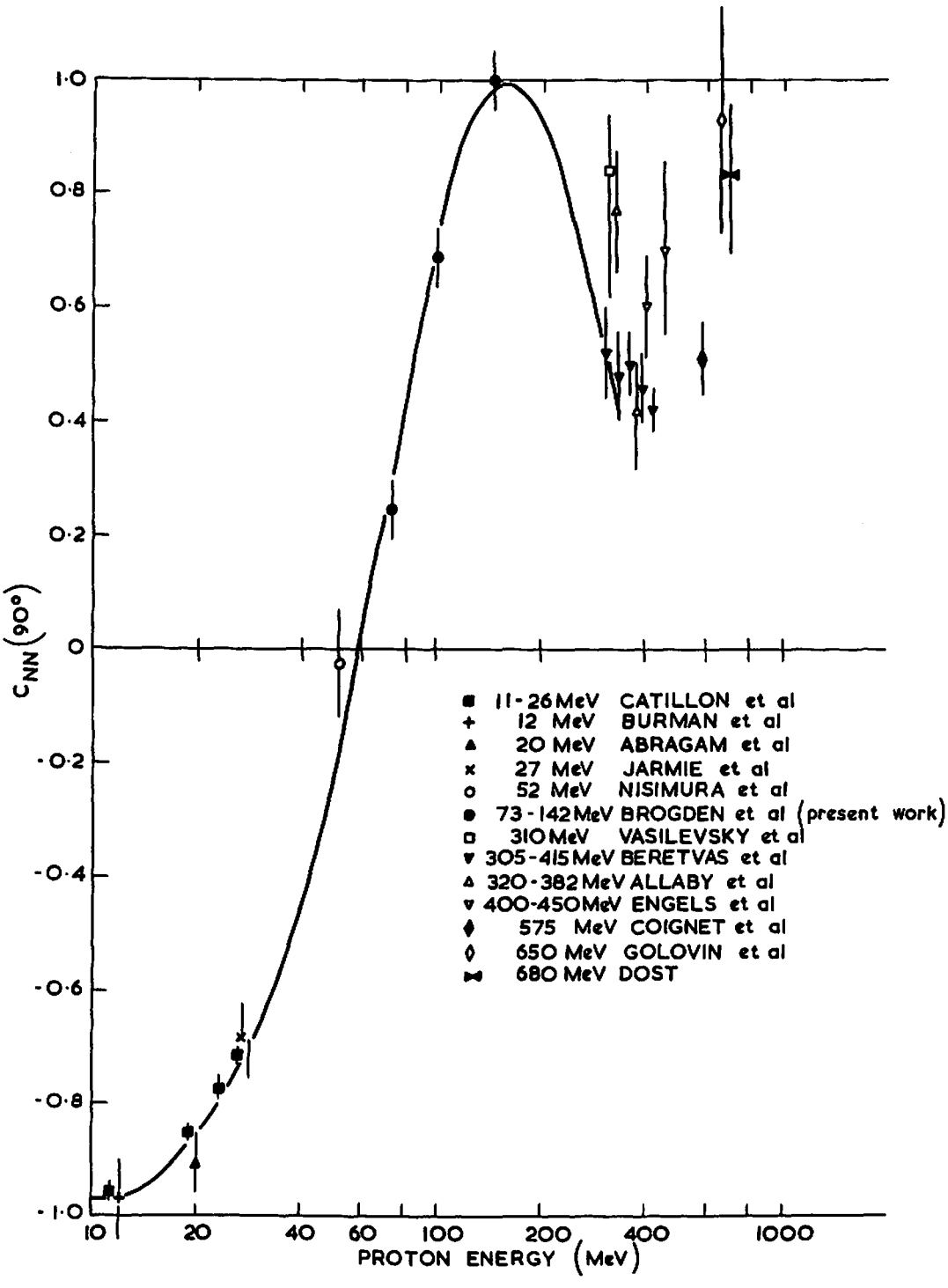

C_{NN} (90° C.M.) IN PROTON-PROTON SCATTERING

7.2 The determination of the energies of the measurements

In all cases the energy quoted for a measurement is referred to a range curve taken in copper, and interpreted using the revised Sternheimer tables listed in Ref.105.

The precision of the data is such that an error of 1 Mev would be of some concern, and this is the order of magnitude of the disagreements between theory and experiment found at McGill[124] near 100 Mev as is shown in FIG.35. For these reasons all the energies quoted are referred to ranges in the same material, interpreted in the same way.

7.3 Comparisons with other data

The polarisation data near 95 Mev is shown in FIG.32 together with the Harvard and previous Harwell measurements. It is evident that both these earlier data sets contain unresolved systematic errors, as is shown by their failure to extrapolate to zero polarisation at 90^{0} c of m. This fault was also present in $\sim$140 Mev polarisation until the recent Cox et al[13] values were obtained (FIG.37).

The normalisations for polarisation data were in considerable disagreement until Jarvis and Rose[50] showed that polarisations of some of the beams used had been referred to an incorrect value for the polarisation in p-C^{12} scattering measured at Harwell in 1957. The renormalised results for the maximum polarisation in p-p scattering are shown in FIG. 38 over a wide range of energies. A smooth curve may now be drawn between $\sim$ 60 and $\sim$600 Mev, and the 93, 98 and 141 Mev (1967) Harwell values lie on this curve. The polarisation data at 93, 98 Mev fit in well with the data at other energies, and are of adequate precision to provide the stronger constraints on the phase-shift analyses required by

FIG. 35

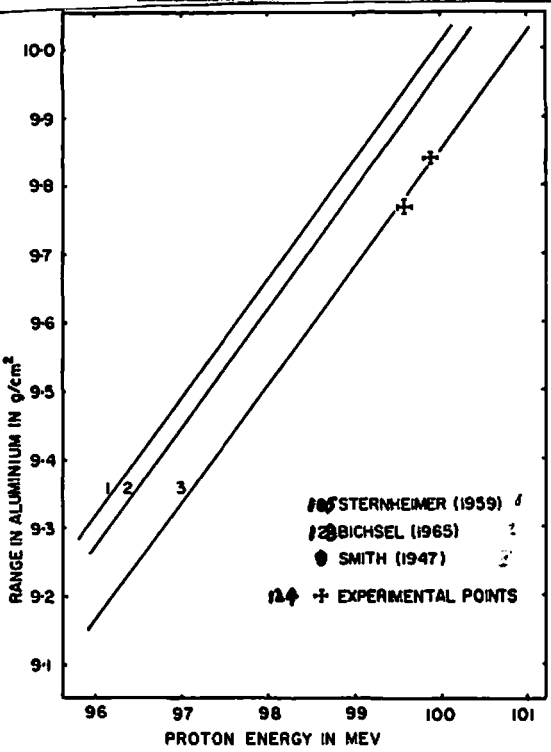

FIG. 35. Comparison between present experimental range–energy values and theoretical range–energy curves.

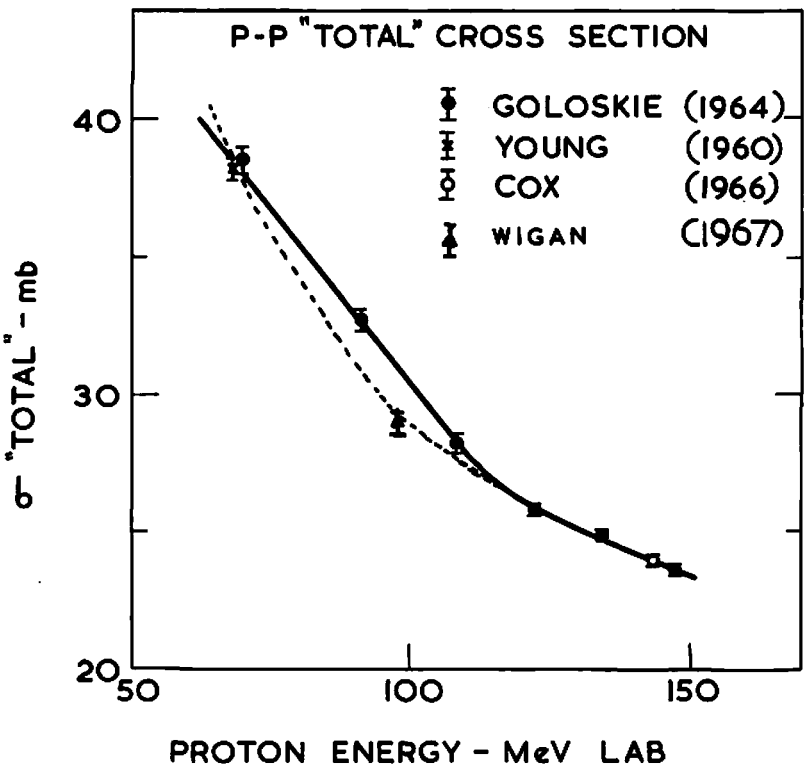

FIG. 36

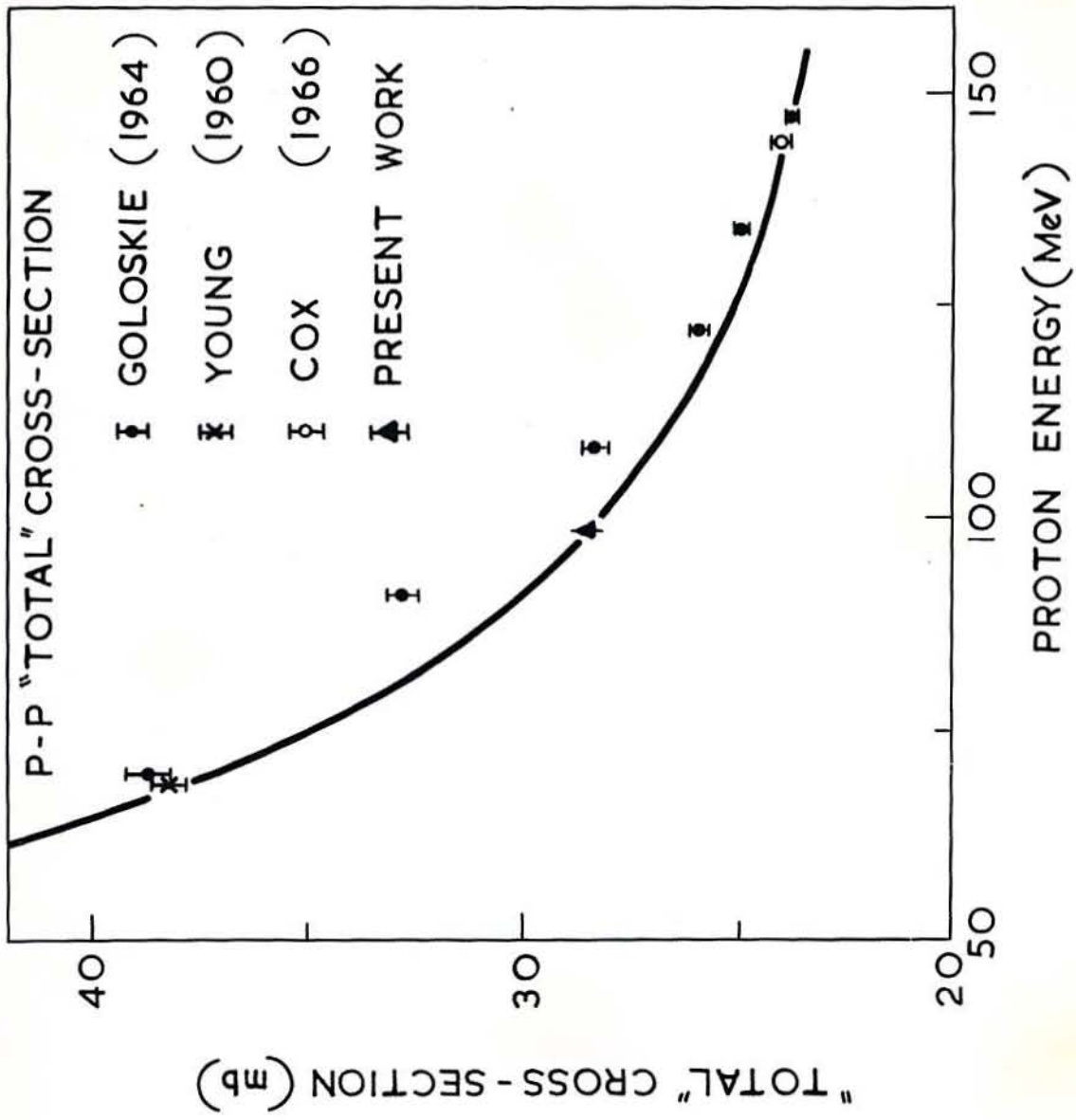

FINAL DATA (1968) SHOWN WITH MCGREGOR AND ARNDT (UCRL-70075) INC

MacGregor et al (16).

The cross-section [149] is the only absolute measurement in this energy region, other than that of Kruse [88] [to ± 5%]. The relative values are also a significant improvement on the previous data. The integrated 'total' cross-section [from 12° -90° c of m] is shown on FIG.36, together with the results of Goloskie [50], Cox, [13] and Young. [54] The Goloskie point at 90 Mev is in disagreement with the new value at 99 Mev, which favours a smooth variation of σ_{total} with energy. The kink required to draw a smooth line through all the Goloskie points has previously been criticised, [91] although this is the first experimental disagreement.

The Cnn (90° c of m) measurements are shown as a function of energy in FIG.39, where the smooth curve is the prediction of the Hamada-Johnston [41] potential model, which fits remarkably well. The references listed on the figure are to be found under Ref. 151. At 140 Mev the Cnn data do not contribute much new information, as the concurrently measured σ, P results of FIG.37 were analysed and used first to closely define the phase-shift solution. At 98 and 74 Mev the Cnn results are valuable, but it is advisable to make some allowance for the possible ± 0.3 Mev error in the mean energies of the measurements. This is made necessary by the rapid variation of Cnn(90°) with energy, (see FIG.39).

7.4 Phase-shift analyses

In TABLE 18 the results of the Perring analyses for T=1 phase shifts are tabulated together with the Livermore (1966) results. The Livermore analyses represent the previous data, and include both n-p and p-p information in the data sets. The Perring data sets contain solely p-p information.

FIG. 37

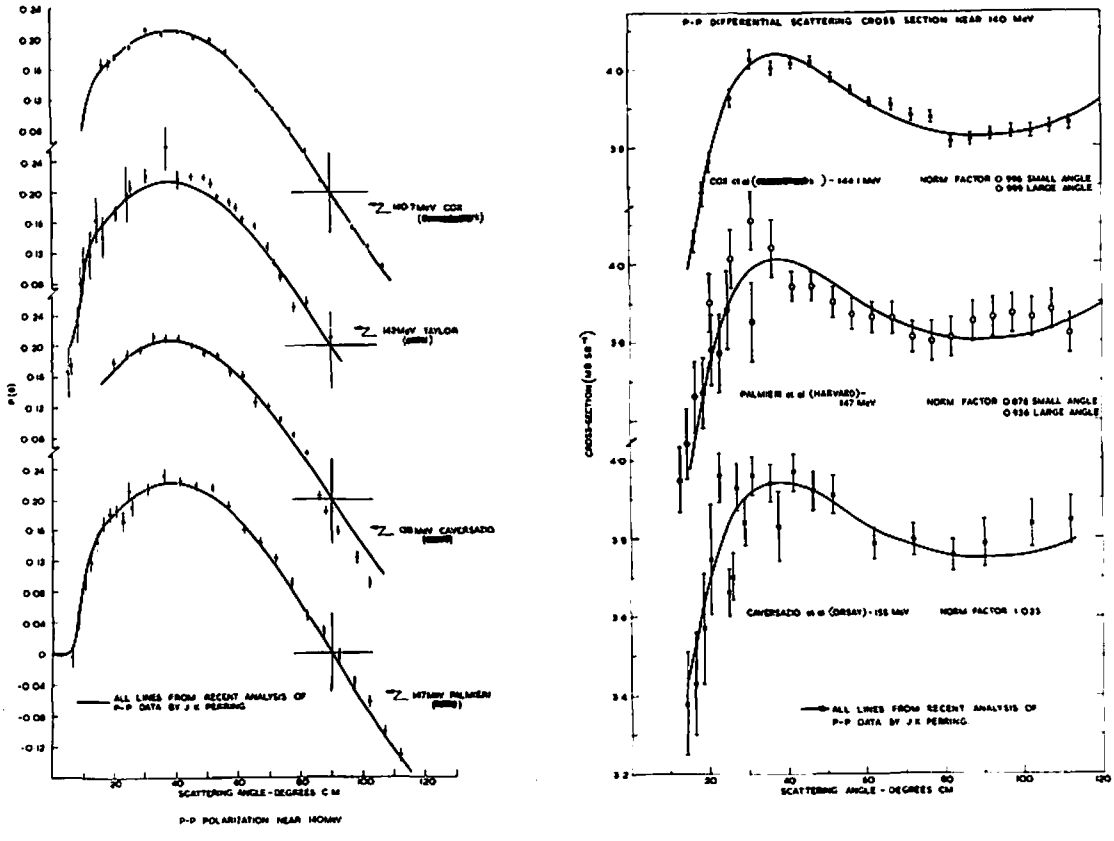

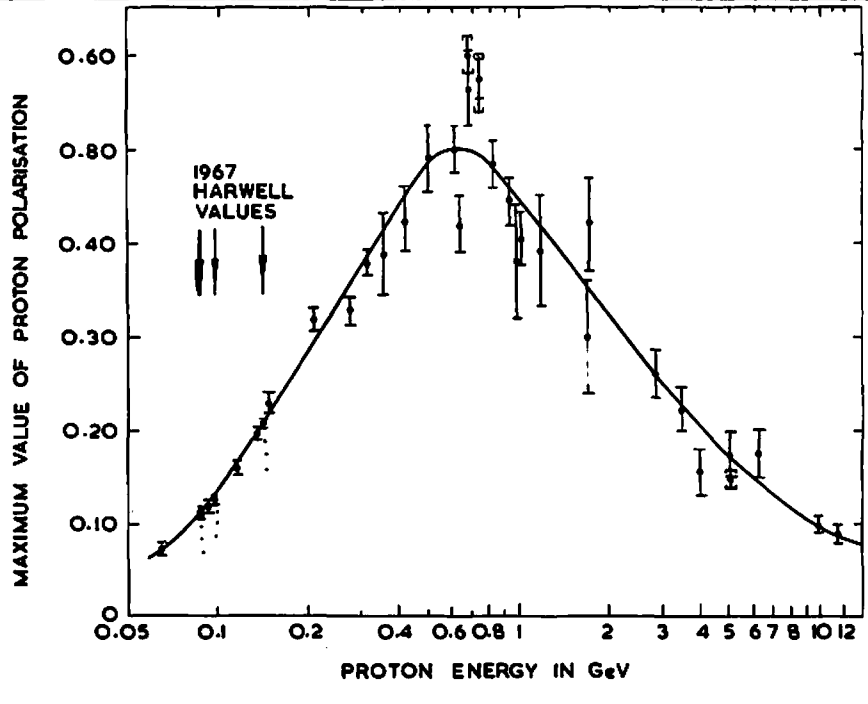

MAXIMUM POLARISATION IN P-P SCATTERING

FIG. 38

In TABLE 18, * indicates that the phase shift has been set at the one-pion exchange value, x indicates an energy independent analysis, and y an energy dependent one.

At 73.5 Mev the data set is the Minnesota σ[54], the Harvard P, σ, and the new Cnn(90°)[78]. Only five free phases are used, the remainder being set at the values given by the one-pion exchange potential. The Cnn point contributes 4.9 to the χ^2. In order to use the measured Cnn value, the value (0.9737)[137] of Cnn at 143.2 Mev, deduced from the precise 140 Mev analysis, was used as a normalisation to give Cnn (90°, 73.5 Mev).

The 95 Mev analysis shows a very marked improvement in precision, many errors being reduced by a factor of two or more when seven phase shifts are allowed to vary. The analysis at 95 Mev is now as well determined as at 140 Mev, but for the 3P0 phase shift, for which a new precise D (depolarisation) measurement is required. The data set used is the Harwell R, R'[91]; Harvard D, σ[52], P[47]; and the new Harwell P, σ, Cnn. The χ^2 contributions of the new data are:

$$\chi^2(\text{Cnn}) = 5.3/1 \text{ point}$$

$$\chi^2[\text{P(93.2 Mev)}] = 4.6/5$$

$$\chi^2[\text{P(97.3 Mev)}] = 13.6/12$$

$$\chi^2[\sigma\text{(98.8 Mev)}] = 14.6/20.$$

The absolute normalisation of polarisation (experimentally 1.000 ± 0.008)[57] and cross-section (experimentally 1.000 ± 0.008)[149] are found to be 0.994 ± 0.008 and 1.001 ± 0.008 respectively, which is a very satisfactory agreement. Further support for the shape is given by the value of δ_c (the average P-wave phase shift). This parameter is determined by the shape of the Coulomb interference minimum, and the value of $2.71^\circ \pm 0.24^\circ$ obtained in this 95 Mev analysis lies

FIG. 39

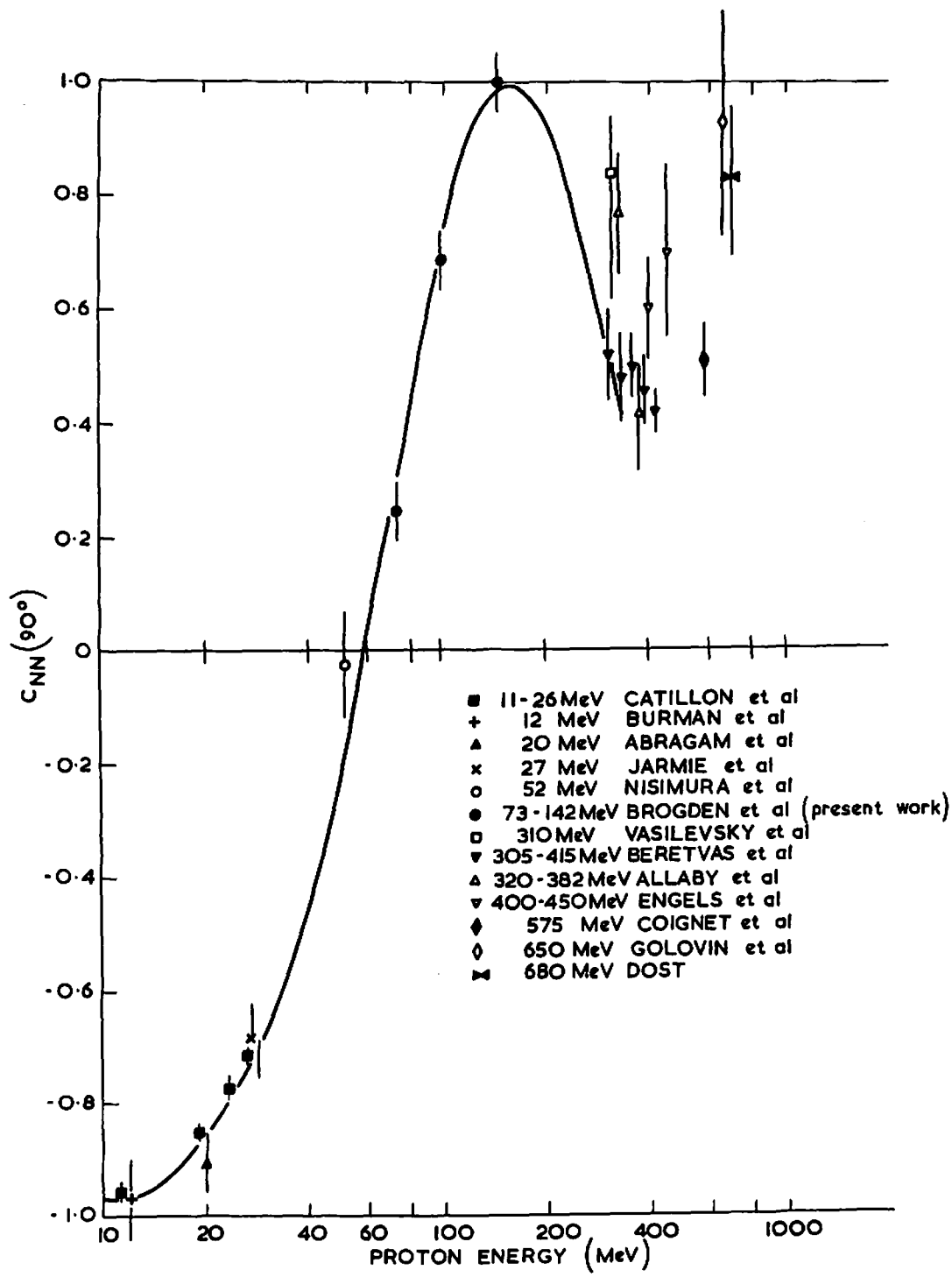

C_{NN} (90° C.M.) IN PROTON-PROTON SCATTERING

on the smooth curve through other accurate[92] values at 10, 18, 68, 140 Mev.

The 95 Mev Harvard[47] data could now be dropped from the analysis as the data is of little weight. The phase shifts are now accurately known at 95 Mev.

7.5 Conclusion

The p-p system is now well determined at both 95 and 140 Mev, and the ambiguities and inconsistencies in the data at these energies have been resolved. There is now no further need to remeasure any quantities (except D at 95 Mev) in the p-p system at either energy until a further order of magnitude in precision may be obtained.

A compilation of the N-N data in the 60-160 Mev region is presented in TABLE 19, and should be used in conjunction with the papers of Jarvis[50] and Rose[152] which discuss the renormalisations in detail. A selected data set near 140 Mev is to be presented in the paper describing the ~140 Mev σ, P measurements.[13]

T = 1 Phase-shift solutions: 70-140 Mev

Phase shift	Energy:	73.5 Mev	72.0 Mev	95 Mev	95 Mev	140 Mev	140 Mev
1S0		30.64±0.58°	31.7°	25.37±0.55°	26.33±2.37°	17.58±0.62°	16.78±0.74°
1D2		2.87±0.08°	2.6°	4.08±0.13°	3.48±0.33°	5.22±0.22°	4.84±0.27°
3P0		13.92±2.57°	12.4°	12.01±1.57°	13.22±1.85°	6.74±0.52°	6.66±0.58°
3P1		-10.91±0.22°	-10.5°	-13.06±0.26°	-12.78±0.47°	-16.61±0.18°	-16.85±0.43°
3P2		8.26±0.53°	8.3°	10.32±0.25°	10.18±0.45°	13.71±0.12°	13.57±0.22°
E2		-2.31°*	-2.9°	-3.08±0.15°	-2.67±0.36°	-2.77±0.09°	-2.88±0.16°
3F2		0.63°*	1.0°	0.62±0.14°	0.64±0.59°	0.40±1.31°	0.67±0.32°
3F3		-1.25°*	-1.9°	-1.69°*	-1.18±0.67°	-1.91±0.20°	-2.13±0.22°
3F4		0.18°*	0.8°	0.22°*	0.48±0.20°	0.52±0.18°	0.87±0.18°
E4		*	0.7°	*	*	-0.70±0.14°	-0.66±0.07°
3H4		*	0.2°	*	*	0.18±0.14°	0.44±0.18°
1G4		*	0.6°	*	*	0.58±0.09°	0.62±0.13°
3H5		*	-0.5°	*	*	-0.38±0.16°	-0.62±0.17°
3H6		*	0.1°	*	*	0.11±0.09°	0.25±0.11°
χ^2/Points		29/48		78/92			
		I Perring 1967x	II Livermore 1966y	III Perring 1967x	IV Livermore 1966x	V Perring 1967x [9a]	VI Livermore 1966x

TABLE 18

Collected nucleon-nucleon scattering data in the range 60-160 Mev

P-P

Parameter	Energy	Renormalisation factor	Author		Reference
Total Cross-section	70-147	-	Goloskie	(1964)	(56)**
Differential Cross-section	68.3	-	Young	(1960)	(54)
..	40- 95	-	Kruse	(1956)	(88)
..	95-147	Relative only	Palmieri	(1958)	(47)
..	98		This work	(1966-7)	(147)
..	142.0	-	Taylor	(1960)	(49)*
..	144.1	-	Cox	(1967)	(13)
..	155	-	Caversazio	(1961)	(53)
Polarisation	70, 97	0.89	Christmas	(1961)	(55)*
..	66-147	0.933	Palmieri	(1958)	(47)
..	98	0.911±0.03	Taylor	(1959)	(70)
..	93, 98	-	This work	(1966-7)	(39)
..	138	-	Caversazio	(1963)	(53)
..	140.7	-	Cox	(1967)	(13)

TABLE 19

P-P

Parameter	Energy	Renormalisation factor	Author		Reference
Polarisation	142	0.911±0.03	Taylor	(1960)	(49)
Depolarisation	98	-	Thorndike	(1960)	(52)
••	138	-	Caversazio	(1963)	(53)
••	142	-	Hwang	(1960)	(62)
••	143	-	Bird	(1961)	(63)
R-Parameter	98	-	Jarvis	(1965)	(51)
••	140	-	Thorndike	(1960)	(64)
••	142	-	Bird	(1963)	(65)
R -parameter	98	-	Jarvis	(1965)	(51)
••	137.5	-	Hee	(1963)	(66)
••	140	-	Jarvis	(1965)	(67)
A-parameter	139	-	Hee	(1963)	(68)
••	143	-	Jarvis	(1965)	(69)
Cnn-parameter	73, 98, 143	-	This work	(1966-)	(38)

TABLE 19

N-P

Parameter	Energy	Renormalisation	Normalisation error	Author		Reference
Total Cross-section	38-153	-	-	Taylor	(1953)	(71)
..	88	-	-	Hillman	(1954)	(72)
..	16-112	-	-	Bowen	(1961)	(73)
..	129-151	-	Relative only	Measday	(1966)	(74)
Differential Cross-section	70-109	-	-	Bowen	(1961)	(73)
..	91	-	Relative only	Stahl	(1954)	(75)
..	128	-	Relative	Hobbie	(1960)	(76)*
..	137	-	-	Thresher	(1955)	(77)
..	133, 153	-	Relative	Randle	(1956)	(78)
..	129, 150	-	Relative	Measday	(1966)	(74)
Polarisation	20-120	-	-	Langsford	(1965)	(79)
..	77	-	Relative only	Whitehead	(1960)	(80)
..	95	-	-	Stafford	(1962)	(81)
..	126	-	10 %	Carrol	(1964)	(82)

TABLE 19

N-P

Parameter	Energy	Renormalisation	Normalisation error	Author		Reference
Polarisation	128	-	10 %	Hobbie	(1960)	(83)
..	140	1.097	7%	Stafford	(1962)	(84)
Transfer Depolarisation	128	-	-	Patel	(1962)	(85)
..	128	-	-	Collins	(1964)	(86)*
P-P Bremsstrahlung (e.g.)						
	140	-	-	Edgington	(1966)	(17)*
	158	-	-	Gottshalk	(1966)	(87)
Triple scattering parameters measured using deuterons, and corrected by Cromer (89) for binding.						
A,R in N-P	135, 137 resp.		-	Hoffman	(1962)	(92)*

*It is recommended[16)153)91)] that these data are ignored.

** 90, 108 Mev points suspect[91)]: see FIG.36.

TABLE 19

VIII Appendices

8.1 Calculation of the proton flight paths in the magnetic field of Cnn magnet

The technique used was that of F.J.M.Farley,[97] as published in a CERN report. The paths of the individual protons in the magnetic field are traced by a step by step calculation. The parameters used are shown in FIG.41, and are defined as follows:

x = radial distance from centre of magnet in cm.

y = azimuth angle in radians.

z = inclination of track to radius vector in radians.

ϱ = radius of curvature of trajectory.

y and z are both measured in the same rotational direction. By moving a distance h along the particle trajectory from (x,y,z) to (x',y',z')

(a) $x' = x + h\cos(z) - h^2 \sin(z)/2\varrho + h \sin(z)/2x$

(b) $y' = y + h \sin(z)/x' + h^2 \cos(z)/2\varrho x'$

(c) $z' = z + h/\varrho - (y'-y)$

In (a) and (b) ϱ enters only to second order, and thus the value of ϱ at the beginning of the step may be used in (c) $\bar{\varrho}$ is the value of ϱ at the midpoint of the step. This can be calculated from (a) and from

(d) $\varrho = 3.336\ P/B$ where P is momentum in Mev/c

B is field in kilogauss.

Two programmes were written: one using a fitted polynomial to the fringeing field, the other using the fringeing field at 0.5 cm. intervals and an interpolation routine. The results computed in each way were in good agreement.

Reference (97)

F.J.M.Farley C.E.R.N Report 59-12 Geneva (1959)

FIG. 40

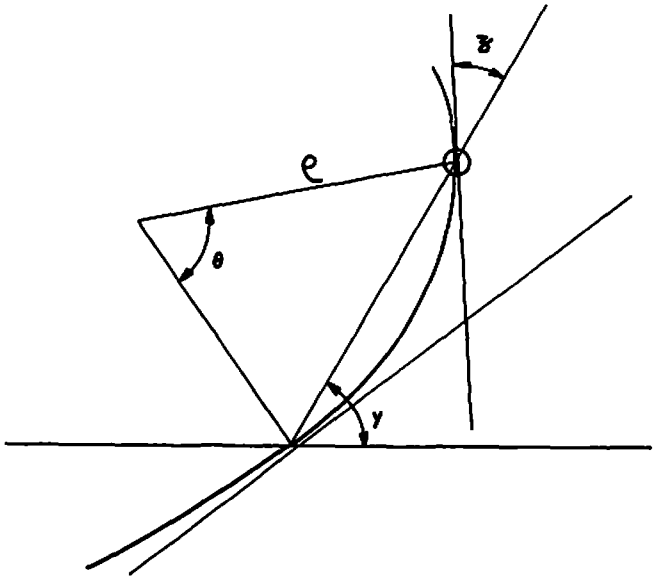

PARAMETERS USED IN ORBIT CALCULATION

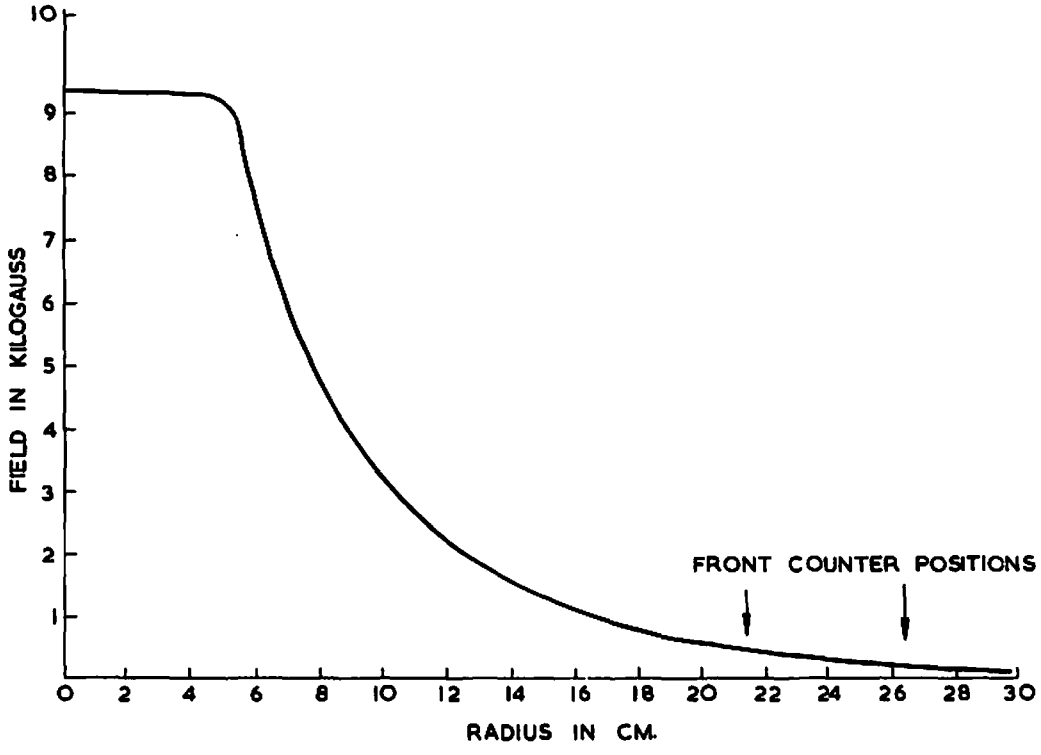

FIELD OF C_{NN} MAGNET

FIG. 41

8.2 Use of the error matrices obtained in Cnn analysis

The analysis carried out for the 143.2 Mev Cnn data has been shown to give a value of 0.1656 ± 0.0019 for the polarisation in proton-proton scattering at the overall mean angular setting of the 30° telescopes. This is supposed to be 30° Lab (61.8° centre of mass). The values for Cnn are quite independent of this angle, as the only effect of the arm was to provide an admixture of analysing power for the polarisation measurement. If it is taken that the angle was in fact 30° Lab, then the result obtained may be checked against the recent measurements of Cox et al[13] at 140.7 Mev. These measurements were made using the same beam, and thus the value of the proton-proton polarisation (P3) given by their data is 0.162 ± 0.003 when corrected to 143.2 Mev using the known energy dependence of P3 from the literature, see FIG.19.

If this value of P3 is imposed on our results, then by using the error matrices of TABLE 5, we may give the corrected value of Cnn. We take the two-variable regression equation of y[=Cnn(90°)] on x(=P3).

$$E(y|x) = \beta_{yx} + \rho_{xy}\frac{\sigma_y}{\sigma_x}[x - \mu_x]$$

As we have moved 1.9 standard deviations σ_x (note: we are not here using the values renormalised for overall χ^2/point),

$[E(y/x)] = -0.47\ \sigma_y = -0.018$;

thus Cnn (90°) becomes 0.982 ± 0.0039

The derivation of the equation for E(y|x) is now given.

We have a bivariate distribution $f(x|y) = \frac{f(x,y)}{f(y)}$.

If we take a normal distribution:

$$f(x|y) = \frac{1}{2\pi\sqrt{1-\rho^2}\,\sigma_x\sigma_y} \text{Exp}\left[-\frac{1}{2(1-\rho^2)}\left(\frac{x-\mu_x}{\sigma_x}\right)^2 - 2\rho\left(\frac{(x-\mu_x)(y-\mu_y)}{\sigma_y\sigma_x}\right) + \left(\frac{y-\mu_y}{\sigma_y}\right)^2\right]$$

$$\frac{1}{\sqrt{2\pi}\,\sigma_y}\text{Exp}\left[-1/2\left(\frac{y-\mu_y}{\sigma_y}\right)^2\right]$$

This is the P.D.F. of $N(\mu_x + \rho_{xy}\frac{\sigma_x}{\sigma_y}(y-\mu_y), \sigma_x^2(1-\rho^2))$

thus the regression line is $E(x|y) = \mu_x + \rho_{xy}\cdot\frac{\sigma_x}{\sigma_y}\cdot(y-\mu_y)$.

8.3 Asymmetry formulae

The general form for the cross-section for the scattering of a beam of polarised protons from an unpolarised target has been given in chapter one. If we restrict our attention to the case of scattering in the plane perpendicular to the plane of incident polarisation, we may express the count rates recorded in two telescopes set at angles θ_L and θ_R (to proton left and right respectively of the beam), in the following manner. L,R = left or right; U,D = incident proton spin up or down, set by the spin precession solenoid.

$$\text{L.U.} = N_u e_L I(\theta_L)[1 + P_1 P_2(\theta_L)]$$

$$\text{L.D.} = N_D e_L I(\theta_L)[1 - P_1 P_2(\theta_L)]$$

$$\text{R.U.} = N_U e_R I(\theta_R)[1 - P_1 P_2(\theta_R)]$$

$$\text{R.D.} = N_D e_R I(\theta_R)[1 + P_1 P_2(\theta_R)]$$

where $I(\theta)$, $P_2(\theta)$ are the differential cross-section and polarisation for proton-proton scattering of an unpolarised beam from an unpolarised target at an angle θ: e_L, e_R are the efficiencies of the two arms Left and Right: P_1 is the polarisation of the incident beam: and N_u, N_D are the number of protons incident on the target for one monitor count when the incident proton spins are up or down respectively.

Defining r as $\left\{\frac{LU}{RU}\frac{RD}{LD}\right\}^{\frac{1}{2}}$, and $\xi_L = P_1 P_L(\theta_L)$

$$\xi_R = P_1 P_L(\theta_R)$$

$r = \left\{\frac{1+\xi_L}{1-\xi_R}\right\}^{\frac{1}{2}} \times \left\{\frac{1+\xi_R}{1-\xi_L}\right\}^{\frac{1}{2}}$; independent of e_L, e_R, N_L, N_D.

if we now take θ_L to be $\simeq \theta_R$, and write $\varepsilon_L = \varepsilon + \delta$, $\varepsilon_R = \varepsilon - \delta$

then $r \simeq \frac{1+\varepsilon}{1-\varepsilon}(1 + 2\varepsilon\delta^2)$

where δ^4 and higher terms are neglected; and ε^2 is neglected compared to 1 in the second term. As in the case of 98 Mev p-C^{12} the maximum value of ε^2 is ~ 0.08, this is acceptable. Thus $\varepsilon = \left(\frac{r-1}{r+1}\right) - \varepsilon\delta^2$ to the same order of accuracy. As an estimate of the size of the second term, consider $\theta_L - \theta_R = 2^\circ$ then δ refers to 1° and $\delta = P_1 \frac{\partial P_1}{\partial \theta}$. The highest value of $P_1 \frac{\partial P_1}{\partial \theta}$ obtained in the proton-proton scattering gives $\delta^2 \sim 10^{-5}$. The term was thus neglected, and the formula $\varepsilon = \left(\frac{r-1}{r+1}\right)$ used for the asymmetry, which then refers to the angle $\left(\frac{\theta_L + \theta_R}{2}\right)$.

8.4 Statistical error on the asymmetry

We label the four counts at a given angle Xi (i=1-4) when $r = \sqrt{\frac{X_1 \cdot X_3}{X_2 X_4}}$. We have already shown that this expression is not dependent on monitoring, and thus the standard deviation of each count is given by its square root.

$$\left\{\frac{\Delta(r^2)}{r^2}\right\}^2 = \sum_{i=1}^{4} \left\{\frac{\Delta(x_i)}{x_i}\right\}^2 = \sum_{i=1}^{4} \left(\frac{1}{x_i}\right)$$

now $\frac{d\varepsilon}{dr} = \frac{2}{(r+1)^2}$; as $\varepsilon = \frac{r-1}{r+1}$

thus $\Delta\varepsilon = \frac{2}{(r+1)^2} \cdot \frac{1}{2} r \cdot \frac{\Delta(r^2)}{r^2} = \frac{r}{(r+1)^2}\left(\sum_i^4 \left(\frac{1}{x_i}\right)\right)^{\frac{1}{2}} = (1-\varepsilon^2)\sqrt{\sum_i^4 \left(\frac{1}{x_i}\right)}$

As $a \simeq b \simeq c \simeq d$ (as a consequence of the small asymmetries measured) $\Delta\varepsilon = \frac{1-\varepsilon^2}{\sqrt{N}}$ where $N = a + b + c + d$.

8.5 Effects of beam movements on the measured asymmetries

If the beam alters position between the two solenoid settings, or if the beam spot varies in position at a given

solenoid setting, false asymmetries may be introduced. These asymmetries come from two sources: (a) the change in cross-section with angle, (b) the change in polarisation with angle. The previous appendix has shown that the values of the asymmetry calculated in the manner described are independent of small differences between the left and right scattering angles. This allows us to assume that the spin-up beam has equal left and right angles of scattering (θ), and the spin-down beam, is displaced $\Delta\theta$ to proton left.

For case (a) $r = \frac{1+\epsilon}{1-\epsilon} \cdot \left[\frac{\sigma(\theta)\,\sigma(\theta-\Delta\theta)}{\sigma(\theta)\,\sigma(\theta+\Delta\theta)}\right]^{\frac{1}{2}}$ neglecting $P(\theta)$effects

For case (b) $r = \left(\frac{1+P_1 P_2(\theta)}{1-P_1 P_2(\theta)} \cdot \frac{1+P_1 P_2(\theta-\Delta\theta)}{1-P_1 P_2(\theta+\Delta\theta)}\right)^{\frac{1}{2}}$

neglecting $\sigma(\theta)$ effects.

Expressing r to first order terms in $\Delta\theta$, and writing $P_1P_2(\theta) = \epsilon$, and $P_1P_2(\theta+\Delta\theta) - P_1P_2(\theta) = \Delta\epsilon$

(a) becomes $r = \frac{1+\epsilon}{1-\epsilon}\left(1-\Delta\theta\frac{1}{\sigma}\frac{d\sigma}{d\theta}\right)$

(b) becomes $r = \frac{1+\epsilon}{1-\epsilon}\left(1+\epsilon\Delta\epsilon\right)$

Rearranging again to first order in $\Delta\theta$

(a) gives $\epsilon \doteq \frac{r-1}{r+1} + \frac{1}{2}\Delta\theta\left[\frac{1}{\sigma}\frac{d\sigma}{d\theta}\right]$

(b) gives $\epsilon \doteq \frac{r-1}{r+1}\left[1-\frac{1}{2}\Delta\theta\left(P_1\frac{\partial P_2}{\partial\theta}\right)\right]$

For hydrogen the magnitudes of these effects are, in the worst cases, (a) 1 part in 500

(b) 1 part in 3000

although the effects can be larger for the carbon case. The beam lines for spin-up and spin-down cases differ only slightly, the measured angular difference between the two

lines being $0.005^{\circ} \pm 0.003^{\circ}$. As the beam position is defined by the last collimator up-stream of the hydrogen target, movements of the beam during runs with constant spin-up (or down) are negligible. The centre of gravity of the beam spot incident on the ionisation chambers could be held steady to better than 0.1 mm. without difficulty, thus reducing any effect still further.

8.6 Application of the background asymmetry correction

The asymmetry (ε_F) measured in scattering from a full hydrogen target may be written $\varepsilon_F = \frac{L_F - R_F}{L_F + R_F}$ where $L_F (R_F)$ is the count in the left (right) hand telescope. The count L_F is made up of L_H from the liquid hydrogen and L_B from other material in the beam.

Thus $$\varepsilon_F = \frac{L_H - R_H + L_B - R_B}{L_H + R_H + L_B + R_B}$$

and if we write $\frac{L_B + R_B}{L_H + R_H}$ as f, the background fraction

$$\varepsilon_F = \frac{\varepsilon_H}{1+f} + \frac{\varepsilon_B}{1+f}$$

or $$\varepsilon_H = \varepsilon_F + [\varepsilon_F - \varepsilon_B] f$$

8.7 Asymmetry correction due to the finite size of the defining scintillators

The finite vertical extent of the defining scintillators causes a reduction in the asymmetry measured, as scattering at an angle ϕ to the horizontal is included with the scattering in the horizontal plane. The effective asymmetry is then reduced to $P_1(\cos\delta)P_2(\theta)$, where δ is the angle between the normals to the horizontal and the ϕ-inclined planes see FIG. 42. The measured asymmetry is then $P_1 P_2 (\theta) \overline{\cos(\delta)}$

$$\varepsilon_{meas} = P_1 P_2 \int \cos\delta \, dy$$

FIG. 42

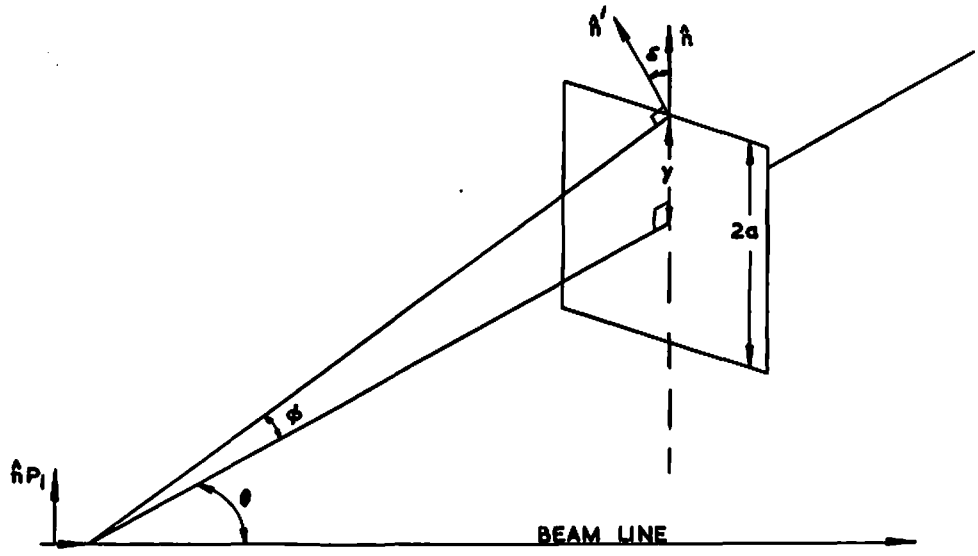

FIGURE FOR EFFECT OF FINITE SIZE OF THE COUNTER ON THE ASYMMETRY.

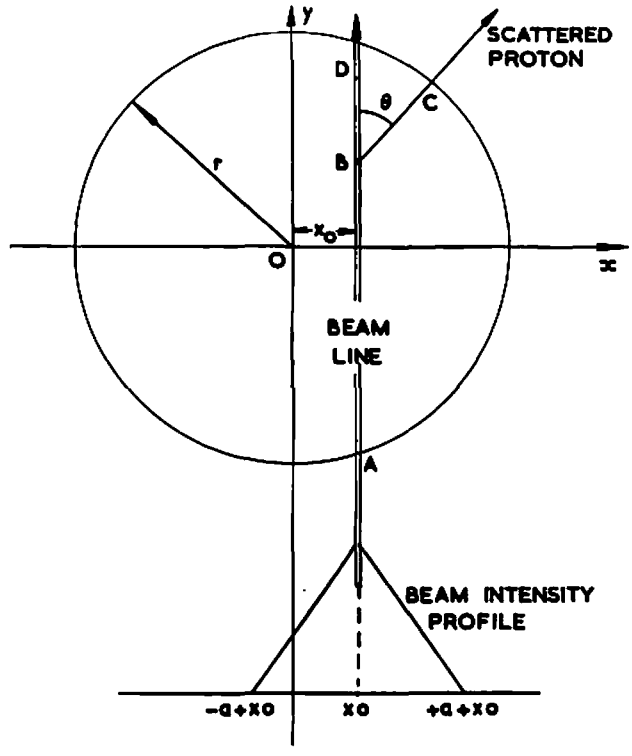

FIGURE FOR COMPUTER CODE DISCUSSION.

FIG. 43

Now $\delta = \tan^{-1}\left[\frac{y}{l\sin\theta}\right]$, where l is the distance between target and counter. Thus, expanding the expression for $(\cos\delta)$ in terms of y, a term by term integration may be made,

$$\varepsilon_{meas.} = P_1P_2 - \frac{1}{6}P_1P_2\left(\frac{a}{l\sin\theta}\right)^2 + \text{higher terms.}$$

The fractional correction is thus: $-\frac{1}{6}\left(\frac{a}{l\sin\theta}\right)^2$, and amounts to 0.5 % in the worst case.

8.8 Computer code used for the absorbers and various effects on P and $d\sigma/d\Omega$ measurements

A computer code was written for the I.B.M. 7030 to compute the copper absorbers required for the 98 Mev experiments, and to define as consistently as possible an energy threshold to remove protons, e.g. at 13 or 20 Mev down from the mean energy of the incident proton beam, taken at the mean centre of scattering. The effects of beam size, target position, target shape and beam intensity profile were included in the calculations. The loss of protons due to absorption in the hydrogen was included in the computation, and the losses after scattering could conveniently be obtained for all angles. The total cross-section data of Goloskie et al were used for this stage. The range curves of Sternheimer as published in the N.I.R.N.S. High Energy and Nuclear Physics Handbook (Chilton 1963)[105] were used for losses in Cu, CH, CH_2, Al and air. The curves of UCRL 2426 (1960) were used for the energy losses in hydrogen.

All range curves were reduced to the form:
Range (gm/cm**2) = A.Exp (BT), where T = energy in Mev, for the energy range 20-60 Mev. The parameters used are given here

	H_2	CH	CH_2	AIR	Al	Cu
A	0.72×10^{-3}	1.85×10^{-3}	1.758×10^{-3}	2.22×10^{-3}	2.66×10^{-3}	3.44×10^{-3}
B	1.843	1.810	1.805	1.800	1.785	1.761

The mean thickness of the target depends on the beam intensity profile used: a trapezoidal shape was chosen as it could give a close fit to the gaussian distribution observed in the beam spot. The parameters of the trapezium were chosen by taking a microphotodensitometer trace of the beam spot at the target position and comparing the shapes and areas graphically.

8.9 Spin precession in the solenoid

The precession of the proton spins produced by passing protons down the axis of the solenoid is due to the interaction of the axial field (H) of the solenoid with the magnetic moment of the proton ($\underline{\mu}$). From the classical statement of the problem, $\underline{\mu} \times \underline{H} = \underline{P} \cdot \underline{\omega}$, where $\underline{P}$ is the angular momentum of the proton. Also, $\omega = g_p \mu_N \frac{H}{\hbar}$ in the semi-classical approximation, where g_p is the gyromagnetic ratio of the proton and μ_N the nuclear magneton. As the time for the proton of velocity v to traverse a distance L along the solenoid is given by $\frac{L}{v}\left(1 - v^2/c^2\right)^{\frac{1}{2}}$, the length of solenoid (L) required to precess the proton spins through π radians about the beam axis is given by

$$t_\pi = \frac{\pi \hbar}{g_p H \mu_N} = \frac{L}{v}\left(1 - v^2/c^2\right)^{\frac{1}{2}}$$

$$\text{Thus } L.H = \frac{\hbar v \pi}{g \mu_N \left(1 - v^2/c^2\right)^{\frac{1}{2}}}$$

The beam spread before the degrader is less than $\pm$ 1.4 Mev (FWHM) , which would introduce a % reduction of the incident- beam polarisation of < 0.15 % , which is negligible compared to the experimental error of 0.85 % on the absolute value of the beam polarisation.[57]

A precise derivation of this effect has been described by Bargmann et al.[78]

8.10 p-p Differential cross-section at 98.8 + 0.3 Mev

The data shown in preliminary form in FIG.34 and listed in TABLE 17 was taken while this thesis was being written. As these preliminary results were used in the phase-shift analysis discussed in 7.5, a short account of the experiment is given here.

The experimental layout is shown in FIG.44, and the scintillation counter sizes and distances are those listed in TABLE 6. Shielding and antiscattering collimation was used in addition to that shown in FIG.44.

The experimental techniques were similar to those of Ref.13, however more care was taken in the measurement of the absorption losses in copper used in the scattering arms. The hydrogen scattering chamber differed slightly from that used for 97.7 Mev p-p P(θ) work, and thicker (.013cm) Kapton was used for the entry and exit windows of the vacuum chamber.

The energy discrimination level used, rejected protons more than 20 Mev down from the mean beam energy at the centre of the target, which was $\sim$8.6 Mev thick. Details of the beam shape are shown in FIG.45.

The absolute calibration of the monitor was carried out by the method reported in Refs. 13 and 152 using the long duty cycle beam.[116] The block diagram in FIG.45 shows the fast-slow system used. The resolving times of all the fast circuits were set at 18 ns, so that the fast systems could count once and only once each r.f. cycle (100 MHz units) or once every cycle - other than one following a cycle in which it had counted - (1 MHz units), giving counts in a given time of $N_{/00}$, $N_{/0}$ respectively.

The actual number (N) of protons passing through the

FIG. 44

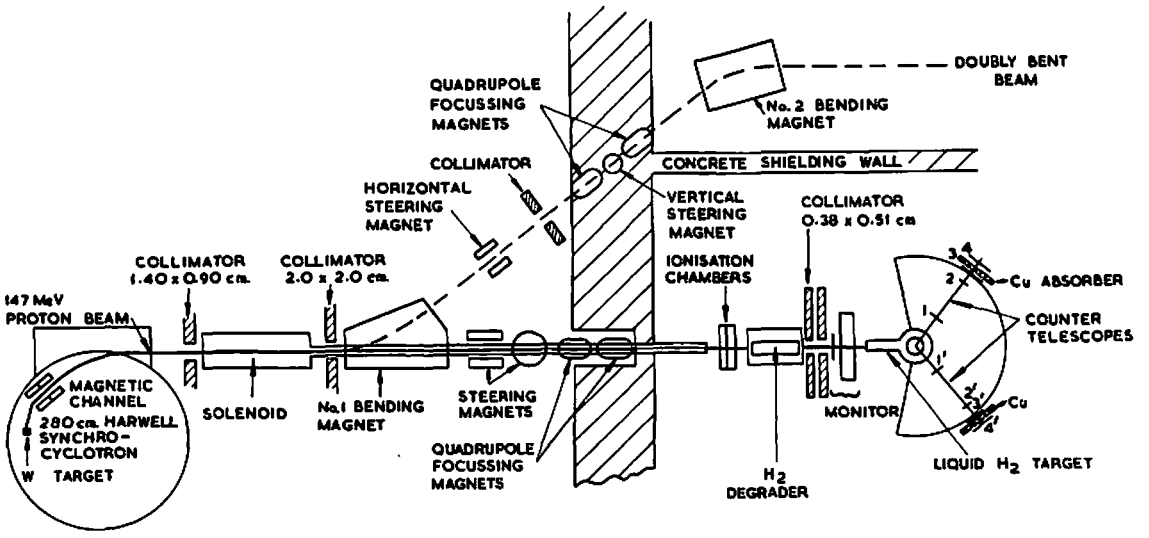

EXPERIMENTAL LAYOUT FOR 98 MeV P-P: $\sigma(\theta)$

ELECTRONICS USED TO CALIBRATE THE BEAM MONITOR.

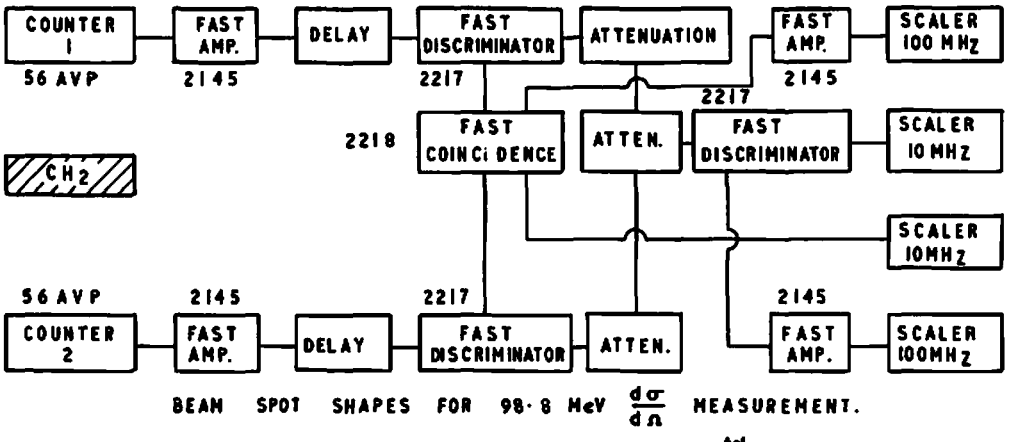

BEAM SPOT SHAPES FOR 98·8 MeV $\frac{d\sigma}{d\Omega}$ MEASUREMENT.

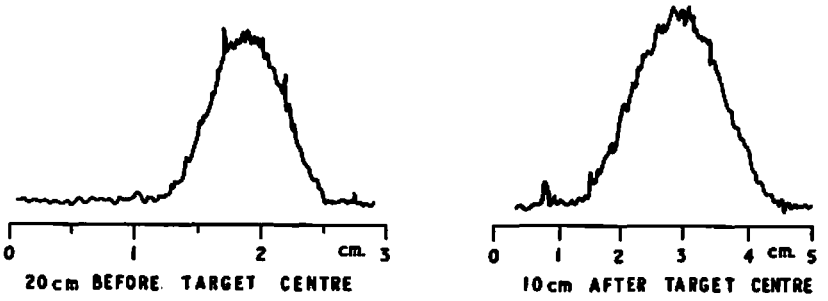

FIG. 45

fast-slow counter system is given by:

(a) $N = N_{/\infty}\ N_{/o}\ \log[\ N_{/o}/(2N_{/o} - N_{/\infty}\ )]/[N_{/\infty} - N_{/o}\ ]$

which reduces to

(b) $N \simeq N_{/\infty} + [\ N_{/\infty} - N_{/o}\ ]/2$

when $N_{/\infty}$ is close to $N_{/o}$. This relation (a) was tested over a wide range of intensities and duty cycles, and found to give the same value for protons/monitor count. An absolute normalisation of 1.0000 ± 0.0082 was finally obtained for the cross-section data.

References (1)

1) R.Wilson: The Nucleon-Nucleon Interaction Wiley (1963)

2) M.Moravcsik: The Two Nucleon Interaction O.U.P (1963)

3) H.A.Bethe: Ann.Phys. (3)190 (1958)

4) A.G.Petschek: Ann.Rev.Nuclear Science 14 p29 (1964)

D.M.Brink,R.E.Peierls: Comments on Nuc. and Part.Phys. 1,4 p110 (1967)

J.Mahalanabis: Thesis University of London (1964)

A.H.Cromer,J.N.Palmieri: Ann.Phys. 30 p32 (1964)

A.K.Kerman,H.McManus,R.M.Thaler: Ann.Phys. 8 p551 (1959)

D.W.L.Sprung,P.C.Bargava,T.K.Dahlblom: Phys.Lett. 21,5 p538 (1966)

6) J.M.Pearson: Can.J.Phys. 45,3 p1290 (1967)

7) J.P.Elliot,H.A.Mavromatis,E.A.Sanderson: Phys.Lett. 24B,8 p358 (1967)

8) P.Cziffra,M.H.MacGregor,M.J.Moravcsik,H.P.Stapp: Phys.Rev. 114 p880 (1959)

A.P.Grashin: Soviet Physics JETP (9) p1223 (1959)

9) D.Amati,E.Leader,B.Vitale:Nuovo Cim. 18 p458 (1960)

10) P.Signell: Phys.Rev. 133,4B pB982 (1964)

11) A.Scotti,D.Y.Wong: Phys.Rev. 138,1B pB145 (1965)

J.S.Ball,A.Scotti,D.Y.Wong: Phys.Rev. 142 p1000 (1966)

12) R.A.Bryan,B.L.Scott: Phys.Rev. 135 pB434 (1964)

13) O.N.Jarvis,G.F.Cox,G.H.Eaton,B.Rose,C.P.van Zyl: Proceedings of Williamsberg conference on Intermediate Energy Physics: College of William and Mary II p595 (1966) (also to be submitted to N.P.)

G.F.Cox: PhD thesis Birmingham (1965)

14) G.Kopp,G.Kramer: Phys.Lett. 19,7 p593 (1965)

15) R.A.Arndt,R.A.Bryan,M.H.MacGregor: Phys.Rev. 152 4 p1490(1966)

References (2)

16) R.A.Arndt,M.H.MacGregor: Phys.Rev. 141 3 p873 (1966)

17) J.A.Edgington,B.Rose: Phys.Lett. 20 5 p552 (1966)

18) L.Wolfenstein,J.Ashkin: Phys.Rev. 85 p847 (1952)
L.Wolfenstein: Ann.Rev.Nuc.Sci. 6 p43 (1956)

19) A.E.Woodruff: Ann.Phys. 7 p65 (1959)

20) R.J.N.Phillips: Nuovo Cim. 10,8 p265 (1958)

21) R.J.N.Phillips: A.E.R.E. R5138 (1966)

22) L.Puzikov,R.Ryndin,Ia Smorodinskii: Soviet Physics JETP (5) p489 (1957)

23) C.R.Schumacher,H.A.Bethe: Phys.Rev. 121 p1534 (1961)

24) Proceedings of conference on polarised targets and ion sources Dec. 1966 (Saclay 1967)
V.I.Lushikov,Y.V.Tarn,A.I.Frank: JETP Letters I 2 April (1965)

25) P.Hillman,A.Johannson,G.Tibell: Phys.Rev. 110 p1218 (1958)

26) R.Beurtey: These Rapport C.E.A. R2366 (C.E.N. Saclay France

27) the earliest being A.Abragam,M.Borghini et al: Phys.Lett. 2,7 p310 (1962)

28) R.C.Tolman: The principles of statistical mechanics p78 O.U.P. (1938)

29) H.R.Stapp: Phys.Rev. 103 p425 (1956)

30) L.Wolfenstein: Phys.Rev. 96 p1654 (1954)

31) M.H.MacGregor,M.J.Moravcsik,H.P.Stapp: Ann.Rev.Nuc.Sci. 10 p291 (1960)

32) H.P.Stapp: Thesis U.C.L.A Report UCRL 3098 (1956)
H.P.Stapp,T.J.Ypsilantis,N.Metropolis: Phys.Rev. 105 p302 (1957)
D.W.L.Sprung: Phys.Rev. 121 3 p925 (1961)
A.Garren: Thesis Carniegie Tech. Report NYO-7102 (1955)

33) J.M.Blatt,L.C.Biedenharn: Phys.Rev. 86 p399 (1952)

References (3)

34) E.H.Thorndike: Phys.Rev. 138 3B pB586 (1965)
E.H.Thorndike: Univ. of Rochester Report UR-895-67

35) E.Fermi,N.Metropolis,E.F.Alei: Phys.Rev. 95 p1581 (1954)

36) P.Cziffra,M.H.MacGregor,M.J.Moravcsik,H.P.Stapp:
Phys.Rev. 114 p880 (1959)
A.F.Grashin: Soviet Physics JETP 9 p1223 (1959)

37) G.Breit,M.H.Hull,K.E.Lassila,K.D.Pyatt: Phys.Rev.
120 p2227 (1960)

38) O.N.Jarvis,T.W.P.Brogden,B.Rose,J.Orchard-Webb,J.P.Scanlon,
M.R.Wigan: A.E.R.E. Report R-5556 (1967) ~~to be~~ pub.
in Nuc. Phys. (Jan 29 1968)

39) M.R.Wigan,P.M.Martin: to be published

40) L.Eisenbud,E.P.Wigner: Proc.Nat.Acad.Sci. 27 p281 (1941)

41) T.Hamada,I.D.Johnston: Nuc.Phys. 34 p382 (1962)
K.E.Lassila,M.H.Hull,H.M.Ruppel,F.A.MacDonald,G.Breit:
Phys.Rev. 126 p881 (1962)

42) R.Jastrow: Phys.Rev. 81 p165 (1951)

43) C.Bressel,A.K.Kerman,E.L.Lomon: Bull.Am.Phys.Soc.
10 p584 (1965)

44) G.Breit: Proc. of the Conf. on Intermediate En. Phys.
Vol. 2,p1 College of William and Mary (1966)

45) A.E.S.Green,T.Sawada: Nuc.Phys. B2 p267 (1967)

46) G.Breit: Rev.Mod.Phys. 34 4 p766 (1962)

47) J.N.Palmieri,A.M.Cormack,N.F.Ramsey,R.Wilson:
Ann.Phys. 5 p299 (1958)

48) J.W.Durso,P.Signell: Phys.Rev. 135B1057 (1964)

49) A.E.Taylor,E.Wood,L.Bird: Nuc.Phys. 16 p320 (1960)

50) O.N.Jarvis,B.Rose: Phys.Lett. 15 p271 (1965)

51) O.N.Jarvis,B.Rose,G.F.Cox,G.H.Eaton: Nuc.Phys. 61 p194 (1965)

52) E.H.Thorndike,T.R.Ophel: Phys.Rev. 119 p362 (1960)

References (4)

53) C.Caversazio,K.Kuroda,A.Michaelowicz:
J.Phys.Rad. 22 p628 (1961)
C.Caversazio,A.Michaelowicz,K.Kuroda,M.Poulet,N.Poutcherov:
J.Phys.Rad. 24 p1048 (1963)

54) D.E.Young,L.H.Johnston: Phys.Rev. 119 p313 (1960)

55) P.Christmas,A.E.Taylor: Nuc.Phys. 41 p388 (1963)

56) R.Goloskie,J.N.Palmieri: Nuc.Phys. 55 p453 (1964)

57) O.N.Jarvis,B.Rose,J.P.Scanlon: Nuc.Phys. 77 p161 (1966)

58) C.D.Jeffries: Dynamic Nuclear Orientation Interscience NY (1963)
A.Abragam,M.Borghini: Prog. in Low Temp. Phys. Vol. 4 (1964)
G.Shapiro: Prog. in Nuc. Tech. and Inst. Vol 1 (1964)

59) Proc. of the Saclay Conf. on Polarised Targets and Ion Sources Dec. 1966 Saclay (1967)

60) P.L.Scott,C.D.Jeffries: Phys.Rev. 127 p32 (1962)

61) T.W.P.Brogden: A.E.R.E. Harwell report (1966)

62) C.F.Hwang,T.R.Ophel,G.H.Thorndike,R.Wilson: Phys.Rev. 119 p352 (1960)

63) L.Bird,P.Christmas,A.E.Taylor,E.Ward: N.P. 27 p586 (1961)

64) E.Thorndike,J.Le Francois,R.Wilson: Phys.Rev. 120 p1819 (1960)

65) L.Bird,D.N.Edwards,B.Rose,A.E.Taylor,E.Wood: N.P. 42 p280 (1963)

66) S.Hee,R.Wilson: Phys.Rev. 132 p744 (1963)

67) O.N.Jarvis,B.Rose,G.H.Eaton,C.P.van Zyl: N.P. 50 p529 (1964)

68) S.Hee,E.Thorndike: Phys.Rev. 132 p744 (1963)

69) O.N.Jarvis,B.Rose,J.P.Scanlon,E.Wood: N.P. 42 p294 (1963)

70) A.E.Taylor,E.Wood: Proc.Phys.Soc. A69 p645 (1956)

71) A.E.Taylor,E.Wood: Phil.Mag. 44 p95 (1952)

72) P.Hillman,R.H.Stahl,N.F.Ramsey: Phys.Rev. 96 p115 (1954)

73) P.Bowen,G.C.Cox,G.B.Huxtable,A.Langsford,J.P.Scanlon, J.J.Thresher: Phys.Rev.Lett. 7 p248 (1961)

74) D.F.Measday,J.N.Palmieri: N.P. 85 p142 (1966)

75) R.H.Stahl,N.F.Ramsey: Phys.Rev. 96 p1310 (1954)

76) R.K.Hobbie,D.Miller: Phys.Rev. 120 p2201 (1960)

77) R.G.P.Voss,J.J.Thresher,R.Wilson: Proc.Roy.Soc. A224-493 (1955)

78) T.C.Randle,D.M.Skyrme,M.Snowden,A.E.Taylor,F.Uridge, E.Wood: Proc.Phys.Soc. A69 p360 (1956)

79) A.Langsford,P.H.Bowen,G.C.Cox,G.B.Huxtable,R.A.J.Riddle: N.P. 74 p241 (1965)

80) C.Whitehead,S.Tornabene,G.H.Stafford: Proc.Phys.Soc. 75 p345 (1960)

81) G.H.Stafford,C.Whitehead: Proc.Phys.Soc. 79,2 p430 (1962)

82) A.S.Carroll,P.M.Patel,N.Strax,D.Miller: Phys.Rev. 134B p595 (1964)

83) R.K.Hobbie,D.Miller: Phys.Rev. 120 p2201 (1960)

84) G.H.Stafford,C.Whitehead: Proc.Phys.Soc. 79 p508 (1962)

85) P.M.Patel,A.S.Carroll,N.Strax,D.G.Miller: Phys.Rev.Lett. 8 p491 (1962)

86) W.G.Collins Jr.,D.G.Miller: Phys.Rev. 134 B575 (1964)

87) B.Gottshalk,W.J.Schlaer et al: Nuc.Phys. 75 3 p549 (1966)

88) U.E.Kruse,J.M.Teem,N.F.Ramsey: Phys.Rev. 101 3 p1079 (1956)

89) A.Cromer: Phys.Rev. 113,1607 (1959)
A.Cromer,E.H.Thorndike: Phys.Rev. 131 p1680 (1963)

90) R.Hoffman,J.Le Francois,E.H.Thorndike,R.Wilson: Phys.Rev. 125 p973 (1962)

91) P.Signell,N.R.Yoder: Phys.Rev. 134 1B (1964)
H.P.Noyes,P.Signell,N.R.Yoder,R.M.Wright: SLAC-PUB-269(1967)

References (6)

92) J.K.Perring: Rev.Mod.Phys. July (1967)

93) A.J.George,D.T.Teaney: Rev.Sci.Instr. 31 p997 (1960)

94) V.Petriceck: preprint (1967)
C.Ryter: Nuc.Inst.Meth. 49 p267 (1967)
V.Petriceck,M.Odenhal C.E.N.Saclay Report April (1967)

95) J.Butterworth,J.Orchard Webb,J.Riley,M.R.Wigan:
Proc.Phys.Soc. 91 p605 (1967)

96) T.W.P.Brogden,J.Butterworth: Proc.Roy.Soc. 86 p877 (1965)

97) F.J.M.Farley C.E.R.N. Report 59-12 Geneva (1959)

98) V.Bargemann,L.Michel,V.L.Telegdi: Phys.Rev.Lett. 2
10 433 (1959)

99) R.A.Arndt,M.J.Moravcsik,R.M.Wright: Nuov.Cim IL A 4
p606 (1967)

100) D.Garreta: Private communication

101) T.W.P.Brogden: Proc.Roy.Soc. A283 p480 (1965)

102) A.Abragam,M.Borghini,M.Chapellier: Compt.Rend. 255 p1343
(1962)
A.Abragam: Compt.Rend. 258 p1773 (1964)
M.Chapellier: Compt.Rend. 258 p112 (1964)
A.Abragam,M.Chapellier Phys.Lett. 1103 p207 (1964)

103) L.J.Challis Proc.Roy.Sos. A26 p31 (1961)
L.J.Challis Proc.Phys.Soc. 80 p759 (1962)

104) B.Bleaney,W.Hayes,P.M.Llewellyn Nature 179 p140 (1957)

105) High Energy and Nuclear Physics Handbook, ed. W.S.C.Williams
and W.Galbraith N.I.R.N.S. Chilton (1963)

106) L.Van Gerven,A.Van Itterbeck,L.De Laet: Proc.First Int.Conf.
on Paramagnetic Resonance: Jerusalem 1962 Vol 2 p605 (1963)

107) O.S.Liefson,C.D.Jeffries: Phys.Rev. 122 p1781 (1961)

108) P.G.De Gennes: J.Phys.Chem.Solids 7 p345 (1958)

1 9) T.J.Schmugge,C.D.Jeffries Phys.Rev. 138 pA1785 (1965)

11) G.R.Khutsishvili: Soviet Physics-JETP 15 p909 (1962)

111) J.Ramakrishna,F.N.H.Robinson: Proc.Phys.Soc. 87 p945 (1966)

112) W.N.Hardy,G.Shapiro: C.E.N.Saclay Report June (1966)

113) M.A.Preston: Physics of the Nucleus Addison-Wesley (1963)

114) R.J.N.Phillips,W.Rarita: U.C.R.L. 16185 (1965)

115) J.K.Perring: Proc. of Antwerp conf. on Nuclear structure studies with Neutrons July 1965. North Holland (1966)

116) O.N.Jarvis,B.Rose,J.P.Scanlon,E.Wood: Nuc.Phys. 42 p294 (1963)

117) C.Whitehead,L.Bird,E.Wood,E.G.Auld,D.G.Crabb,J.G.McEwen: A.E.R.E. Report NP.GEN. 33 (1964)

118) G.B.Huxtable,P.S.Rogers,F.M.Russell: Nuc.Inst.Meth. 23 p357 (1963)

119) E.Leader,R.C.Slansky: Phys.Rev. 148 4 p1491 (1966)

120) P.B.Kantor: Phys.Rev. 148 4 p1411 (1966)

121) J.H.Tinlot,R.E.Warner: Phys.Rev. 124 3 p890 (1960)

122) F.N.H.Robinson: Rev.Sci.Inst. 34 p1260 (1963)

123) B.Rose: A.E.R.E. Harwell Report A.E.R.E HL66/1362 (1966)

124) P.M.Portner,R.B.Moore: Can.J.Phys. 43 p104 (1965)

125) L.S.Azhgirey,V.I.Chizikov: JINR Preprint E1-3420 Dubna (1967)

126) P.G.O.Freund,S.Y.Lo: Phys.Rev. 140 No 4 pB927 (1965)

127) R.M.Sternheimer: Phys.Rev. 115 p137 and later revisions [e.g see Ref. 105]

128) H.Bichsel: a private communication acknowledged in Ref. 124 (1965)

129) J.M.Dickson,D.C.Salter: Nuov.Cim. VI,1 p235 (1957)

130) S.K.Mark,P.M.Portner,R.B.Moore: Can.J.Phys. 44 p2961 (1966)

131) C.Rolland,B.Geoffrion,N.Marty,M.Morlet,B.Tatischeff, A.Willis: Nuc.Phys. 80 p625 (1966)

132) T.W.P.Brogden,O.N.Jarvis,J.Orchard-Webb,M.R.Wigan: Proc.2nd Int.Symp. on Polarisation Phenomena of Nucleons, Karlsruhe (1965): Huber p293 (1966)

133) H.Atkinson: Private communication (1965)

134) M.Powell: Computer Journal 7 2 p155 (1964)

135) M.Powell: Computer Journal 7 4 p303 (1965)

136) G.Breit,R.E.Seamon,K.A.Freidman: Private communications (1965-7)

137) J.K.Perring: Private communications (1965-7)

138) G.Felsner: Phys.Lett. 25,4 p290B (1967)

139) B.Tatischeff: Nuc.Phys. A98 p384 (1967)

140) R.Moss,C.F.Kellars,A.J.Bearden: Rev.Sci.Inst. 34 p1267 (1963)

141) R.L.Collins,K.Mayer,J.C.Travis: Rev.Sci.Inst. 38 p3446 (1967)

142) D.M.Warschauer,W.Paul: Rev.Sci.Inst. 27,6 p419 (1956)

143) D.N.Astrov,L.B.Belyanskii: Cryogenics p111 April (1967)

144) A.M.Koehler,D.F.Measday,D.H.Morrill Nuc.Inst.Meth. 33 p341 (1965)

145) DuPont information sheet on H-film

146) M.R.Wigan,P.M.Martin,E.Wood: to be published (1967): Nuc. Inst. M. 57 (1) (19

147) M.R.Wigan,P.M.Martin: unpublished (1967): Nuc. Phys. (A) (19 A.E.R.E. - R 5685 (19

148) A.M.Cormack: Nuc.Phys. 52,286 (1964)

149) M.R.Wigan,P.M.Martin,O.N.Jarvis Preliminary data, unpublished (1967): Final data . AERE-R5685 (1968): Nuc. Phys A 117-91 (1968)

150) G.O.Jones: The Optical Model Interscience NY (1963)
E.J.Squires: A.E.R.E. Harwell Report A.E.R.E. T/P.75 (1959)

References (9)

151) P.Catillon,M.Chapellier,D.Garreta: Nuc.Phys. B2 p93 (1967)
R.L.Burman,B.Elbeck,B.Herskind: C.I.P.N. Paris 1964 Conference p180 (1965)
A.Abragam,M.Borghini,P.Catillon,J.Coustham,P.Roubeau, J.Thirion Phys.Lett. 2 p310 (1962)
N.Jarmie,J.E.Brolley,H.Kruse,H.C.Bryant,R.Smythe: Phys.Rev. (to be published)
K.Nisimura,N.Ruy,D.C.Worth,H.Imada et al: Proc.Theor. Phys. (Kyoto) 30 p719 (1963)
T.W.P.Brogden et al: (Ref. 38)
I.M.Vasilevsky,V.V.Vishnyakov,E.I.Ilescu,A.A.Tyapkin: Sov.Phys. J.E.T.P. 12 p616 (1961)
A.Beretvas,N.E.Booth,C.Dolmick,R.J.Esterling,R.E.Hill, J.Scheid,D.Sherdin,A.Yokosawa: Chicago Univ.Preprint EFINS 67-8 (1967)
J.V.Allaby,A.Ashmore,A.N.Diddens,J.Eades,G.B.Huxtable, K.Skarsvag: Proc.Phys.Soc.(Lond.) 77 p234 (1961)
E.Engels,T.Bowen,J.N.Cronin,R.L.McIlwain,L.G.Pondrom: Phys.Rev. 129 p1858 (1963)
G.Coignet,D.Cronenberger,K.Kuroda,A.Michaelowicz, J.C.Oliver,M.Poulet,J.Teillac,M.Borghini,C.Ryter: Nuov.Cim. 43A p708 (1966)
B.M.Golovin,V.P.Dzelepov,R.V.Zulkarneev: Sov.Phys. J.E.T.P. 14 p63 (1962)
H.E.Dost: UCRL-11877 (1965)
152) O.N.Jarvis,G.F.Cox: Nuc.Phys. 79 p297 (1966)
153) B.Rose: Phys.Lett. 20 p86 (1966)
154) R.D.Sharma,A.E.S.Green: Nuc. Phys. B3 p33 (1967)